ARCTIC CIRCULATION PATHWAYS, HEAT AND FRESHWATER FLUXES: RESULTS FROM NUMERICAL MODEL INTEGRATIONS

By

Jonathan Whitefield

RECOMMENDED:

Dr. Thomas Weingartner

Dr. Russ Hopcroft

Dr. Peter Winsor
Advisory Committee Chair

Dr. Sarah Mincks Hardy
Program Head, Marine Sciences and Limnology

APPROVED:

Dr. S. Bradley Moran
Dean, School of Fisheries and Ocean Sciences

Dr. John Eichelberger
Dean of the Graduate School

19 May 2016
Date

# ARCTIC CIRCULATION PATHWAYS, HEAT AND FRESHWATER FLUXES: RESULTS FROM NUMERICAL MODEL INTEGRATIONS

A

THESIS

Presented to the Faculty

of the University of Alaska Fairbanks

In Partial Fulfillment of the Requirements

for the Degree of

MASTER OF SCIENCE

By

Jonathan David Whitefield, B.Sc (Hons), M.Sc.

Fairbanks, Alaska

May 2016

Abstract

With increasing attention on Arctic warming and consequent reductions of sea ice, many studies are focusing on the "gateways" to the Arctic Ocean - the regions where water enters and exits the Arctic Basin. The Chukchi Sea is the only pathway for Pacific water to enter the Arctic Ocean. While the Chukchi naturally undergoes large seasonal and interannual variability, currently it is also undergoing larger and rapid changes, which include transition to a longer ice-free season. Numerical models are often used to explore this region, due to observational restrictions associated with sea-ice. Most past and current models tend to represent riverine inputs in a non-realistic manner; adding freshwater on or past the shelf break, not accounting for seasonality of the river discharge, and omitting riverine heat content. In addition, in many of these models, buoyant coastal currents are not well resolved. Here, I present a new river discharge and river temperature data set (at 1/6° resolution). Employing this new data set within a high-resolution pan-Arctic model, freshwater content on the Arctic shelves increased by ~3600 $km^3$ and summer heat fluxes increased by 8 TW (compared to previous models), resulting in a reduction of the Arctic-wide September sea ice extent by up to ~10%. With both the improved riverine forcing included in the model calculations, and the model's ability to resolve the Alaskan Coastal Current, the model suggests an additional 0.25 Sv of flow to the long-term Bering Strait volume transport. This translates to a 64% increase in the heat transport and a 32% increase in freshwater transport (including 4% from sea ice). The model also resolves individual transport pathways in the Chukchi Sea, including that of Bering Sea Water, which could influence species composition and distribution in the eastern Chukchi Sea. Increased computing power and improved observational tools lead to more accurate reproductions of coastal currents and riverine influences in these numerical models. Greater understanding of this near-shore

region and its influences is vital to further interpret larger connections between terrestrial and marine ecosystems, as well as Arctic-wide and global oceanic changes.

Table of Contents

Page

List of Figures

Page

List of Tables

Page

Acknowledgements

This work was supported in part by a Graduate Student Research Award from the North Pacific Research Board, and a UAF Center for Global Change Student Research Grant with funds from the Cooperative Institute for Alaska Research. Model integrations were supported in part by a grant of high-powered computing resources from the Arctic Region Supercomputing Center at the University of Alaska Fairbanks. Additional funding was provided by the Bureau of Ocean Energy Management (BOEM), the National Science Foundation (ARC-0856786) with ship time for moorings from the NOAA-RUSALCA program, and a TA-ship through UAF's Physics department.

Additional thanks must be given to Dr. Rebecca Woodgate (University of Washington) for generously providing access to the moored instrument data, Dr. Kevin Wood (NOAA/JISAO) for supplying data from a wave glider which sparked the finding that the model was not recreating riverine heat, and without which my first chapter would not exist, Dr. Alan Condron (UMass Dartmouth) for access to, and assistance with, the model output and analysis, and also Dr. Eddy Carmack (DFO-Canada) for many constructive comments and discussions. More critiques and extremely helpful discussions and suggestions were also welcomed from Drs. Mark Johnson, Seth Danielson, and Andrew McDonnell (all UAF), who were all instrumental in shaping final drafts of papers, presentations and posters.

The most help, guidance and patience came from my advisory committee, especially from my graduate chair Dr. Peter Winsor. Dr. Tom Weingartner was instrumental in keeping me grounded in the "real world", and not believing all that I saw in the model. Dr. Russ Hopcroft provided many comments and questions from outside the physical oceanography realm, and encouraged me to think further outside the box.

Finally, thanks goes out to the other staff and students from UAF's School of Fisheries and Ocean Sciences (and one from the UAF Physics department). Innocuous questions and comments at the lunch table changed my research, or provided thoughts to include in the work, plus their support as I neared completion of my thesis was invaluable. My family back in the United Kingdom was vital to keeping me sane, accepting several late night/early morning phone calls, and always being willing to Skype when needed. Lastly, I would like to thank my wife Charlotte for all the support and motivation she provided, even when she didn't realize she was doing it.

## Introduction

Referring to a region as estuarine usually implies a nearshore or coastal area where freshwater from terrestrial sources (i.e. rivers) dilute the salinity of ocean water. Pritchard (1967) also includes the stipulation that estuaries are semi-enclosed, and have free connections with the open ocean. However, entire ocean basins have been considered to have estuarine qualities – Tully and Barber (1960) interpreted the North Pacific as an estuary, and Stigebrandt (1984) referred to exchanges between the Pacific and Arctic oceans as estuarine. Based on the definition of Pritchard (1967), the Arctic Ocean is indeed an estuary; it is a mediterranean sea, completely surrounded by land, with connections to the saltier Atlantic Ocean at one end, and fresher water from the Pacific Ocean at the other. While input from the Pacific is not strictly freshwater from terrestrial sources, a massive amount of riverine water is carried into the Arctic Ocean; for a basin that is only ~1% of the total ocean volume, it receives over 10% of the total global river discharge (McClelland et al., 2012).

This large amount of riverine freshwater, coupled with net precipitation and seasonally melting sea ice serves to form the buoyant fresh layer, akin to a single river in the "normal" coastal estuarine environment. The saltier Atlantic Ocean is the proxy for the salt wedge in the "normal" situation. This division between the water masses is perhaps more pronounced than in lower latitudes, due to stratification in high-latitude seas being controlled primarily by salinity (known as beta-type oceans), compared to subtropical, alpha-type oceans having stratification controlled primarily by changes in temperature (Carmack, 2007). Surface waters of the central Arctic are typically near freezing (Aagaard et al., 1981), but Atlantic waters at 200-600 m are normally over 0 °C (Rudels et al., 1994). With the Arctic as a beta-type ocean, the transition between these two water masses, the halocline region and corresponding pycnocline act as an

inhibitor for mixing, essentially insulating the Arctic from the warming by the Atlantic water. It also acts to block winter mixing and convection by the surface layers to the Atlantic layer, subsequently promoting ice growth in winter. A weakening or disappearance of this insulating layer would lead to mixing of the warmer water, increasing the sensible heat available to reduce the ice thickness (Björk et al., 2002).

This insulating surface is one of the reasons that the Arctic Ocean plays such an important role in global climate, in particular through surface heat exchange. Most of the heat transfer in the Arctic occurs on the shelves, where there is seasonal ice cover, polynyas and other areas of open water. The Arctic also has a large effect on the thermohaline circulation, with freshwater export controlling the intensity of the circulation (Aagaard and Carmack, 1994). In the northern hemisphere, trade winds transport water vapor from the Atlantic to the Pacific over the Isthmus of Panama, making the equatorial Pacific fresher than the Atlantic. Oceanic transport north leads to further freshening of Pacific waters due to net precipitation and input from rivers, which results in a high-latitude Pacific that is fresher (by 2-3) than the Atlantic (Carmack and McLaughlin, 2011). This difference leads to a higher sea surface in the Pacific, and this "downhill" flow drives the waters into the Arctic Ocean. The fresh Arctic Ocean waters then exit through Fram Strait and the Canadian Archipelago into the sub-Arctic North Atlantic, before being carried back to the tropics in fresher, colder deep water masses such as North Atlantic Deep Water, completing the global thermohaline circulation "conveyor belt" (Carmack and McLaughlin, 2011). Thermohaline circulation is key in redistributing atmospheric heat over the globe (Aagaard and Carmack, 1994), and in the North Atlantic, regulates European climate (Broecker et al., 1985). Increasing freshwater content would reduce convection, and such reductions have been documented on both small (the "Great Salinity Anomaly" in the late 60s

and 70s; Dickson et al., 1988) and large (the Younger Dryas event; Broecker et al., 1985) scales. Decreasing freshwater content, however, would serve to intensify the thermohaline circulation, reducing northward transport of Atlantic water and increasing Arctic sea ice extent (Aagaard and Carmack, 1994).

As climate changes, notably through the warming of the atmosphere, more moisture will be carried in the atmosphere. For every 1 °C of temperature increase, the atmosphere can hold another 7% of water vapor (Mauritzen, 2012). Thus, a warming climate will also lead to an increase in evaporation in the lower latitudes, and a subsequent increase in precipitation at higher latitudes, followed by an increase in both temperature and magnitude of river discharge. In the Arctic, this warm river discharge then leads to an increase in sea ice melt, or a decrease in ice formation (see Chapter 1). Increasing Arctic river discharge is already being documented – discharge from Russian rivers has been monitored since at least the 1930s (Lammers et al., 2007) with a 7% increase in discharge (Peterson et al., 2002), and most of the increase in the recent decades (McClelland et al., 2004). North American rivers have been gauged only since the 1960s, but analyses of those data sets show an increase in discharge from glacially fed rivers (Hinzman et al., 2005).

Currently, river discharge makes up 38% of the annual mean freshwater input to the Arctic Ocean, with input through the Bering Strait contributing 30% and precipitation adding a further 24% (Serreze et al., 2006). While the inflows and outflows are largely balanced (Serreze et al., 2006), there is still a large amount of freshwater stored in the Arctic Ocean, both in liquid form (e.g. the Beaufort Gyre) and as sea ice. Estimates show that the amount of freshwater currently stored in the Arctic is similar to the amount released as the Great Salinity Anomaly (Curry and Mauritzen, 2005), yet during this period, there was little to no effect on ocean

circulation from the freshwater release. With potential increases in freshwater from Arctic river input and ice melt leading to increased freshwater storage, significant change to the thermohaline circulation in the northern North Atlantic could be possible.

Although river discharge has been gauged since the 1930s (at least for the Eurasian rivers), oceanic freshwater pathways have been monitored for considerably less time. Larger scale regional studies have only studied the sub-Arctic seas since the early 1990s, but river discharge volumes are already showing signs of change due to climatic variations. For example, reductions in Arctic sea ice extent, volume and thickness are only evident since the use of satellite imagery (cf. Kwok and Rothrock, 2009), with corresponding warming of Atlantic inflow (Schauer et al., 2008), water on Arctic shelves (Dmitrenko et al., 2010), and in the Arctic basin (Polyakov et al., 2005; McLaughlin et al., 2009). Arctic-ward fluxes through the Barents Sea Opening and Fram Strait have been monitored since 1997 through a series of regional efforts, beginning with the 1997-2000 Variability of Exchanges in Northern Seas (VEINS) project. This was followed by the 2003-2006 Arctic-Subarctic Ocean Fluxes (ASOF) study, which transitioned into the Developing Arctic Modelling and Observing Capabilities for Long-term Environmental Studies (DAMOCLES) as the European portion of the International Polar Year. ASOF and DAMOCLES were Arctic-wide studies, aiming to observe the complete coupled ocean-atmosphere-ice system, of which fluxes in the Atlantic pathways were only a part.

The Barents Sea Opening (BSO) is the most significant of the inflow pathways from the Atlantic, with a long-term mean volume transport of ~2 Sv (1 Sv $\equiv 10^6$ $m^3$ $s^{-1}$) through the main channel, although this value can vary by 50% (Smedsrud et al., 2010). However, some of this inflow is cooled and outflows through the northern BSO (Skagseth et al., 2008). A coastal current brings an additional 2.6 Sv along the Norwegian coast (Beszczynska-Möller et al., 2011).

Observations show that waters passing through the BSO have increased in both temperature (~1 °C between 1997 and 2006) and volume (0.1 Sv $yr^{-1}$). This warm inflow means that the Barents Sea is ice-free year round, and 71 TW (1 terawatt = $10^{12}$ watts, or J $s^{-1}$) is transferred to the atmosphere over the Barents Sea (Beszczynska-Möller et al., 2011), which is likely to increase with rising global ocean temperatures, and thus further contribute to warming of the Arctic.

Fram Strait, between Greenland and Svalbard, is a two-way exchange between the Arctic and the Atlantic Oceans. Atlantic waters passing through Fram Strait are much deeper than in the BSO, flowing under the fresher, colder waters exiting from the Arctic. As such, less heat is lost to the atmosphere in this region. A large, 16 mooring observational array has been in place since 1997 in deep waters, and additional shallower moorings are closer to Greenland in order to capture freshwater transport in the East Greenland Current. These moorings show that there is high variability in the inflowing volume transport through Fram Strait, with a long-term value of 2 ± 2.7 Sv (Schauer et al., 2008). However, some of this uncertainty comes from the mooring spacing poorly resolving the ~10 km Rossby radius in the deeper parts of the Fram Strait. The East Greenland Current is a key outflow for both water and sea ice from the Arctic basin. Approximately 51% of the total freshwater outflow from the Arctic passes through Fram Strait, with an equal split between sea ice and liquid components (Serreze et al., 2006), and most of the sea ice exiting the Arctic being transported by the East Greenland Current (Kwok, 2009). There is an increasing trend in volume transport through Fram Strait, with transport in the East Greenland Current increasing from 4 Sv in 2002 to 10 Sv in 2007 (Beszczynska-Möller et al., 2011), in part due to varying contributions from precipitation, riverine sources, and the melting of the Greenland ice sheets (Dodd et al., 2009; Rabe et al., 2009).

The third main gateway to the Arctic Ocean, the comparatively narrow Bering Strait (85 km compared to the 350 km wide Fram Strait), is primarily an inflow pathway, and is the only way that oceanic waters can enter the Arctic from the Pacific Ocean. Pacific waters passing through the Bering Strait add ~30% of the total freshwater input to the Arctic Ocean (Serreze et al., 2006), and 10-20% of oceanic heat (Woodgate et al., 2012). The Bering Strait has been sampled the longest of the main entrances, with occasional observations dating back several hundred years, including by James Cook (1778-1779). One of the first estimates of the volume transport through the Bering Strait was taken by the United States Coast and Geodetic Survey, and (when converted from $ft^3\ d^{-1}$) was estimated to be 1.2 Sv (Dall, 1880). This value is ~ 50% greater than estimates from present-day moorings, which have been monitoring the Bering Strait throughflow since 1990 (Woodgate et al., 2006), although it is acknowledged that these moorings do not account for flow in seasonally present coastal currents.

The Bering Strait is divided into two channels by the Diomede Islands, and a boundary current exists in each channel. The western Anadyr Current is nutrient rich, and tends to be colder and saltier than the eastern current – the Alaskan Coastal Current, which is seasonally present during summer and autumn. Based on observations, the long-term mean volume transport through the Bering Strait is 0.8 Sv northwards, due to a Pacific-Arctic sea level difference of ~0.7 m (Aagaard et al., 2006). However, more recent measurements suggest that volume transport is greater than the climatology (Woodgate et al., 2006) and on an increasing trend, largely due to an increase in the sea level difference (Woodgate et al., 2012). Short term transport variability is strongly correlated with the local winds (Coachman and Aagaard, 1981), and can result in transport values ranging between -2 Sv and 3 Sv (Woodgate and Aagaard, 2005).

After passing through the Bering Strait, waters flow across the wide (500 km), shallow (50 m) Chukchi Sea, although the transport across the shelf is variable. Maximum transport occurs during the summer, as the Alaskan Coastal Current increases in strength, and during the winter prevailing northeasterly winds oppose the northward flow resulting in transport minima (Roach et al., 1995; Woodgate et al., 2005). Flow patterns across the shelf region are largely controlled by the bathymetry – western Bering Strait throughflow typically exits through Herald Canyon, and eastern Bering Strait throughflow (including the Alaskan Coastal Current, when present) exits through Barrow Canyon. Measurements by Weingartner et al. (2005) show a third exit pathway through the region between Hanna and Herald Shoals, termed the Central Channel. However, with complications due to the seasonal sea ice coverage, observations are typically limited to summer, making a full understanding of the Chukchi flow structure and its seasonal transitions difficult. What is known is that the nutrient concentrations in the flow pathways during summer and fall months are markedly different in each channel (Walsh et al., 1989; Cooper et al., 1997). Waters to the west are typically from the deeper Bering Sea basin, are upwelled and advected through the Gulf of Anadyr, and are more nutrient rich (with surface nitrate and silicate concentrations >20 $\mu g\ l^{-1}$; Walsh et al., 1989) than the eastern waters which have passed through the biologically productive Bering Sea shelf (Lomas et al., 2012). There is some mixing of water masses to the north of Bering Strait, and the high nutrient content makes the Chukchi Sea shelf one of the most productive shelf regions in the world (Grebmeier and Maslowski, 2014), with ~15% of all Arctic primary productivity occurring on the Chukchi shelf (Sakshaug, 2004).

The shallow depths of the Chukchi Sea mean that, in the ice-free summer months, the entire water column can be atmospherically influenced, particularly through a strong Beaufort

High (Overland et al., 2012). With the increasing loss of summer sea-ice (Duarte et al., 2012), an environment that is tuned to a specific cycle of ice extent, temperature and mixing cycles is undergoing pronounced changes. A longer ice-free period creates a negative feedback, with the open ocean warming due to decreased albedo and greater stratification, and thus storing more heat (Jackson et al., 2010). Additional observations show that the Chukchi Sea is also experiencing an increase in primary productivity rates, which could lead to a regime shift similar to those already documented in other Arctic regions (Arrigo and van Dijken, 2011). Observations over the Chukchi Sea shelf, however, are typically limited to the ice-free months, and normally confined to the eastern side of the International Date Line. However, concerted international efforts to sample the Chukchi Sea as a whole began with the Russian-American Long-term Census of the Arctic (RUSALCA) program in 2004. Three extended, multidisciplinary cruises in 2004, 2009 and 2013 comprehensively surveyed the southern Chukchi Sea, but only managed to observe periods where summer conditions were progressively cooler, not representative of the longer-term Arctic warming trends (Wood et al., 2015).

Most, if not all forms of observation of the Arctic gateways are susceptible to data omissions. Cruises only capture a short-term picture of long-term variability (as above), and are subject to logistical difficulties. Technologies such as autonomous underwater vehicles can run "missions" for longer than traditional cruises, and sample at resolutions that are impractical for CTDs. Gliders can also operate in shallower waters than vessels, providing increased spatial coverage. However, they cannot be safely used in shallow, seasonally ice-covered regions– gliders cannot surface and communicate through ice, and higher velocity currents (such as through Barrow Canyon and in the Alaskan Coastal Current) can make navigation to waypoints difficult. Moored arrays provide better estimates of long-term changes, but even these have

impracticalities. For instance, it becomes cost prohibitive to measure the variation of flow in the Arctic pathways at a spatial resolution on the order of the Rossby radius (~10 km), and moorings which are deployed need to be designed with the changing ice extent in mind. Ice keels in the Bering Strait can reach upwards of 20 m (Woodgate et al., 2015), and so the shallowest instruments in this array do not sample the summer stratified layer, and thus cannot account for heat and freshwater transported in this layer. It has thus become common to combine observations and results of numerical simulations in order to provide a more complete picture of the region of interest. Yet, there are few models that are used in studies of the Pacific-Arctic region.

The complex Bering Strait throughflow, with three distinct water masses, can be poorly represented due to complex boundary conditions in regional models, while global models are run either with a closed Bering Strait (e.g. Maslowski et al., 2000), or with a single grid cell representing the Bering Strait with a spatially constant transport value (e.g. Steele et al., 2001; Clement et al., 2005). These models also tend to be forced with transports derived from observations (either long-term means or seasonal cycles; Winsor and Chapman, 2004; Spall, 2007), which, due to the inability to resolve the entire water column, contain uncertainties in estimates of volume, heat and freshwater transport.

The model used in this thesis, the Massachusetts Institute of Technology general circulation model (MITgcm; Marshall et al., 1997), uses a high enough resolution (~1/6°) to resolve the different currents in the Bering Strait, and is a global model, so is not restricted by boundary condition problems. It is coupled to the MIT sea ice model (Losch et al., 2010), and was used as one developed as part of the Estimating the Circulation and Climate of the Ocean, Phase II (ECCO2) project (Menemenlis et al., 2005a; Menemenlis et al., 2008). An overview of

the model configuration is detailed in Condron et al. (2009). The model was run for a 35-year period (1979 – 2013) with initial conditions created by taking a Green's function approach to blend several salinity, temperature and sea ice climatologies (Menemenlis et al., 2005b), and atmospheric forcing from the Japan Meteorological Agency's Japanese 25 year reanalysis (JRA-25; Onogi et al., 2007). Initial model simulations used a monthly-mean river discharge climatology with 1° × 1° resolution based on the Arctic Runoff Data Base; this comparatively coarse resolution forcing compared to the model resolution resulted in discharge being input on or past the shelf break in some instances, and did not account for seasonal heating in the river discharge. In fact, preliminary sea surface temperature contours showed no signal from large river plumes which were clearly evident in observations.

Therefore, this thesis begins by creating a new climatological river forcing data set for the pan-Arctic region with 1/6° resolution, six times higher than the 1° × 1° resolution data sets currently used in the MITgcm. The new data set, Arctic River Discharge and Temperature (ARDAT) incorporates observations from 30 Arctic rivers into monthly mean river discharge and water temperature climatologies. Results of a comparison between two model runs (one using the original 1° resolution forcing and no discharge temperature, and one using the ARDAT data set), including basin-scale analysis, and more focused analyses of differences over the Arctic shelf domain and around the Mackenzie River delta, is presented in Chapter 1, "A new river discharge and river temperature climatology data set for the pan-Arctic region" (Whitefield et al., 2015). Chapter 2 then uses results from a simulation incorporating the more realistic riverine heat and freshwater fluxes from ARDAT to both estimate Bering Strait throughflow (including contributions from the Alaskan Coastal Current, sea-ice, and in stratified surface

layers), and to recreate seasonal variations in the flow pathways across the Chukchi Sea shelf region. The overall results of both papers are then summarized in the conclusions section.

***References***

Aagaard, K., Carmack, E.C., 1994. The Arctic Ocean and Climate: A Perspective. Geophysical Monograph Series 85, 5-20.

Aagaard, K., Coachman, L.K., Carmack, E.C., 1981. On The Halocline of the Arctic Ocean. Deep Sea Research 28A, 529-545.

Aagaard, K., Weingartner, T.J., Danielson, S.L., Woodgate, R.A., Johnson, G.C., Whitledge, T.E., 2006. Some Controls on Flow and Salinity in Bering Strait. Geophysical Research Letters 33, L19602.

Arrigo, K.R., van Dijken, G.L., 2011. Secular Trends in Arctic Ocean Net Primary Production. Journal of Geophysical Research: Oceans (1978–2012) 116, C09011.

Beszczynska-Möller, A., Woodgate, R.A., Lee, C., Melling, H., Karcher, M., 2011. A Synthesis of Exchanges through the Main Oceanic Gateways to the Arctic Ocean, in: The Changing Arctic Ocean: Special Issue on the International Polar Year (2007-2009), Oceanography, 24 (3), 76-93.

Björk, G., Söderkvist, J., Winsor, P., Nikolopoulos, A., Steele, M., 2002. Return of the Cold Halocline Layer to the Amundsen Basin of the Arctic Ocean: Implications for the Sea Ice Mass Balance. Geophysical Research Letters 29 (11), 1513-1516.

Broecker, W.S., Peteet, D.M., Rind, D., 1985. Does The Ocean-Atmosphere System Have More Than One Stable Mode Of Operation? Nature 315, 21-26.

Carmack, E., McLaughlin, F., 2011. Towards Recognition of Physical and Geochemical Change in Subarctic and Arctic Seas. Progress in Oceanography 90, 90-104.

Carmack, E.C., 2007. The Alpha/Beta Ocean Distinction: A Perspective on Freshwater Fluxes, Convection, Nutrients and Productivity in High-Latitude Seas. Deep Sea Research Part II: Topical Studies in Oceanography 54, 2578-2598.

Clement, J.L., Maslowski, W., Cooper, L.W., Grebmeier, J.M., Walczowski, W., 2005. Ocean Circulation and Exchanges through the Northern Bering Sea – 1979-2001 Model Results. Deep Sea Research II 52, 3509-3540.

Coachman, L.K., Aagaard, K., 1981. Re-Evaluation of Water Transports In The Vicinity Of Bering Strait, in: Hood, D.W., Calder, J.A. (Eds.), the Eastern Bering Sea Shelf: Oceanography and Resources. National Oceanic and Atmospheric Administration, Washington D.C., pp. 95-110.

Condron, A., Winsor, P., Hill, C., Menemenlis, D., 2009. Simulated Response Of The Arctic Freshwater Budget To Extreme NAO Wind Forcing. Journal of Climate 22, 2422-2437.

Cooper, L.W., Whitledge, T.E., Grebmeier, J.M., Weingartner, T., 1997. The Nutrient, Salinity, and Stable Oxygen Isotope Composition of Bering and Chukchi Seas Waters In and Near the Bering Strait. Journal of Geophysical Research: Oceans (1978–2012) 102, 12563-12573.

Curry, R., Mauritzen, C., 2005. Dilution of the Northern North Atlantic Ocean in Recent Decades. Science 308, 1772-1774.

Dall, W.H., 1880. Report On The Currents And Temperatures Of Bering Sea And The Adjacent Waters, Report Of The Superintendent Of The U.S. Coast And Geodetic Survey, Washington D.C., pp. 297-340.

Dickson, R.R., Meincke, J., Malmberg, S.-A., Lee, A.J., 1988. The "Great Salinity Anomaly" In the Northern North Atlantic 1968–1982. Progress in Oceanography 20, 103-151.

Dmitrenko, I.A., Kirillov, S.A., Tremblay, L.B., Bauch, D., Hölemann, J.A., Krumpen, T., Kassens, H., Wegner, C., Heinemann, G., Schröder, D., 2010. Impact of the Arctic Ocean Atlantic Water Layer on Siberian Shelf Hydrography. Journal of Geophysical Research: Oceans (1978–2012), 115 (C8), C08010.

Dodd, P.A., Heywood, K.J., Meredith, M.P., Naveira-Garabato, A.C., Marca, A.D., Falkner, K.K., 2009. Sources and Fate of Freshwater Exported in the East Greenland Current. Geophysical Research Letters 36 (19), L19608.

Duarte, C.M., Lenton, T.M., Wadhams, P., Wassmann, P., 2012. Abrupt Climate Change in the Arctic. Nature Climate Change 2, 60-62.

Grebmeier, J.M., Maslowski, W., 2014. The Pacific Arctic Region: Ecosystem Status and Trends in a Rapidly Changing Environment. Springer, New York.

Hinzman, L.D., Bettez, N.D., Bolton, W.R., Chapin, F.S., Dyurgerov, M.B., Fastie, C.L., Griffith, B., Hollister, R.D., Hope, A., Huntington, H.P., 2005. Evidence and Implications of Recent Climate Change in Northern Alaska and Other Arctic Regions. Climatic Change 72, 251-298.

Jackson, J., Carmack, E., McLaughlin, F., Allen, S.E., Ingram, R., 2010. Identification, Characterization, and Change of the Near-Surface Temperature Maximum in the Canada Basin, 1993–2008. Journal of Geophysical Research: Oceans (1978–2012) 115 (C5), C05021.

Kwok, R., 2009. Outflow of Arctic Ocean Sea Ice into the Greenland and Barents Seas: 1979-2007. Journal of Climate 22, 2438-2457.

Kwok, R., Rothrock, D., 2009. Decline in Arctic Sea Ice Thickness from Submarine and ICEsat Records: 1958–2008. Geophysical Research Letters 36 (15), L15501.

Lammers, R.B., Pundsack, J.W., Shiklomanov, A.I., 2007. Variability in River Temperature, Discharge, and Energy Flux from the Russian Pan-Arctic Landmass. Journal of Geophysical Research 112, G04S59.

Lomas, M.W., Moran, S.B., Casey, J.R., Bell, D.W., Tiahlo, M., Whitefield, J., Kelly, R.P., Mathis, J.T., Cokelet, E.D., 2012. Spatial and Seasonal Variability of Primary Production on the Eastern Bering Sea Shelf. Deep Sea Research II 65-70, 126-140.

Losch, M., Menemenlis, D., Campin, J.-M., Heimbach, P., Hill, C., 2010. On the formulation of sea-ice models. Part 1: Effects of different solver implementations and parameterizations. Ocean Modelling 33, 129-144.

Marshall, J., Adcroft, A., Hill, C., Perelman, L., Heisey, C., 1997. A Finite-Volume, Incompressible Navier Stokes Model for Studies of the Ocean on Parallel Computers. Journal of Geophysical Research 102, 5753-5766.

Maslowski, W., Newton, B., Schlosser, P., Semtner, A., Martinson, D., 2000. Modeling Recent Climate Variability in the Arctic Ocean. Geophysical Research Letters 27, 3743-3746.

Mauritzen, C., 2012. Oceanography: Arctic freshwater. Nature Geoscience 5, 162-164.

McClelland, J.W., Holmes, R., Dunton, K., Macdonald, R., 2012. The Arctic Ocean Estuary. Estuaries and Coasts 35, 353-368.

McClelland, J.W., Holmes, R.M., Peterson, B.J., Stieglitz, M., 2004. Increasing River Discharge in the Eurasian Arctic: Consideration of Dams, Permafrost Thaw, and Fires as Potential Agents of Change. Journal of Geophysical Research: Atmospheres (1984–2012) 109 (D18), D18102.

McLaughlin, F.A., Carmack, E.C., Williams, W.J., Zimmermann, S., Shimada, K., Itoh, M., 2009. Joint Effects of Boundary Currents and Thermohaline Intrusions on the Warming Of Atlantic Water in the Canada Basin, 1993–2007. Journal of Geophysical Research: Oceans (1978–2012) 114 (C1), C00A12.

Menemenlis, D., Campin, J.-M., Heimbach, P., Hill, C., Lee, T., Nguyen, A., Schodlok, M., Zhang, H., 2008. ECCO2: High Resolution Global Ocean and Sea Ice Data Synthesis. Mercator Ocean Quarterly Newsletter 31, 13-21.

Menemenlis, D., Hill, C., Adcroft, A., Campin, J.M., Cheng, B., Ciotti, B., Fukumori, I., Koehl, A., Heimbach, P., Henze, C., Lee, T., Stammer, D., Taft, J., Zhang, J., 2005a. NASA Supercomputer Improves Prospects for Ocean Climate Research. EOS Transactions AGU 86, 89.

Menemenlis, D., Fukumori, I., Lee, T., 2005b. Using Green's Functions to Calibrate an Ocean General Circulation Model. Monthly Weather Review 133, 1224-1240.

Onogi, K., Tsutsui, J., Koide, H., Sakamoto, M., Kobayashi, S., Hatsushika, H., Matsumoto, T., Yamazaki, N., Kamahori, H., Takahashi, K., 2007. The JRA-25 Reanalysis. Journal of the Meteorological Society of Japan 85, 369-432.

Overland, J.E., Francis, J.A., Hanna, E., Wang, M., 2012. The Recent Shift in Early Summer Arctic Atmospheric Circulation. Geophysical Research Letters 39 (19), L19804.

Peterson, B.J., Holmes, R.M., McClelland, J.W., Vorosmarty, C.J., Lammers, R.B., Shiklomanov, A.I., Shiklomanov, I.A., Rahmstorf, S., 2002. Increasing River Discharge to the Arctic Ocean. Science 298, 2171-2173.

Polyakov, I.V., Beszczynska, A., Carmack, E.C., Dmitrenko, I.A., Fahrbach, E., Frolov, I.E., Gerdes, R., Hansen, E., Holfort, J., Ivanov, V.V., 2005. One More Step toward a Warmer Arctic. Geophysical Research Letters 32 (17), L17605.

Pritchard, D.W., 1967. What Is An Estuary: Physical Viewpoint. Estuaries 83, 3-5.

Rabe, B., Schauer, U., Mackensen, A., Karcher, M., Hansen, E., Beszczynska-Möller, A., 2009. Freshwater Components and Transports in the Fram Strait–Recent Observations and Changes since the Late 1990s. Ocean Science 5, 219-233.

Roach, A.T., Aagaard, K., Pease, C.H., Salo, S.A., Weingartner, T., Pavlov, V., Kulakov, M., 1995. Direct Measurements Of Transport And Water Properties Through The Bering Strait. Journal of Geophysical Research 100, 18443-18457.

Rudels, B., Jones, E., Anderson, L., Kattner, G., 1994. On the Intermediate Depth Waters of the Arctic Ocean, in: The Polar Oceans and Their Role in Shaping the Global Environment, O. M. Johannessen, R. D. Muench and J. E. Overland (eds), American Geophysical Union, Washington, D. C., pp. 33-46.

Sakshaug, E., 2004. Primary and Secondary Production in the Arctic Seas, in: The Organic Carbon Cycle in the Arctic Ocean, R. Stein and R. MacDonald (eds), Springer, New York, pp. 57-81.

Schauer, U., Beszczynska-Möller, A., Walczowski, W., Fahrbach, E., Piechura, J., Hansen, E., 2008. Variation of Measured Heat Flow through the Fram Strait between 1997 and 2006, in: Arctic–Subarctic Ocean Fluxes, R. Dickson, J. Meincke, and P. Rhines (eds), Springer, New York, pp. 65-85.

Serreze, M.C., Barrett, A.P., Slater, A.G., Woodgate, R.A., Aagaard, K., Lammers, R.B., Steele, M., Moritz, R., Meredith, M., Lee, C.M., 2006. The Large-Scale Freshwater Cycle of the Arctic. Journal of Geophysical Research 111, C11010.

Skagseth, Ø., Furevik, T., Ingvaldsen, R., Loeng, H., Mork, K.A., Orvik, K.A., Ozhigin, V., 2008. Volume And Heat Transports To The Arctic Ocean Via The Norwegian And Barents Seas, in: Arctic–Subarctic Ocean Fluxes, R. Dickson, J. Meincke, and P. Rhines (eds), Springer, New York, pp. 45-64.

Smedsrud, L.H., Ingvaldsen, R., Nilsen, J.E.Ø., Skagseth, Ø., 2010. Heat in the Barents Sea: Transport, Storage, and Surface Fluxes, Ocean Science, 6, 219-234.

Spall, M.A., 2007. Circulation and Water Mass Transformation in a Model of the Chukchi Sea. Journal of Geophysical Research: Oceans (1978–2012), 112 (C5), C05025.

Steele, M., Ermold, W., Hakkinen, S., Holland, D., Holloway, G., Karcher, M., Kauker, F., Maslowski, W., Steiner, N., 2001. Adrift In the Beaufort Gyre: A Model Intercomparison. Geophysical Research Letters 28, 2935-2938.

Stigebrandt, A., 1984. The North Pacific: A Global-Scale Estuary. Journal of Physical Oceanography 14, 464-470.

Tully, J., Barber, F., 1960. An Estuarine Analogy in the Sub-Arctic Pacific Ocean. Journal of the Fisheries Board of Canada 17, 91-112.

Walsh, J.J., McRoy, C.P., Coachman, L.K., Goering, J.J., Nihoul, J.C.J., Whitledge, T.E., Blackburn, T.H., Parker, P.L., Wirick, C.D., Shuert, P.G., Grebmeier, J.M., Springer, A.M., Tripp, R.D., Hansell, D.A., Djenidi, S., Deleersnijder, E., Henriksen, K., Lund, B., Andersen, P., Muller-Karger, F.E., Dean, K., 1989. Carbon and Nitrogen Cycling Within the Bering/Chukchi Seas: Source Regions for Organic Matter Affecting AOU Demands of the Arctic Ocean. Progress in Oceanography 22, 277-359.

Weingartner, T., Aagaard, K., Woodgate, R., Danielson, S., Sasaki, Y., Cavalieri, D., 2005. Circulation on the North Central Chukchi Sea Shelf. Deep Sea Research Part II: Topical Studies in Oceanography 52, 3150-3174.

Whitefield, J., Winsor, P., McClelland, J., Menemenlis, D., 2015. A New River Discharge And River Temperature Climatology Data Set For The Pan-Arctic Region. Ocean Modelling 88, 1-15.

Winsor, P., Chapman, D.C., 2004. Pathways of Pacific Water across the Chukchi Sea: A Numerical Model Study. Journal of Geophysical Research, 109 (C3), C03002.

Wood, K.R., Wang, J., Salo, S., Stabeno, P., 2015. The Climate of the Pacific Arctic during the First RUSALCA Decade 2004–2013. Oceanography 28, 24-35.

Woodgate, R.A., Aagaard, K., 2005. Revising the Bering Strait Freshwater Flux into the Arctic Ocean. Geophysical Research Letters 32, L02602.

Woodgate, R.A., Aagaard, K., Weingartner, T.J., 2005. Monthly Temperature, Salinity, and Transport Variability of the Bering Strait Through Flow. Geophysical Research Letters 32, L04601.

Woodgate, R.A., Aagaard, K., Weingartner, T.J., 2006. Interannual Changes in the Bering Strait Fluxes of Volume, Heat and Freshwater Between 1991 and 2004. Geophysical Research Letters 33, L15609.

Woodgate, R.A., Stafford, K.M., Prahl, F.G., 2015. A Synthesis of Year-Round Interdisciplinary Mooring Measurements in the Bering Strait (1990-2014) and the RUSALCA Years (2004-2011). Oceanography 28, 46-67.

Woodgate, R.A., Weingartner, T., Lindsay, R., 2012. Observed Increases In Bering Strait Oceanic Fluxes From The Pacific To The Arctic From 2001 To 2011 And Their Impacts On The Arctic Ocean Water Column. Geophysical Research Letters 39, L24603.

# Chapter 1. A new river discharge and river temperature climatology data set for the pan-Arctic region [1]


***Abstract***

Most regional ocean models that use discharge as part of the forcing use relatively coarse river discharge data sets (1°, or ~110 km) compared to the model resolution (typically 1/4° or less), and do not account for seasonal changes in river water temperature. We introduce a new climatological data set of river discharge and river water temperature with 1/6° grid spacing over the Arctic region (Arctic River Discharge and Temperature; ARDAT), incorporating observations from 30 Arctic rivers. The annual mean discharge for all rivers in ARDAT is 2817 ± 330 $km^3$ $yr^{-1}$. River water temperatures range from 0 °C in winter to 14.0 – 17.6 °C in July, leading to a long-term mean monthly heat flux from all rivers of 3.2 ± 0.6 TW, of which 31% is supplied by Alaskan rivers and 69% is supplied by Eurasian rivers. This riverine heat flux is equivalent to 44% of the estimated ocean heat flux associated with the Bering Strait throughflow, but during the spring freshet can be ~10 times greater, suggesting that heat flux associated with Arctic rivers is an important component of the Arctic heat budget on seasonal time scales.

We apply the ARDAT data set to a high-resolution regional ocean-ice model, and compare results to a model integration using a 1° resolution discharge data set. Integrated freshwater content on the Arctic shelves (<200 m) increases by ~3600 $km^3$ in the ARDAT forced model run compared to the coarser forcing, suggesting that river discharge is contained on the Arctic shelves when forced with the ARDAT data set. Modeled summer heat fluxes over the shelves increase by 8 TW when river water temperature is included, which subsequently reduces basin-wide September sea ice extent by ~10%. Regional differences are larger, where e.g., sea


[1] Whitefield, J., Winsor, P., McClelland, J., Menemenlis, D., 2015. A new river discharge and river temperature climatology data set for the pan-Arctic region. Ocean Modelling 88, 1-15.

ice extent on the Beaufort shelf is reduced by ~36%. Using a non-linear free surface parameterization along with the ARDAT data set, we find an increase in the sea surface height gradient around river mouths. Geostrophic velocities increase to form quasi-continuous, fast-moving near-shore boundary currents not reproduced using the 1° resolution data set. Omitting river water temperature, or using a lower resolution data set, can therefore lead to incorrect model estimates of coastal transport, sea ice formation/melt rates, and other regional and basin scale processes. Using a high-resolution discharge data set, and accounting for the considerable heat carried by the Arctic rivers is recommended for future modelling efforts.

### *1.1. Introduction*

The Arctic Ocean is a uniquely structured mediterranean sea with a low salinity surface mixed layer on the order of a few tens of meters thick, on top of a 150-200 m thick halocline layer (Aagaard et al., 1981). The low surface salinity is in part the result of freshwater discharge from some of the largest rivers on the planet, such as the Lena and Yenisey Rivers (Figure 1.1; Holmes et al., 2013). Most of the annual river discharge enters the Arctic Ocean over a short period of ~ 2 months, as river ice breaks up and snow melts during the spring freshet between May and June (McClelland et al., 2012). During the spring freshet period, river discharge can reach temperatures of >10 °C (Lammers et al., 2007), indicating that river discharge may contribute significantly to both the Arctic heat and freshwater budget.

The river discharge portion of freshwater input is 18% greater than the relatively fresh (~32.5) water from the Pacific Ocean which enters through the shallow Bering Strait (Woodgate et al., 2005) (3200 $km^3$ $yr^{-1}$ compared to 2700 $km^3$ $yr^{-1}$; Condron et al., 2009) and 60% greater than atmospheric sources (2000 $km^3$ $yr^{-1}$; Serreze et al., 2006). Saltier water (35–35.2; Aagaard

and Carmack, 1989) enters from the deep North Atlantic creating the halocline layer. Due to the strong dependence of density on salinity at high latitudes (Carmack, 2007), this halocline serves to insulate the surface Arctic Ocean from the warmer, saltier (35 – 35.2) Atlantic layer below (Aagaard et al., 1981). The high lateral and vertical gradients often lead the Arctic Ocean to be considered an estuarine system (e.g., Tully and Barber, 1960; Stigebrandt, 1984; Aagaard and Carmack, 1994; Carmack, 2007; McClelland et al., 2012).

As the global climate warms, both precipitation (Houghton et al., 2001) and air temperatures (Rouse et al., 1997) are predicted to increase. These changes will likely lead to increased and warmer river discharge, potentially affecting factors such as nutrient transport (Manizza et al., 2011; McClelland et al., 2012) or sea ice formation and melt (e.g., Dean et al., 1994; Searcy et al., 1996; Bareiss et al., 1999).

Although modelling studies that focus on the role of Arctic river discharge may resolve the major transport pathways (e.g., Bering Strait and Canadian Arctic Archipelago), they often use a relatively coarse river discharge forcing (1°; Dai and Trenberth, 2002) compared to the model resolution (typically on the order of 1/4° or smaller), and do not account for seasonal changes in the temperature of river water. These models can also underestimate pan-Arctic freshwater budgets. For example, total integrated Arctic freshwater content in the Ocean Circulation and Climate Advanced Model from the National Oceanography Centre is ~58,000 $km^3$ compared to the observed 74,000 $km^3$ (Serreze et al., 2006; Jahn et al., 2012), a discrepancy of 22%.

Here we present a new climatological river forcing data set for the pan-Arctic region with 1/6° resolution, six times higher than the 1° × 1° resolution data sets currently used. It incorporates observations from 30 Arctic rivers and consists of a climatological seasonal cycle

for both river discharge and water temperature. We describe our methods for constructing the new data set in section 2, before presenting the data set in section 3. We compare results of two high-resolution ocean-sea ice coupled model runs, one using a 1° resolution forcing with no associated river water temperature, and one incorporating the new discharge/temperature data set. These comparisons include a basin-scale analysis, as well as more focused analyses of differences over the Arctic shelf domain and around the Mackenzie River delta in particular. We discuss our results in section 4, and present our conclusions in section 5.

### *1.2. Methods*

#### *1.2.1. Data Sources*

The Arctic River Discharge and Temperature (ARDAT) data set is comprised of monthly mean river discharge and temperature data. Discharge for the Eurasian rivers was obtained from two openly available data sets; R-ArcticNET (http://www.r-arcticnet.sr.unh.edu/v4.0/index.html; Lammers et al., 2001) and the Regional Integrated Hydrological Monitoring System for the Pan-Arctic Landmass (ArcticRIMS; http://rims.unh.edu). Alaskan river discharge observations were downloaded as monthly means from the US Geological Survey's National Water Information System (NWIS; http://waterdata.usgs.gov/nwis). Canadian rivers in Baffin and Hudson Bays were not included in the data set, as we use the definition of the pan-Arctic watershed from Holmes et al. (2013). This only includes rivers that empty in to the Arctic Ocean, plus the watershed of the Yukon and all rivers entering the Bering Sea north of the Yukon, although due to the proximity of the watersheds we also include the Kuskokwim River in ARDAT. In all cases, observations from the most downstream station on each river were used. The only exception to this was for the Lena River; the most downstream station on the Lena is at

Polyarnaya, within the delta, which receives only 25% of the June discharge when compared to the monitoring station at Kusur.

ARDAT only includes temperature observations for the six largest Arctic rivers (hereafter referred to as the "Big 6" following Holmes et al. (2013); Figure 1.1; Table 1.1). Data for the Eurasian rivers combine observations from the ART-Russia data set (http://www.r-arcticnet.sr.unh.edu/RussianRiverTemperature-Website/; Lammers et al., 2007), and the Pan-Arctic River Transport of Nutrients, Organic Matter, and Suspended Sediments (PARTNERS) and Arctic Great Rivers Observatory (AGRO; http://www.arcticgreatrivers.org/) projects (McClelland et al., 2008). Temperature observations for Alaskan rivers are also available as part of NWIS.

### *1.2.2 Data set compilation*

A monthly seasonal cycle of discharge and, in the case of the large rivers, river water temperature was created for each river by averaging observations for each calendar month. With the exception of the Mackenzie River, there were sufficient data available to complete the mean seasonal cycle of water temperature for each river without interpolation over the May-October timeframe. In the case of the Mackenzie, temperature data were not available during May or October; these points were filled by using a linear interpolation between the two adjacent months. River water temperature observations for the Mackenzie are also scarce during the winter months (November to April). We therefore assigned a value of 0 °C during these months. This assumption was supported by temperature data from the other "Big 6" rivers that were consistently near zero during the November-April timeframe.

The data set was mapped to a polar stereographic projection on a 1/6° grid. This corresponds to the mean horizontal resolution of several models used in the Arctic Ocean Model Intercomparison Project (AOMIP; Jahn et al., 2012). Geographic positions of the river mouths were determined from publicly available satellite imagery, with the 1/6° grid superimposed. Grid cells closest to the river mouth (or channels, in the case of large deltas such as the Lena) were then assigned a long-term mean monthly discharge climatology, divided equally between the number of grid cells needed to reproduce the river mouth. Rivers that had a mouth width of < 1 grid cell (e.g., the Kobuk, and several rivers that empty in to the White Sea) were assigned the grid cell closest to the mouth.

The seasonal cycle of river water temperature was assigned to the corresponding discharge grid cell. For the larger rivers that were assigned > 1 grid cell for discharge, each grid cell was set to the same temperature as the others for that river. As river water temperatures are not available for all 30 rivers in the data set, we only use temperatures for the "Big 6" rivers (Figure 1.1, Table 1.2), and the Kuskokwim as a representative of sub-Arctic rivers. Comparisons between smaller rivers and the "Big 6" show that river water temperatures are similar (e.g., both the Yana and Lena rivers peak at 14.0 °C, and the Pur River's warmest temperature is 16.1 °C compared to the Ob's 15.8 °C). Riverine heat fluxes (Table 1.2) were calculated using $H = \rho C_p T_{river} Q$, where H is the monthly mean heat flux (Watts), $\rho$ is water density (kg $m^{-3}$), $C_p$ is specific heat capacity of water (J $kg^{-1}$ $°C^{-1}$), $T_{river}$ is river temperature (°C), and Q is monthly mean river discharge ($m^3$ $s^{-1}$). The data set, along with documentation and continuing updates is available at http://mather.sfos.uaf.edu/~jwhitefield/river/.

### *1.3. Results*

#### *1.3.1. Data*

Data from 30 river gauges were used to construct the ARDAT discharge data set. These include 26 from the Eurasian side of the Arctic and four from the North American side of the Arctic (Table 1.1). The gauge with the earliest available data was on the Severnaya Dvina, which started in June 1886 (Table 1.1). The Severnaya Dvina also has the longest available record, with only 10 months missing between the start of the record and September 2009. The three largest Eurasian rivers (Ob', Yenisey, Lena) have been gauged since 1936, and data are available for many other Eurasian rivers starting in the 1950s and 1960s (Table 1.1). Four of the Eurasian rivers included in the ARDAT climatology were not gauged before 1994 (Table 1.1).

Although the longest discharge records came from the Eurasian side of the Arctic, some of the records included significant gaps. The Nadym and the Amguema had 9.25 years of missing data over 46 and 44-year records respectively, and four other Eurasian rivers were missing at least 4 years of data in records of 30-50 years. The Eurasian river with the largest data gap was the Khatanga, with 22 years missing over a 33-year record. Data coverage was also notably sparse during winter months on the Khatanga. This is due to the Khatanga being dominated by inflow from the ocean during low discharge, leading to a reversed flow direction and negative discharge values (A. Shiklomanov, pers. comm.). An experimental directional current meter was used for 3 years, providing the only winter discharge rates for the Khatanga included in ARDAT.

Most of the North American rivers have been gauged since the 1970s (Table 1.1). Observations on the Kuskokwim started in 1951, making it the longest observed North American

river in this data set. Unlike the Eurasian rivers, there are no data gaps in the North American river observations.

River water temperature observations for most of the Eurasian rivers starts in 1936, but the Kolyma has the longest data record, starting in 1929. Data are available continuously until between 1995 and 2001, depending on the river (Table 1.2), and then additional observations from the PARTNERS/AGRO project cover the period from August 2003 – November 2011 (Table 1.2). Alaskan river water temperatures are available over the same period as discharge data (April 1975 – September 2012 for the Yukon, June 1951 – September 2010 for the Kuskokwim; Table 1.2). The sparsest temperature data set is from the Mackenzie, with observations only during the PARTNERS/AGRO project; 29 months of data exist, compared to 727 months for the Yenisey River. Overall, much less temperature data are available for winter months than summer months in the Arctic rivers. However, where winter data are available, values are typically near zero and do not vary strongly among rivers.

### *1.3.2. Climatologies*

The long-term mean annual discharge for all rivers in ARDAT is 2817 ± 330 $km^3$ $yr^{-1}$. The mean seasonal cycle integrated over all rivers (Figure 1.2a) shows a peak in June for the spring freshet, followed by a rapid decline. The Lena and Yenisey Rivers contribute 48.1% of the long-term mean 831 $km^3$ $month^{-1}$ discharged by all rivers in ARDAT during peak flow in June (Figure 1.2a). Discharge is measureable in the "Big 6" throughout the winter. In contrast, discharge from many of the smaller Arctic rivers is either zero or is too low to measure accurately during the winter (A. Shiklomanov, pers. comm.). The Yenisey has the highest mean winter discharge (18 $km^3$ $month^{-1}$, averaged over the complete data record, 1936 – 2009), which

is equivalent to about half of the discharge from the Yukon River in June (Figure 1.3), and also the largest mean June discharge (208 $km^3$ $month^{-1}$; Figure 1.3). Seasonal cycles of river discharge in the Yenisey, Lena and Kolyma follow the same cycle as the total monthly discharge for all rivers in ARDAT, with May discharge being 9.5% – 33.7% of the June discharge (Figure 1.3). Discharge then decreases sharply to reach 32.6% – 53.6% of the June levels in July (Figure 1.3). There is a second distinct seasonal cycle on the Ob', Mackenzie and Yukon Rivers; these rivers have comparatively high May discharge values (46.4% – 66.6% of the June discharge), and the subsequent decrease in discharge is also more gradual (Figure 1.3). This difference is likely related to distinct regional air temperature climatologies that affect the timing of snow melt and permafrost distribution.

In comparison to the discharge climatologies, the seasonal cycle of river water temperature is less variable among the "Big 6" rivers. For most of the rivers, water temperatures are ~1-2 °C during May and October, 6-10 °C during June and September, and reach maximum values in July and August (Figure 1.4). The exceptions are seen in the Mackenzie, Yukon and Kuskokwim Rivers, where May river water warms to 6-10 °C and temperatures average ~14 °C by June (Figure 1.4). The sub-Arctic Yukon and Kuskokwim Rivers also remain warmer in the autumn months; water temperatures are 4-5 °C in October, compared to ~2 °C for the other Arctic rivers. The minimum monthly water temperature was ~0 °C during the winter months (November – April) for all rivers (Figure 1.2b). Peak water temperature lags peak discharge by one month, and occurs in July in all rivers (Figure 1.2b). The July water temperature ranges from 14.0 °C in the Lena to 17.6 °C in the Yukon (Figure 1.4, Table 1.2). The mean monthly river water temperature for the "Big 6" reaches 15.8 °C in July (Figure 1.4), and the long-term mean annual water temperature is 4.5 °C.

The seasonal change in heat flux is mainly determined by changes in discharge volume, rather than an increase (or decrease) in river water temperature. Consequently the maximum monthly mean heat flux of 13.4 ± 5.6 TW occurs during June (Figure 1.2c). The long-term mean monthly heat flux for all rivers is 3.2 ± 0.6 TW, and average annual heat flux for all rivers is 38.4 ± 6.7 TW. There are also two distinct patterns in the heat flux seasonal cycles, as with freshwater discharge. The Eurasian rivers show a sharp increase in heat flux starting in May and peaking in June, before slowly decreasing to ~0 TW in the early winter months. For example, the Yenisey contributes 0.01 TW in May, and increases to 2.1 TW in June. There is then an almost linear decrease to 0.09 TW in October, with zero heat flux from November to the following April. The North American rivers have smoother transitions (Figure 1.3): 21% – 29% of the June heat flux on the Mackenzie and Yukon, and 61% of the June heat flux on the Kuskokwim, occurs during May, heat fluxes in June and July are of similar magnitudes (e.g., 0.93 TW and 0.92 TW for the Yukon), and heat fluxes in October are 15% – 24% of June heat fluxes. Due to the large contributions from the Lena and Yenisey, the overall (cumulative) pattern of heat fluxes is dominated by the Eurasian rivers with a distinct peak in June (Figure 1.3). With temperatures at 0 °C during the winter months, heat fluxes are zero for all rivers. All four Eurasian rivers also show negligible heat flux (< 0.01 TW) in May, whereas the large North American rivers (i.e. Yukon and Mackenzie) contribute 0.2 – 0.3 TW as the earlier onset of the spring freshet is coupled with warmer discharge (Figures 1.3 and 1.4). Although river discharge peaks in the spring, with the Yenisey as the greatest single contributor, the largest monthly heat flux among major Arctic rivers occurs in July on the Lena River (2.32 TW; Figure 1.3, Table 1.2). Mean July discharge from the Yenisey River is 32.6% of the mean June discharge, whereas discharge from the Lena River during July is 53.6% of the mean June discharge. This higher discharge rate

during July, as well as warmer summer river water temperatures (Figure 1.4), means that the heat flux on the Lena River is 0.12 TW higher in July than in June on the Yenisey River. The heat flux of the Yenisey shows large variability in June, however, with a standard deviation of 1.78 TW (Figure 1.3).

### *1.3.3. Comparison to coarse resolution forcing*

Our new discharge climatologies were applied to a regional Arctic configuration of the Massachusetts Institute of Technology general circulation model (MITgcm; Marshall et al., 1997), coupled to the MIT sea ice model (Losch et al., 2010), in order to analyze heat and freshwater content of Arctic shelves and the response of the coupled ice-ocean system to inclusion of river water temperatures. The particular model configuration that was used is one developed as part of the Estimating the Circulation and Climate of the Ocean, Phase II (ECCO2) project (Menemenlis et al., 2005a; Menemenlis et al., 2008). It has a 1/6° (~16 km) horizontal grid spacing, and uses the optimized model parameters of Nguyen et al. (2011). The model configuration is described in detail in Condron et al. (2009), Manizza et al. (2009) and Manizza et al. (2011). The model was run for a 35-year period (1979 – 2013) with initial conditions created by taking a Green's function approach to blend several salinity, temperature and sea ice climatologies (cf. Menemenlis et al., 2005b). Boundary conditions for the regional configuration were taken from monthly mean output from a global set of ECCO2 integrations. Atmospheric forcing was from the Japan Meteorological Agency's Japanese 25 year reanalysis (JRA-25; Onogi et al. (2007).

Previously, the ECCO2 model used a monthly-mean river discharge climatology with 1° × 1° resolution based on the Arctic Runoff Data Base, which resulted in discharge being input on

or past the shelf break in some instances; river discharge was subsequently rapidly advected to the interior of the Arctic Basin. Model integrations using the ARDAT data set receive river discharge in realistic geographic locations, and subsequently freshwater from river discharge remains in the shelf region. River discharge enters the model as a volume increase, rather than a decrease in salinity, and a non-linear sea surface is enabled (cf. Campin et al., 2008). River water temperature (used only for the run using ARDAT as forcing) is applied to the model as a heat flux, H, where $H = \rho C_p T_{river} Q$, where H is the monthly mean heat flux (W), $\rho$ is water density (kg $m^{-3}$), $C_p$ is specific heat capacity of water (J $kg^{-1}$ $°C^{-1}$), $T_{river}$ is river temperature (°C), and Q is monthly mean river discharge ($m^3$ $s^{-1}$). Two model runs were performed: one using the new ARDAT climatology for discharge forcing, and one using the 1° × 1° resolution discharge climatology.

The phase of the mean seasonal cycle of freshwater content (FWC) does not change between model runs, but the magnitude is increased by 3,700 $km^3$ (Figure 1.5a). The increase seen when using the ARDAT data set reflects not only direct inputs of river water to the shelf region, but also indirect effects of these inputs on the sea-ice balance. Over the shelf region, there is an initial increase in FWC over a period of ~10 years when using the ARDAT data set (Figure 1.6a). This is a spin-up response from the model, as the initial conditions were from the climatology with 1° × 1° resolution (where river discharge was input on or past the shelf break). However, the decreasing trend in FWC after the equilibration period (Figure 1.6a) is also seen in the model run using the original 1° × 1° forcing (not shown here). This suggests that the decrease is not a return to an equilibrium state, rather freshwater is either being stored in the interior of the Arctic Basin or is being exported to the North Atlantic.

Inclusion of river water temperature changed both the magnitude and phase of the heat flux onto the Arctic shelves. Heat fluxes in the winter months (JFM and ND) were reduced to <0.01 TW, and the mean summer (JJA) heat flux is increased by 8 TW over the shelves (<200 m; Figure 1.5b). When divided equally over the shelf area ($4.25 \times 10^6$ km$^2$), this is equivalent to an increase of ~1.5 W m$^{-2}$. Divided over the entire Arctic basin ($15.55 \times 10^6$ km$^2$), this gives an equivalent to ~0.5 W m$^{-2}$, roughly 50% of the heat flux sufficient to explain the decreasing sea-ice trend over the last few decades (Kwok and Untersteiner, 2011). Using ARDAT, the largest heat flux into the shelf region now coincides with the peak discharge (June) and warmest temperatures (July), rather than occurring in September and being driven solely by solar radiation. When riverine heat fluxes are combined with solar radiation, the Arctic shelves have a seasonal minimum in heat content in March, and a maximum in September. These extrema both exhibit upward trends over the 35-year (1979–2012) model run, with September heat content increasing at a rate 72% greater than March heat content ($24 \pm 4 \times 10^{18}$ J yr$^{-1}$ vs $14 \pm 2 \times 10^{18}$ J yr$^{-1}$). The trends are significantly different than both zero and each other at the 95% confidence level. The additional summer heat flux leads to a reduction of basin-wide sea ice of ~10% by the end of the 35-year model run compared to the run which used the 1° resolution forcing. During the 2012 sea ice minimum, the model run which used the coarse forcing overestimates sea ice extent by 3.5% compared to SSM/I observations downloaded from the National Snow and Ice Data Center (http://nsidc.org/data/nsidc-0081). The ARDAT forced run underestimates sea ice extent by 4.2% when compared to the same data set at the same time. This suggests that accounting for riverine heat content in model would lead to more conservative estimates of changes in sea ice extent. Regionally, the reduction in sea ice area is larger. The Beaufort Sea is covered by up to 7300 km$^2$ of sea ice in the model run forced by the coarse resolution discharge,

which decreases by ~36% (2600 $km^2$) when the resolution of the river discharge climatology is increased and river water temperature is included.

### *1.3.4. Modeled response of the Arctic shelf region*

In this section we present long-term freshwater content (FWC) and heat content (HC) changes over the Arctic shelf region, defined as the areas having depth <200 m and extending from the northern tip of Scandinavia (30° E) to the Canadian Arctic Archipelago (CAA; 60° W; Figure 1.1). We do not include shelves within the CAA, or to the west of Scandinavia, as river input here drains southward with negligible effect to the Arctic Basin. Based on this definition, the Arctic shelf region covers an area of $4.25 \times 10^6$ $km^2$.

Sea surface salinity (SSS) over the Arctic Basin clearly shows areas influenced by river discharge (SSS <20) constrained to the Siberian coasts, with regions of SSS <10 around large rivers (e.g., the Lena, Mackenzie and the Gulf of Ob'; Figure 1.1b). After 1990, there is a downward trend in FWC, which suggests that there is an increase in exported liquid FW or sea ice from the shelf region, either to the interior or to the Atlantic. This suggestion is validated by Rabe et al. (2011), who show that there is an increase of up to 8 m of FWC in the Canada Basin from 1992 – 2008, and FWC in the Arctic shelf region decreases by 2-4 m over the same period.

Mean September FWC is 23,170 $km^3$, combining the annual river discharge with FW from melted sea ice. The minimum in FWC occurs in April (19,550 $km^3$), resulting from the previous winter's ice formation, as well as mixing of deeper, saltier waters by winter convection and storms. The difference between mean September and April FWC is 3620 $km^3$, showing that, in this model, all of the river discharge is removed from the shelf region each year along with

freshwater from other sources. When distributed equally over the shelf region, this is equivalent to a vertically integrated freshwater height of 85 cm.

Winter river heat fluxes on the shelf are near to 0 W, resulting from low discharge and ~0 °C river water. River discharge is warmest in August/September (Figure 1.4). By this time, Arctic shelves have warmed to >7 °C around the major rivers (Yenisey/Ob', Lena, Mackenzie) and >3 °C on the remaining shelf region (Figure 1.1a). Heat fluxes associated with river discharge are 9.9 TW in June (peak discharge) and 11.2 TW in August (warmest river water temperatures). This is similar in magnitude to the annual mean heat flux through the Bering Strait (~12.5 TW; Woodgate et al., 2012), although riverine heat input occurs over a short period, as opposed to the nearly constant heat flux through the Bering Strait. When averaged over the entire shelf region, the maximum river heat flux is equivalent to ~2.6 W $m^{-2}$, or 2.7% of the annual mean shortwave radiation measured at NOAA's Barrow Observatory site in Barrow, Alaska (71° 19' N, 156° 369' W; Zib et al., 2012).

The seasonally varying river heat fluxes result in a seasonal cycle of HC that is qualitatively similar to that of FWC; minimum HC occurs on March, and the maximum occurs in September (Figure 1.6b). There is no equilibration period or downward trend as seen in FWC; instead there is an increasing trend over the entire model run. . March HC, corresponding to the annual minima, increases at ~$14 \times 10^{18}$ J $yr^{-1}$ over the entire 35-year model run, and September HC, corresponding to the annual maxima, increases at twice this rate. There is more interannual variability in September HC, as HC is also controlled by incoming solar radiation, and hence sea ice cover. Predictably, the highest HC (~$5 \times 10^{21}$ J) occurs during the sea ice minimum of September 2007.

### *1.3.5. Local response in a high-resolution model*

In this section we analyze the local response of stratification, heat and freshwater content, and ice retreat to river discharge around the Mackenzie River delta. Results for this comparison were taken from a sub-region of the Arctic-wide regional model integrations, rather than a new model run with smaller domain. The Mackenzie shelf was chosen as a case study region to show the effects of both moving the location of discharge to a realistic location, and also of recreating a delta in the ARDAT data set instead of a point source in the original forcing. In the original 1° forcing data set, discharge was input to the model over the 1000 m isobath, and did not account for the shape of the Mackenzie Delta. We report results for two years, 1996 and 1997, which were chosen to show different plume behaviors under different prevailing wind conditions.

The Mackenzie River is the fourth largest river in the Arctic Basin, with a mean annual discharge of 284 $km^3$ $yr^{-1}$. The majority of water discharge from the Mackenzie occurs between May and November. However, flow during the winter is also significant, adding approximately the same amount of cumulative discharge from December through March as is delivered during the month of June. This winter flow is, in part, supported by runoff and groundwater inputs at lower latitudes. The Mackenzie watershed extends far below the Arctic Circle (as far south as 53° N; Macdonald and Yu, 2006) through regions with little or no permafrost. Outflows from large lakes within the Mackenzie watershed also contribute to winter river discharge. In both cases, water remains unfrozen under a ~2m thick layer of river ice as it moves through the high Arctic on its way to the ocean. The input of wintertime freshwater is visible as a decrease in modeled sea surface salinity (SSS; not shown here) near the delta.

Salinity outside the Mackenzie delta decreases further in May and June during the freshet, reaching < 10 in the model (Figure 1.7). River water temperature in June averages 13.8 ±

2.4 °C (Figure 1.4), resulting in a monthly mean heat flux of 0.92 TW on the Beaufort shelf around the delta. Subsequently, this warm discharge initiates the melt-back of ice around the delta, allowing both warm river discharge and solar radiation to heat the upper water column. By mid-August, ocean water influenced by the river plume is >5 °C in the model (Figure 1.7a, b) and a region of open water exists close to the river mouth. The river plume extends ~150 km from the coast and is advected under the offshore sea ice to the east by the winds (Figure 1.7c). River waters then begin to melt ice and lose heat. Advected river water causes a reduction of salinity that extends under the ice edge, while the sea surface temperature (SST) signal drops to ambient ocean temperatures in front of the ice edge (Figure 1.7d).

There is considerable interannual variability in the behavior of the warm waters associated with the river plume. For example, sea ice retreat begins earlier in 1997 than in 1996 (Figure 1.7e, g), and thus the warm waters at the end of the spring freshet (i.e. June) are subjected to direct wind stress, and are advected over a much larger region (Figure 1.7f). The plume is less well defined in 1997 than in 1996; all grid cells within 100 km of the coast reach 6–8 °C (Figure 1.7f). The shelf becomes ice-free by the end of July, compared to 1996 where the eastern shelf remained partially ice covered.

We also see interannual variability in cross-shelf properties along a transect heading approximately due north from the Mackenzie delta. In 1996, we find that the shelf begins to warm at the beginning of July (Figure 1.8a shows the end of June when surface waters are still near freezing), and in August warm water extends just past the shelf break at 50 km offshore in a stratified surface layer (Figure 1.8b). All grid points on the shelf are <0 °C before the end of September. In 1997, the near-shore waters begin to warm at the end of June (Figure 1.8e), and by August/September the river plume reaches 150 km off shore (Figure 1.8f), with warm river water

mixing with deeper water on the shelf break. As the surface cools in the winter, and river water temperatures decrease, a parcel of relatively warm (1 °C) water remains on the shelf break, where it is mixed into a warmer (by 0.2–0.3 °C compared to deeper waters, and ~1 °C warmer than the offshore surface waters) layer at 40–60 m. There is little difference between 1996 and 1997 in the vertical salinity distribution, with fresher waters constrained to within ~100 km of the coast for both years (Figure 1.8c, d, g, h). The river discharge is mixed over both on-shelf model layers, and remains stratified as it crosses the shelf break.

## *1.4. Discussion*

### *1.4.1. Data Set*

The ARDAT data set is comprised of climatological estimates of river discharge rates and temperatures for 30 Arctic rivers. A monthly-mean climatology was constructed from publicly available data sets, with over 60-year long data records for most Eurasian rivers, and 35-year long records for most North American rivers. While discharge data are available for many Canadian rivers in the Hudson Bay region, these data were not used to develop ARDAT because rivers in this region fall outside of the pan-Arctic watershed boundary that was selected for data set development. Inclusion of these rivers would add about 10% more water to the total budget (Déry et al., 2005), but mean ocean circulation in the Hudson Bay region tends to advect river inputs east and southward, away from the Arctic Basin (Prinsenberg, 1986).

Total annual discharge from rivers currently included in ARDAT is 2817 $km^3$ $yr^{-1}$, comparable to the 2500 $km^3$ $yr^{-1}$ from gauged rivers used in Serreze et al. (2006). There are two different patterns in the discharge seasonal cycles; the Ob', Mackenzie and Yukon Rivers discharge more freshwater in May than the Yenisey, Kolyma and Lena (Figure 1.3). This

difference is likely due to regionally distinct air temperature climatologies, as reflected by differences in permafrost coverage among basins. . The drainage basins for rivers with an earlier spring freshet have <25% continuous permafrost (>90% of the land surface underlain by permafrost) compared to rivers such as the Lena or Kolyma, for which continuous permafrost makes up 79% and 100% of the drainage basin respectively (Holmes et al., 2013).

ARDAT also includes long-term monthly mean river water temperatures based on observations from the six largest Arctic rivers, and one sub-Arctic river. Although additional temperature data exist for some other Eurasian rivers (cf. Lammers et al., 2007), we only use temperatures from the major rivers here in order to apply a temperature seasonal cycle to all rivers. Comparisons of temperature data from the "Big 6" with temperature data from a variety of smaller rivers around the Arctic (data not shown) indicate that seasonal river water temperature patterns are similar across wide geographic regions, but that the North American rivers begin to warm sooner than the Eurasian rivers. As discussed above with respect to different seasonal patterns in river discharge rates, the differences in seasonal water temperature patterns are associated with region-specific air temperature climatologies (inferred from permafrost distributions).

The long-term mean monthly heat flux integrated over all rivers in ARDAT is $3.2 \pm 0.6$ TW. When we integrate only the Eurasian rivers, the mean monthly heat flux is $2.2 \pm 0.9$ TW. This is comparable to 2.0 TW from gauged rivers reported by Lammers et al. (2007). Alaskan rivers contribute $1.0 \pm 0.1$ TW of heat to the Arctic shelves. Including ungauged rivers, Lammers et al. (2007) found total Eurasian heat fluxes to be 2.6 TW. This is higher than values reported here, although ARDAT does not at present include heat fluxes derived from ungauged discharge and runoff. The average annual heat flux for all rivers in ARDAT is $38.4 \pm 6.7$ TW, which is

1.9–2.6 times larger than the estimated 2007 Bering Strait heat flux (15–20 TW; Woodgate et al., 2012).

### *1.4.2. Local responses*

The heating and freshening in regions where there is river discharge raises the sea surface height (Figure 1.10). This sea surface height anomaly leads to an increase in along-shore geostrophic velocities in the model run which incorporates ARDAT relative to the run with the coarser river discharge climatology. When coupled with the increase in wind stress resulting from a greater proportion of open water due to increased ice melt, the nearshore velocities are amplified, leading to a quasi-continuous faster moving, near-shore boundary currents similar to the riverine coastal domain (RCD), described in Carmack and Wassmann (2006) and Carmack et al. (2014). The increased nearshore velocities in the RCD could have effects on future modelling of larval and/or zooplankton transport and potentially ice drift estimates, which are not captured by simulations which use $1° \times 1°$ discharge data sets. Higher resolution model runs will need to be carried out (using higher resolution river discharge forcing) to further analyze the existence of the RCD as the radius of deformation in this region is typically 5-15 km, and is therefore not resolved in the current model.

In our regional example, the Mackenzie River delta, discharge initially remains close to the coast as a buoyant fresh plume, which has two characteristic modes of behavior. During the spring freshet, before ice has begun to retreat, the only control on plume direction is the Coriolis force; this deflects the plume to the right and causes the eastern shelf to begin melting (Kasper and Weingartner, 2012). Once ice has melted around the source of freshwater, the winds become an additional control. Depending on both wind magnitude and direction, the plume has two

characteristic modes. The first mode occurs during north-westerly winds on the Mackenzie shelf, or during wind magnitudes that are not sufficient to overcome the buoyant geostrophic current or be rapidly advected off shore. In this case, the plume continues to behave before the ice melts. The second mode occurs during strong easterly winds on the Mackenzie shelf, and the plume is advected away from shore and rapidly dispersed (Macdonald and Yu, 2006). This difference can be seen over 1996 and 1997, where differences in plume behavior caused the shelf region to become ice-free (<15%) on the order of one month sooner — mid July compared to mid-late August — compared to when the plume is advected in to the Arctic Basin (Figure 1.7).

Despite the increase in FWC and HC on the shelves, the model still underestimates SST and SSS around the Arctic rivers. For example, when we compare the model output to AVHRR SST imagery for 26 July 2006 (Figure 1.9), we find that both the modeled and observed Mackenzie plumes extend to the northwest, yet the model shows the plume waters to only be ~2 °C (Figure 1.9a), compared to the observed 9 °C in plume waters, and >13 °C near to the shore (Figure 1.9b). We also compared model output to more recent observations documented in Nghiem et al. (2014). Between 14 June 2012 and 5 July 2012, we found that the SST increased by 6.1 °C adjacent to the delta, comparable to the observed 6.5 °C. However, the maximum temperature in the model river plume was only 5.8 °C in July, compared to satellite observed 13 °C. At mid-range (300 – 350 km), the model plume was ~3 °C compared to 8 – 10 °C in observations, and at 450 km, modeled SST was only -1.4 °C, whereas observations show that the plume warms the surface waters to 2 °C. These discrepancies suggest that there are several factors that can cause the model to not reproduce observed SST.

The first factor is that the river discharge is input to the model's surface level, which is 10 m thick, as opposed to <5 m in the observations (Wood et al., 2013). Thus, the volume heated by

river discharge is much larger in the model than in the observations, resulting in lower simulated vs. observed SST. The second process is that the Arctic rivers are heavily sediment laden (Figure 1.9c), and this fine sediment is often transported far offshore. The turbid plume has a much lower albedo than the surrounding water, and thus absorbs more solar radiation. The plume is thus able to regain heat lost by advection and mixing. Plume turbidity is not represented in our model, and thus we are unable to distinguish heat fluxes due to advection, insolation and the turbid plumes in the calculations presented in this study.

### *1.5. Conclusions*

A new monthly-mean climatology of river discharge and temperature was compiled with a 1/6° resolution (ARDAT). The ARDAT climatology will be valuable as forcing in regional models, as most Arctic Ocean models do not currently include river water temperature and associated heat fluxes (e.g., Maslowski et al., 2004). An example model study that did include a river water temperature set a maximum temperature of only 3.8 °C in August for the Ob' (Harms et al., 2000). Using ARDAT, we find that the maximum temperature on the Ob' occurs during July, and is 15.8 °C.

ARDAT contains 30 rivers in the pan-Arctic watershed and supplies 2,817 $km^3$ of freshwater to the Arctic shelves per year. The seasonal cycle of river water temperature in ARDAT leads to a long-term mean monthly heat flux of 3.2 TW from all rivers in ARDAT, of which Eurasian rivers contribute 68.8%. After incorporating this new data set in to a high-resolution regional ocean-sea ice coupled model, we find an increase in the FWC of 3,700 $km^3$ and mean summer heat fluxes increase by 8 TW. This increase in heat flux is sufficient to melt an additional $0.2 \times 10^6$ $km^2$ of 1-m thick ice on the Arctic shelves over a 3 month summer period

(June–August), equivalent to 44.7% of the area of the Beaufort Sea shelf and basin ($0.45 \times 10^6$ $km^2$; Jakobsson, 2002). Basin-wide, the annual heat flux from all Arctic rivers combined is enough to melt nearly $4 \times 10^6$ $km^2$ of 1 m thick sea ice, 50% of the mean annual sea ice extent range of $8 \times 10^6$ $km^2$ (Kwok and Untersteiner, 2011). The reduced summer sea ice extent (~10% less in the model forced with ARDAT) leads to a greater proportion of open water subject to solar heating and wind stresses. As such, a more accurate representation of the RCD is formed in the ARDAT forced model, which will allow improved estimates of transports of sea ice, plankton, and nutrients.

Anthropogenic changes will likely cause increases in precipitation (Houghton et al., 2001) and air temperatures (Rouse et al., 1997), which will subsequently lead to increased and warmer river discharge. Although changes in Arctic river outflow from these anthropogenic changes are well documented (e.g., Rouse et al., 1997; Peterson et al., 2006; Rabe et al., 2011), previous basin-wide studies focused on changes in river discharge (e.g., Peterson et al., 2002; Wu et al., 2005; McClelland et al., 2006) and did not consider changes in the temperature of river water that is delivered to the ocean. While the total heat added by rivers is minor as part of a long-term, Arctic Ocean-wide heat budget (~1% of 200 TW), on the Arctic shelf region and on seasonal time scales, riverine heat fluxes are much more substantial in their influence. We have shown here that the heat carried in the Arctic rivers plays a large role in ice formation and melt, and can influence estimation of coastal transport pathways, and as such, river water temperatures should not be neglected from future (climate or regional) modelling efforts.

### *1.6. References*


Aagaard, K., Coachman, L.K., Carmack, E.C., 1981. On The Halocline of the Arctic Ocean. Deep Sea Research 28A, 529-545.

Aagaard, K., Carmack, E.C., 1989. The Role of Sea Ice and Other Fresh-Water in the Arctic Circulation. Journal of Geophysical Research 94, 14,485-414,498.

Aagaard, K., Carmack, E.C., 1994. The Arctic Ocean and Climate: A Perspective. Geophysical Monograph Series 85, 5-20.

Bareiss, J., Eicken, H., Helbig, A., Martin, T., 1999. Impact Of River Discharge And Regional Climatology On The Decay Of Sea Ice In The Laptev Sea During Spring And Early Summer. Arctic and Alpine Research 31, 214-229.

Campin, J.-M., Marshall, J., Ferreira, D., 2008. Sea Ice–Ocean Coupling Using a Rescaled Vertical Coordinate Z*. Ocean Modelling 24, 1-14.

Carmack, E., Wassmann, P., 2006. Food Webs and Physical–Biological Coupling On Pan-Arctic Shelves: Unifying Concepts and Comprehensive Perspectives. Progress in Oceanography 71, 446-477.

Carmack, E., Winsor, P., Williams, W.J., 2014. The Contiguous Riverine Coastal Domain. Progress in Oceanography submitted manuscript.

Carmack, E.C., 2007. The Alpha/Beta Ocean Distinction: A Perspective on Freshwater Fluxes, Convection, Nutrients and Productivity in High-Latitude Seas. Deep Sea Research Part II: Topical Studies in Oceanography 54, 2578-2598.

Condron, A., Winsor, P., Hill, C., Menemenlis, D., 2009. Simulated Response Of The Arctic Freshwater Budget To Extreme NAO Wind Forcing. Journal of Climate 22, 2422-2437.

Dai, A., Trenberth, K.E., 2002. Estimates of Freshwater Discharge from Continents: Latitudinal and Seasonal Variations. Journal of Hydrometeorology, 3, 660-687.

Dean, K., Stringer, W., Ahlnas, K., Searcy, C., Weingartner, T., 1994. The Influence of River Discharge on the Thawing Of Sea Ice, Mackenzie River Delta: Albedo and Temperature Analyses. Polar Research 13, 83-94.

Déry, S.J., Stieglitz, M., McKenna, E.C., Wood, E.F., 2005. Characteristics and Trends of River Discharge into Hudson, James, and Ungava Bays, 1964–2000. Journal of Climate, 18, 2540-2557.

Harms, I., Karcher, M., Dethleff, D., 2000. Modelling Siberian River Runoff—Implications For Contaminant Transport In The Arctic Ocean. Journal of Marine Systems 27, 95-115.

Holmes, R.M., Coe, M.T., Fiske, G.J., Gurtovaya, T., McClelland, J.W., Shiklomanov, A.I., Spencer, R.G., Tank, S.E., Zhulidov, A.V., 2013. Climate Change Impacts On The Hydrology And Biogeochemistry Of Arctic Rivers, in: Goldman, C.R., Kumagai, M., Robarts, R.D. (Eds.), Climatic Change And Global Warming Of Inland Waters: Impacts And Mitigation For Ecosystems And Societies. John Wiley & Sons, New York, pp. 3-26.

Houghton, J.T., Ding, Y., Griggs, D.J., Noguer, M., van der Linden, P.J., Dai, X., 2001. Projection Of Future Climate Change, in: Houghton, J.T., Ding, Y., Griggs, D.J., Noguer, M., van der Linden, P.J., Dai, X., Maskell, K., Johnson, C. (Eds.), Climate Change 2001: The Scientific Basis. Cambridge University Press, New York, pp. 525-582.

Jahn, A., Aksenov, Y., Cuevas, B., Steur, L., Häkkinen, S., Hansen, E., Herbaut, C., Houssais, M.N., Karcher, M., Kauker, F., 2012. Arctic Ocean Freshwater: How Robust Are Model Simulations? Journal of Geophysical Research 117, C00D16.

Jakobsson, M., 2002. Hypsometry and Volume of the Arctic Ocean and Its Constituent Seas. Geochemistry, Geophysics, Geosystems 3, 1-18.

Kasper, J.L., Weingartner, T.J., 2012. Modeling Winter Circulation under Landfast Ice: The Interaction of Winds with Landfast Ice. Journal of Geophysical Research 117, C04006.

Kwok, R., Untersteiner, N., 2011. The Thinning Of Arctic Sea Ice. Physics Today, 64, 36-41.

Lammers, R.B., Shiklomanov, A.I., Vörösmarty, C.J., Fekete, B.M., Peterson, B.J., 2001. Assessment Of Contemporary Arctic River Runoff Based On Observational Discharge Records. Journal of Geophysical Research 106, 3321-3334.

Lammers, R.B., Pundsack, J.W., Shiklomanov, A.I., 2007. Variability in River Temperature, Discharge, and Energy Flux from the Russian Pan-Arctic Landmass. Journal of Geophysical Research 112, G04S59.

Losch, M., Menemenlis, D., Campin, J.-M., Heimbach, P., Hill, C., 2010. On The Formulation of Sea-Ice Models. Part 1: Effects of Different Solver Implementations and Parameterizations. Ocean Modelling 33, 129-144.

Macdonald, R.W., Yu, Y., 2006. The Mackenzie Estuary of the Arctic Ocean, in: Estuaries, P Wangersky (ed), Springer, New York, pp. 91-120.

Manizza, M., Follows, M.J., Dutkiewicz, S., McClelland, J.W., Menemenlis, D., Hill, C., Townsend-Small, A., Peterson, B.J., 2009. Modeling Transport And Fate Of Riverine Dissolved Organic Carbon In The Arctic Ocean. Global Biogeochemical Cycles 23, GB4006.

Manizza, M., Follows, M.J., Dutkiewicz, S., Menemenlis, D., McClelland, J.W., Hill, C., Peterson, B.J., Key, R.M., 2011. A Model of the Arctic Ocean Carbon Cycle. Journal of Geophysical Research 116, C12020.

Marshall, J., Adcroft, A., Hill, C., Perelman, L., Heisey, C., 1997. A Finite-Volume, Incompressible Navier Stokes Model For Studies of the Ocean on Parallel Computers. Journal of Geophysical Research 102, 5753-5766.

Maslowski, W., Marble, D., Walczowski, W., Schauer, U., Clement, J.L., Semtner, A.J., 2004. On Climatological Mass, Heat, And Salt Transports through the Barents Sea and Fram Strait from a Pan-Arctic Coupled Ice-Ocean Model Simulation. Journal of Geophysical Research 109, C03032.

McClelland, J.W., Dery, S.J., Peterson, B.J., Holmes, R.M., Wood, E.F., 2006. A Pan-Arctic Evaluation of Changes in River Discharge during the Latter Half of the 20th Century. Geophysical Research Letters 33, L06715.

McClelland, J.W., Holmes, R.M., Peterson, B.J., Amon, R., Brabets, T., Cooper, L., Gibson, J., Gordeev, V.V., Guay, C., Milburn, D., 2008. Development of a Pan-Arctic Database for River Chemistry. Eos, Transactions American Geophysical Union 89, 217-218.

McClelland, J.W., Holmes, R., Dunton, K., Macdonald, R., 2012. The Arctic Ocean Estuary. Estuaries and Coasts 35, 353-368.

Menemenlis, D., Hill, C., Adcroft, A., Campin, J.M., Cheng, B., Ciotti, B., Fukumori, I., Koehl, A., Heimbach, P., Henze, C., Lee, T., Stammer, D., Taft, J., Zhang, J., 2005a. NASA Supercomputer Improves Prospects for Ocean Climate Research. EOS Transactions AGU 86, 89.

Menemenlis, D., Fukumori, I., Lee, T., 2005b. Using Green's Functions to Calibrate an Ocean General Circulation Model. Monthly Weather Review 133, 1224-1240.

Menemenlis, D., Campin, J.-M., Heimbach, P., Hill, C., Lee, T., Nguyen, A., Schodlok, M., Zhang, H., 2008. ECCO2: High Resolution Global Ocean and Sea Ice Data Synthesis. Mercator Ocean Quarterly Newsletter 31, 13-21.

Nghiem, S., Hall, D., Rigor, I., Li, P., Neumann, G., 2014. Effects of Mackenzie River Discharge and Bathymetry on Sea Ice in the Beaufort Sea. Geophysical Research Letters 41, 873-879.

Nguyen, A.T., Menemenlis, D., Kwok, R., 2011. Arctic Ice-Ocean Simulation with Optimized Model Parameters: Approach and Assessment. Journal of Geophysical Research: Oceans (1978–2012), 116 (C4), C04025.

Onogi, K., Tsutsui, J., Koide, H., Sakamoto, M., Kobayashi, S., Hatsushika, H., Matsumoto, T., Yamazaki, N., Kamahori, H., Takahashi, K., 2007. The JRA-25 Reanalysis. Journal of the Meteorological Society of Japan 85, 369-432.

Peterson, B.J., Holmes, R.M., McClelland, J.W., Vorosmarty, C.J., Lammers, R.B., Shiklomanov, A.I., Shiklomanov, I.A., Rahmstorf, S., 2002. Increasing River Discharge to the Arctic Ocean. Science 298, 2171-2173.

Peterson, B.J., McClelland, J., Curry, R., Holmes, R.M., Walsh, J.E., Aagaard, K., 2006. Trajectory Shifts in the Arctic and Subarctic Freshwater Cycle. Science 313, 1061-1066.

Prinsenberg, S., 1986. The Circulation Pattern and Current Structure Of Hudson Bay, in: Canadian Inland Seas, Martini, I.P. (ed.), Elsevier, Amsterdam, pp. 187-204.

Rabe, B., Karcher, M., Schauer, U., Toole, J.M., Krishfield, R.A., Pisarev, S., Kauker, F., Gerdes, R., Kikuchi, T., 2011. An Assessment of Arctic Ocean Freshwater Content Changes From the 1990s to the 2006–2008 Period. Deep Sea Research Part I: Oceanographic Research Papers 58, 173-185.

Rouse, W.R., Douglas, M.S., Hecky, R.E., Hershey, A.E., Kling, G.W., Lesack, L., Marsh, P., McDonald, M., Nicholson, B.J., Roulet, N.T., 1997. Effects of Climate Change on the Freshwaters of Arctic and Subarctic North America. Hydrological Processes 11, 873-902.

Searcy, C., Dean, K., Stringer, W., 1996. A River-Coastal Sea Ice Interaction Model: Mackenzie River Delta. Journal of Geophysical Research 101, 8885-8894.

Serreze, M.C., Barrett, A.P., Slater, A.G., Woodgate, R.A., Aagaard, K., Lammers, R.B., Steele, M., Moritz, R., Meredith, M., Lee, C.M., 2006. The Large-Scale Freshwater Cycle of the Arctic. Journal of Geophysical Research 111, C11010.

Stigebrandt, A., 1984. The North Pacific: A Global-Scale Estuary. Journal of Physical Oceanography 14, 464-470.

Tully, J., Barber, F., 1960. An Estuarine Analogy in the Sub-Arctic Pacific Ocean. Journal of the Fisheries Board of Canada 17, 91-112.

Wood, K.R., Overland, J.E., Salo, S.A., Bond, N.A., Williams, W.J., Dong, X., 2013. Is there a "New Normal" climate in the Beaufort Sea? Polar Research, 32, 19552-19560.

Woodgate, R.A., Aagaard, K., Weingartner, T.J., 2005. Monthly Temperature, Salinity, and Transport Variability of the Bering Strait Through Flow. Geophysical Research Letters 32, L04601.

Woodgate, R.A., Weingartner, T., Lindsay, R., 2012. Observed Increases In Bering Strait Oceanic Fluxes From The Pacific To The Arctic From 2001 To 2011 And Their Impacts On The Arctic Ocean Water Column. Geophysical Research Letters 39, L24603.

Wu, P., Wood, R., Stott, P., 2005. Human Influence on Increasing Arctic River Discharges. Geophysical Research Letters 32, L02703.

Zib, B.J., Dong, X., Xi, B., Kennedy, A., 2012. Evaluation and Intercomparison of Cloud Fraction and Radiative Fluxes in Recent Reanalyses over the Arctic Using BSRN Surface Observations. Journal of Climate 25, 2291-2305.

## *1.7. Figures*

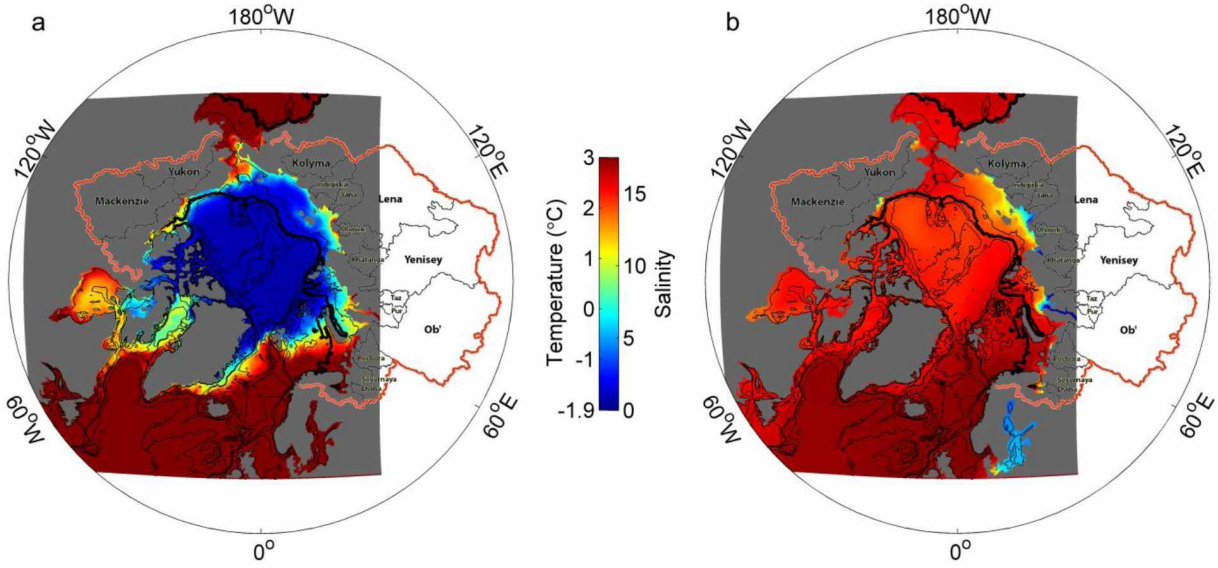


Figure 1.1. Map of the "Big 6" Arctic drainage basins (in green), along with the next 8 largest basins (in yellow) in the pan-Arctic watershed (red line; adapted from Holmes et al., 2013). Overlaid is modeled (a) August sea surface temperature (SST) and (b) June sea surface salinity (SSS) from the MITgcm/ECCO2 model. The model land mask is in grey, model bathymetry (200, 500, 1000, 2500 m) is shown as thin black contours; the thick black contour defines the Arctic shelf region referred to in this paper.

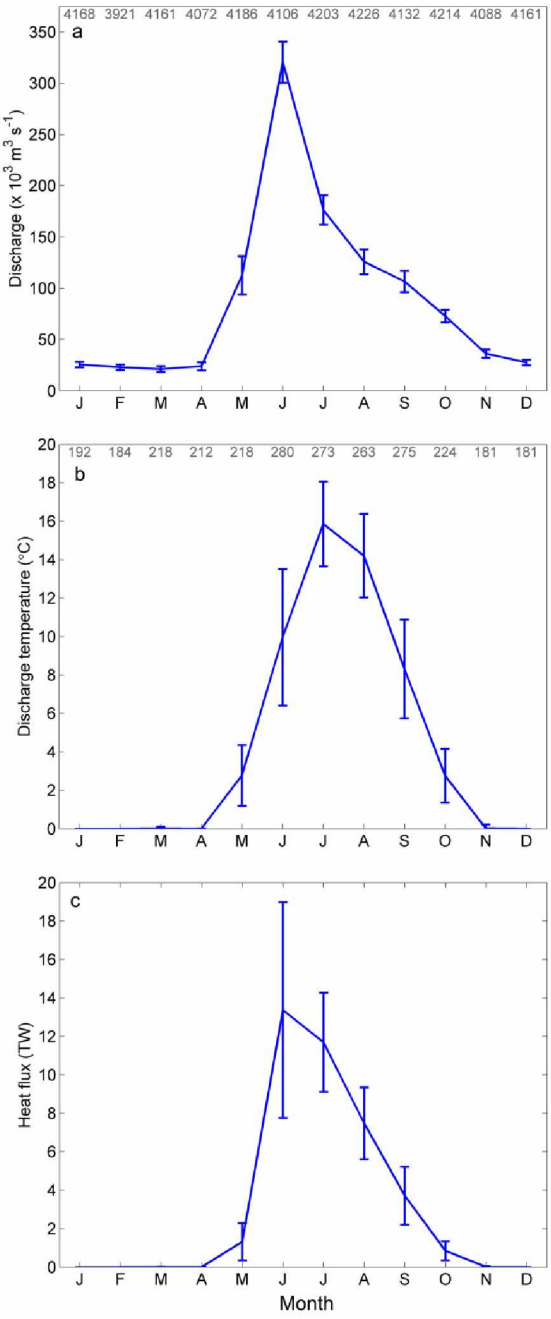


Figure 1.2. Climatologies for (a) integrated discharge (± 1 standard deviation) for all rivers in ARDAT, (b) mean river temperature (± 1 standard deviation) for the "Big 6" Arctic rivers and one sub-Arctic river (Kuskokwim), (c) calculated heat flux (± 1 standard deviation) using integrated discharge from all rivers in ARDAT and mean river water temperatures. Numbers on top axes of (a) and (b) denote total number of monthly-mean observations for each month.

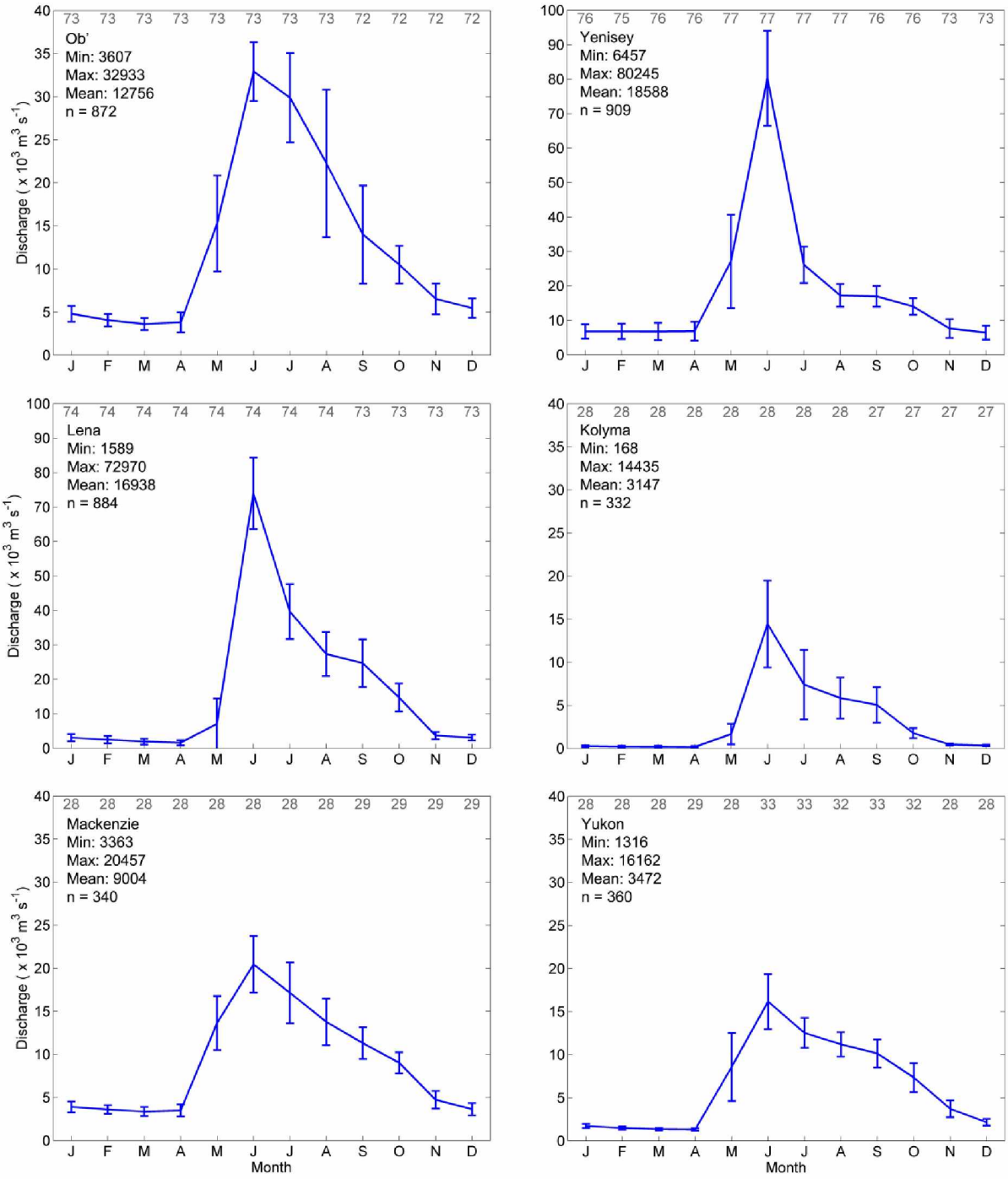


Figure 1.3. Long-term mean discharge for the "Big 6" Arctic rivers (± 1 standard deviation). Numbers along top axes show total number of discharge observations for each month. Legend shows minimum, maximum and annual mean discharge, and n denotes the total number of months with discharge observations.

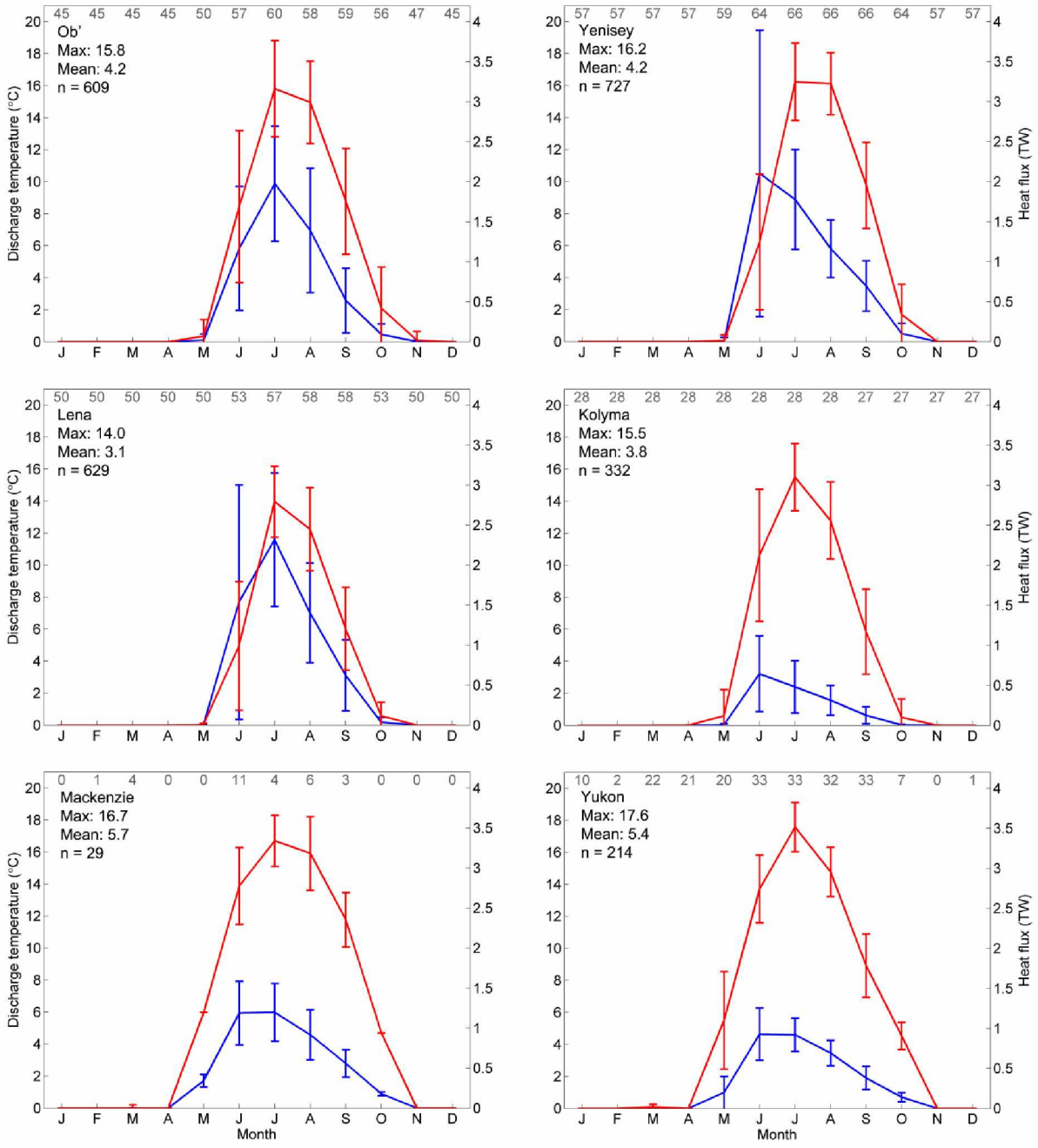


Figure 1.4. Long-term mean river water temperature (± 1 standard deviation; red) and calculated heat fluxes (± 1 standard deviation; blue) for the "Big 6" rivers. Numbers along top axes show total number of river water temperature observations for each month. Legend shows maximum and annual mean river water temperature, and n denotes the total number of months with river water temperature observations.

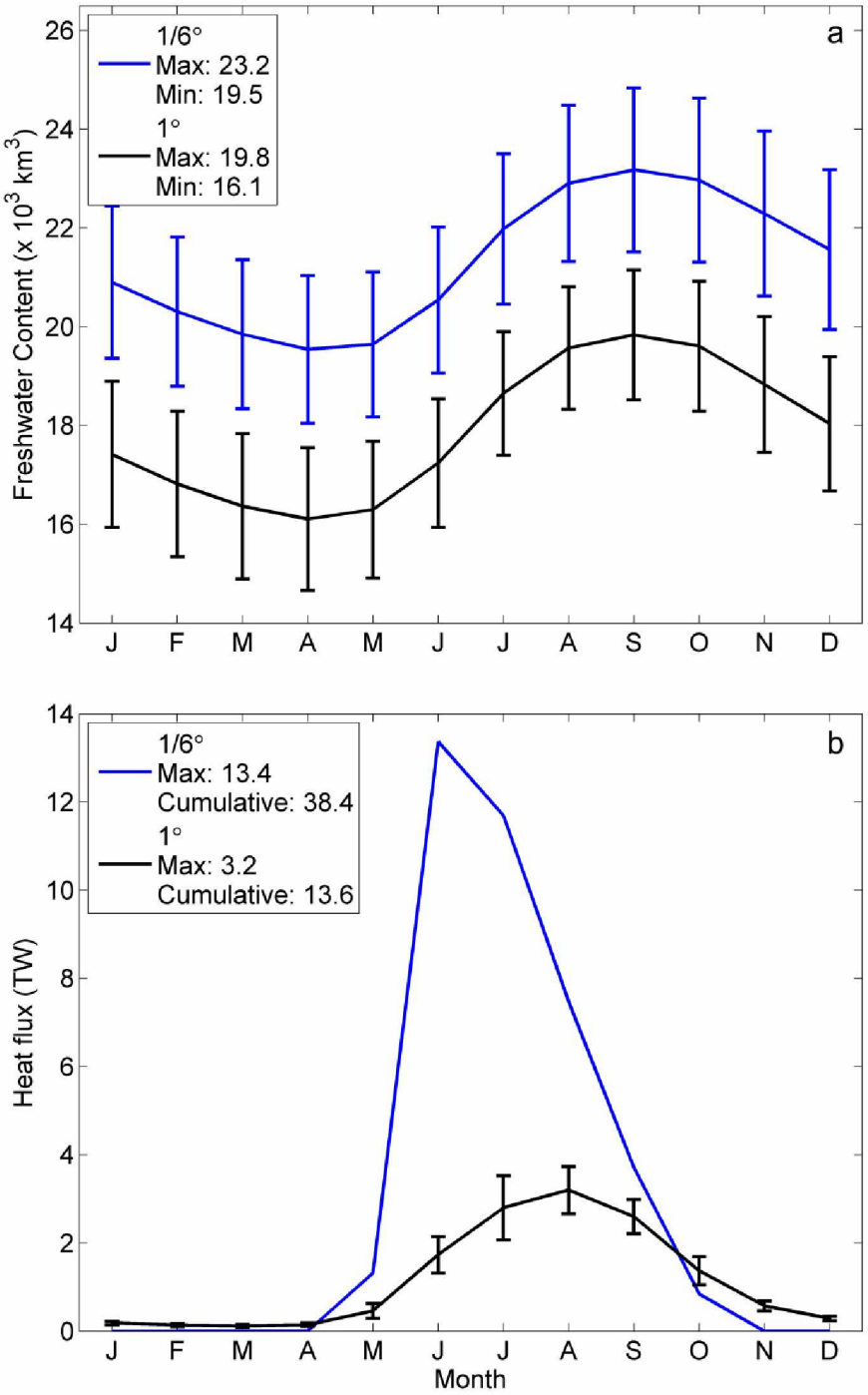


Figure 1.5. Mean modeled seasonal cycles of (a) integrated FWC (± 1 standard deviation) and (b) riverine heat flux (± 1 standard deviation) on the Arctic shelf region (<200 m; see Figure 1.1). Legend text in (a) shows maximum and minimum freshwater content in $km^3$, and in (b) shows annual maximum and cumulative heat flux in TW.

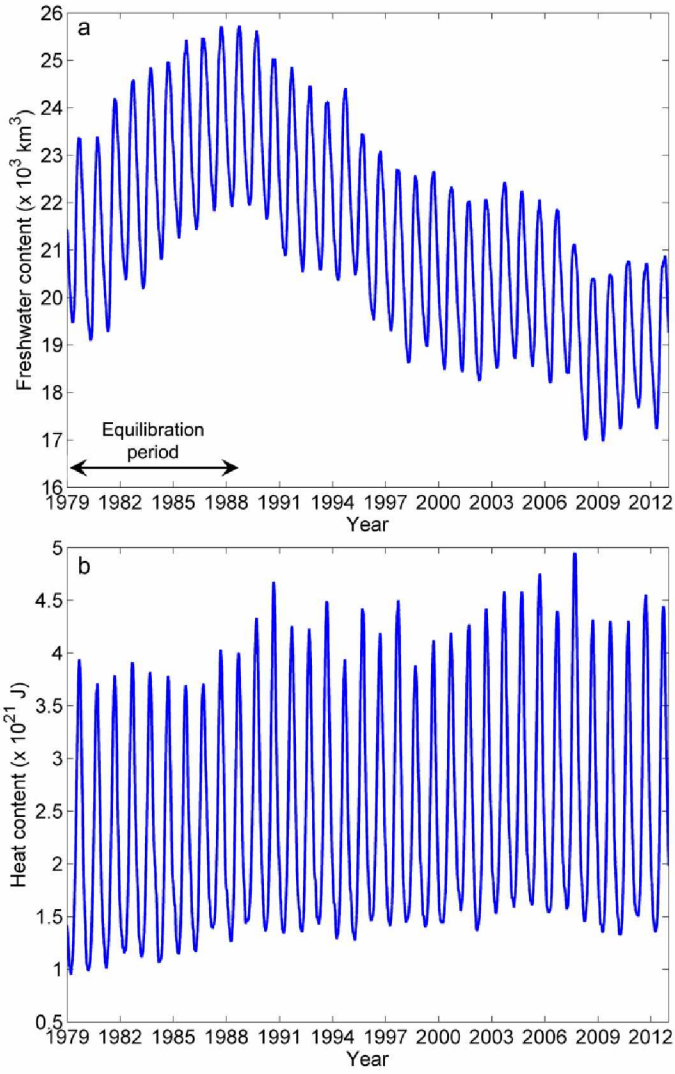


Figure 1.6. (a) integrated FWC ($\times 10^3$ km$^3$) over the Arctic shelf region (<200 m; see Figure 1.1), showing ~10 year period of equilibration to new forcing, (b) integrated HC ($\times 10^{21}$ J) over the Arctic shelf region.

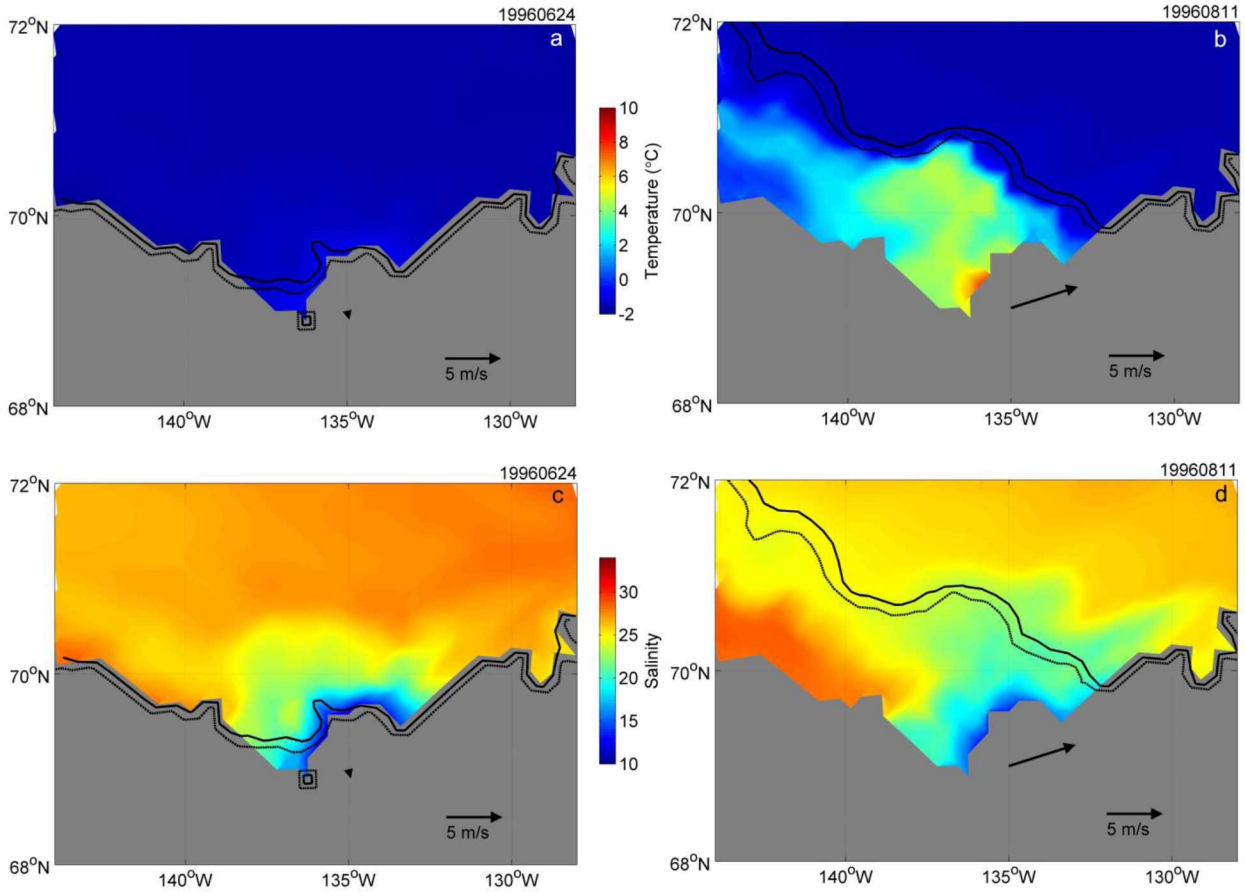


Figure 1.7. Modeled SST (top) and SSS (bottom) for the Mackenzie Delta and shelf region in (a-d) 1996 and (e-h) 1997. Model land mask is in grey, and contours show modeled sea ice concentrations (solid shows 50%, dashed shows 15%). Arrow shows JRA-25 wind velocity at 69° N, 135° W. Date is shown in yyyymmdd format above each panel.

Figure 1.7. cont.

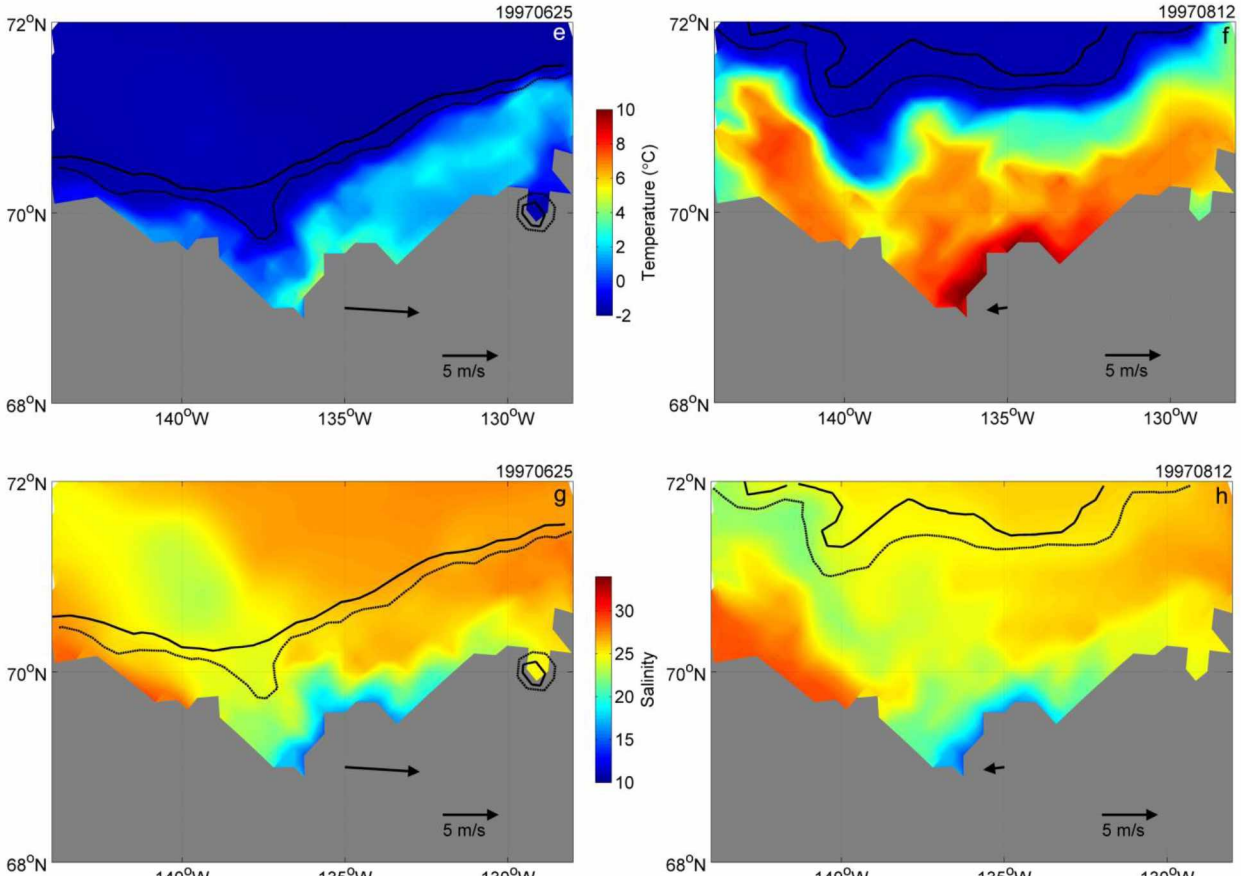
19970625
e
72°N
70°N
68°N
140°W
135°W
130°W
5 m/s
10
8
6
4
2
0
-2
Temperature (°C)
19970812
f
72°N
70°N
68°N
140°W
135°W
130°W
5 m/s
19970625
g
72°N
70°N
68°N
140°W
135°W
130°W
5 m/s
30
25
20
15
10
Salinity
19970812
h
72°N
70°N
68°N
140°W
135°W
130°W
5 m/s

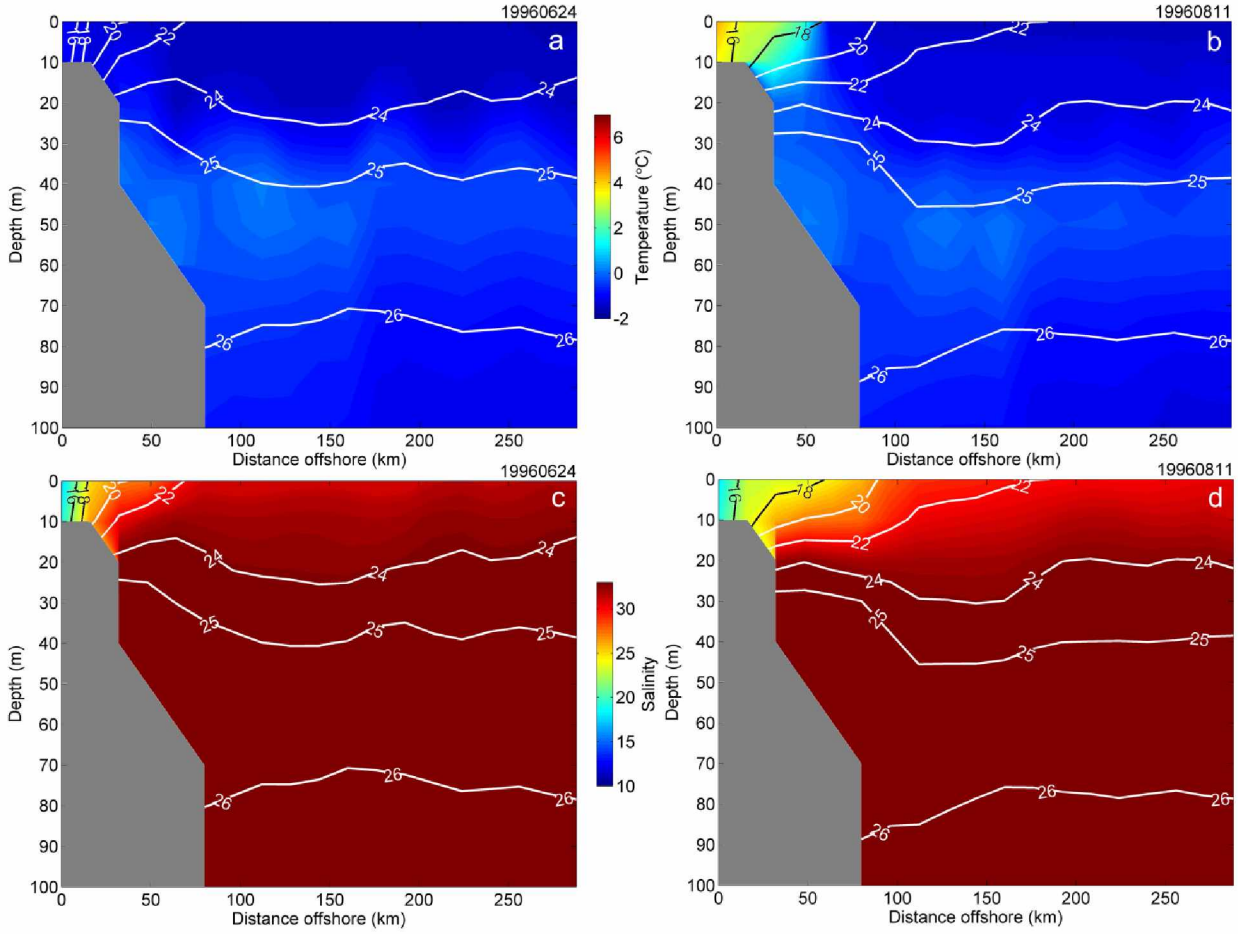


Figure 1.8. Modeled cross-shelf sections of temperature (top row) or salinity (bottom) from the Mackenzie delta in (a-d) 1996 and (e-h) 1997. Contours show density anomalies. Model land mask is in grey. Date is shown in yyyymmdd format above each panel.

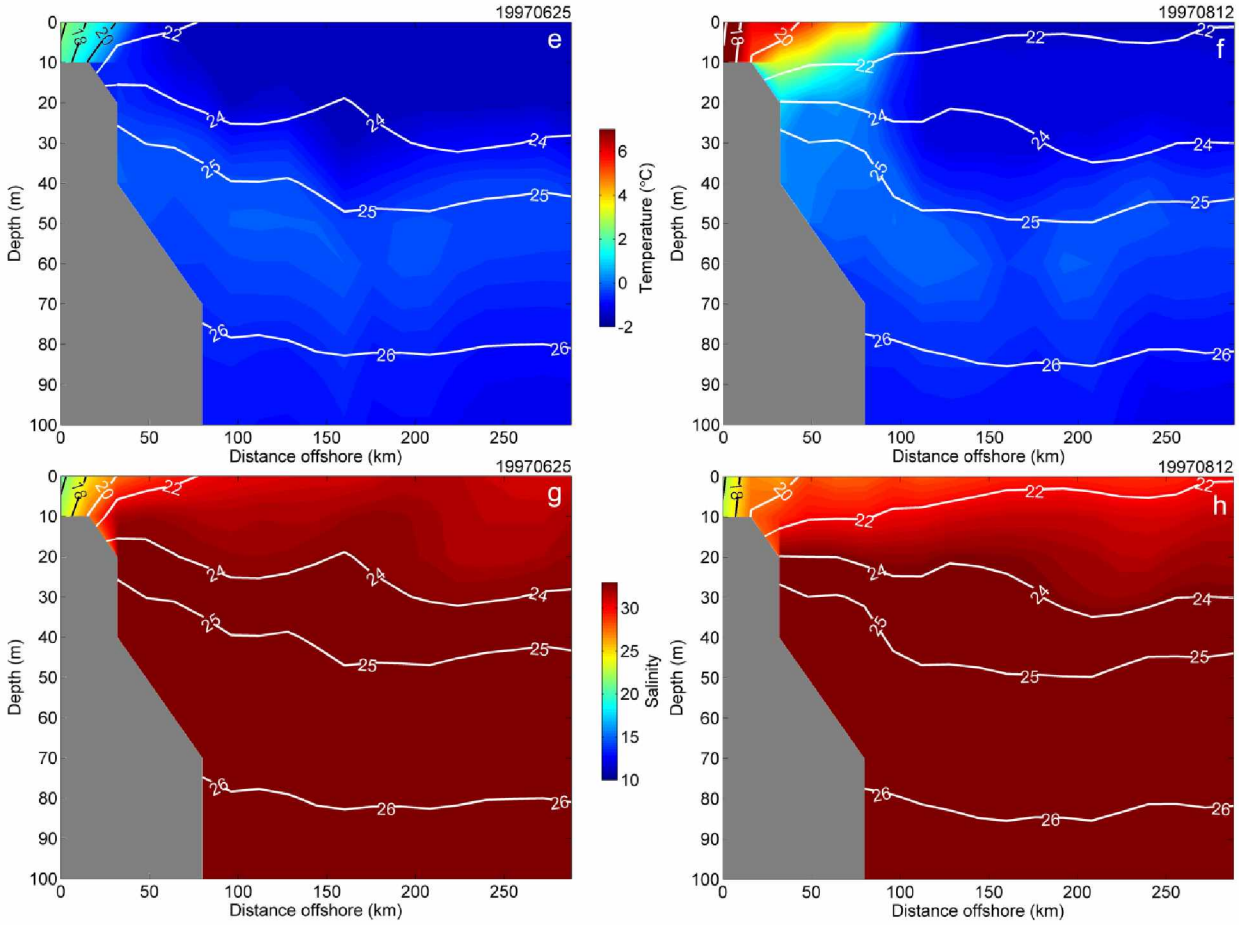


Figure 1.8. cont.

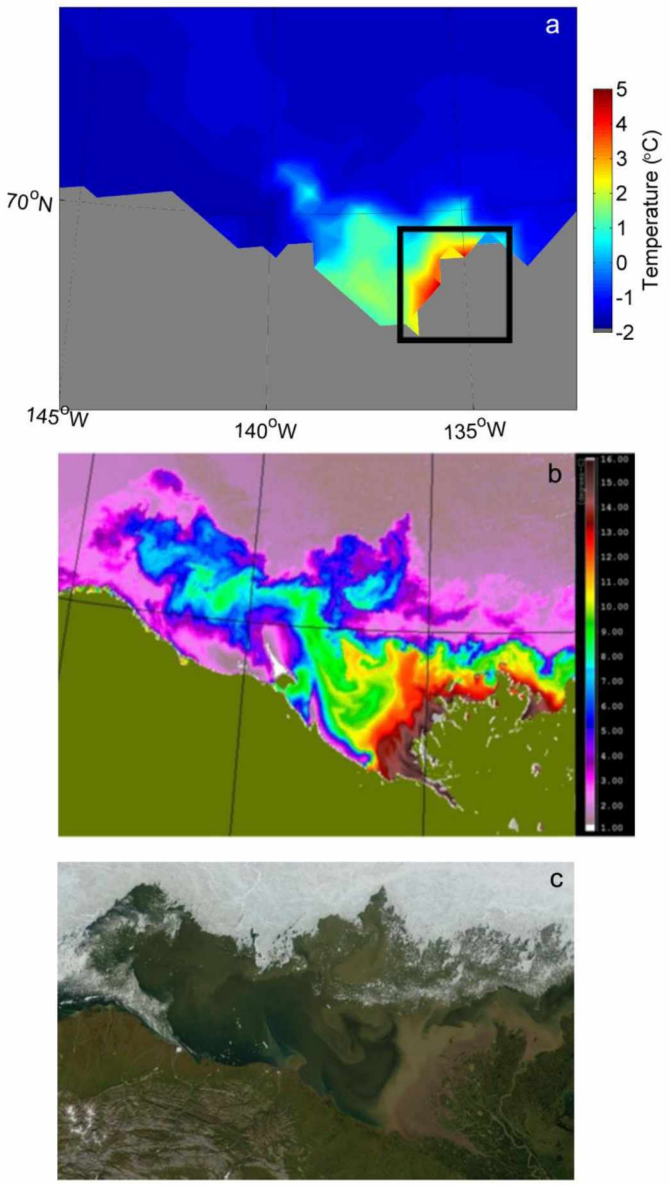


Figure 1.9. (a) Modeled SST (land mask in grey) and (b) SST from AVHRR imagery (land mask in green) from 26 July 2006. Note different color scales have been used to clearly show the modeled plume. The position of the Mackenzie delta in the model is marked with the black box. (c) MODIS-visible band satellite imagery illustrating the turbid waters of the Mackenzie plume.

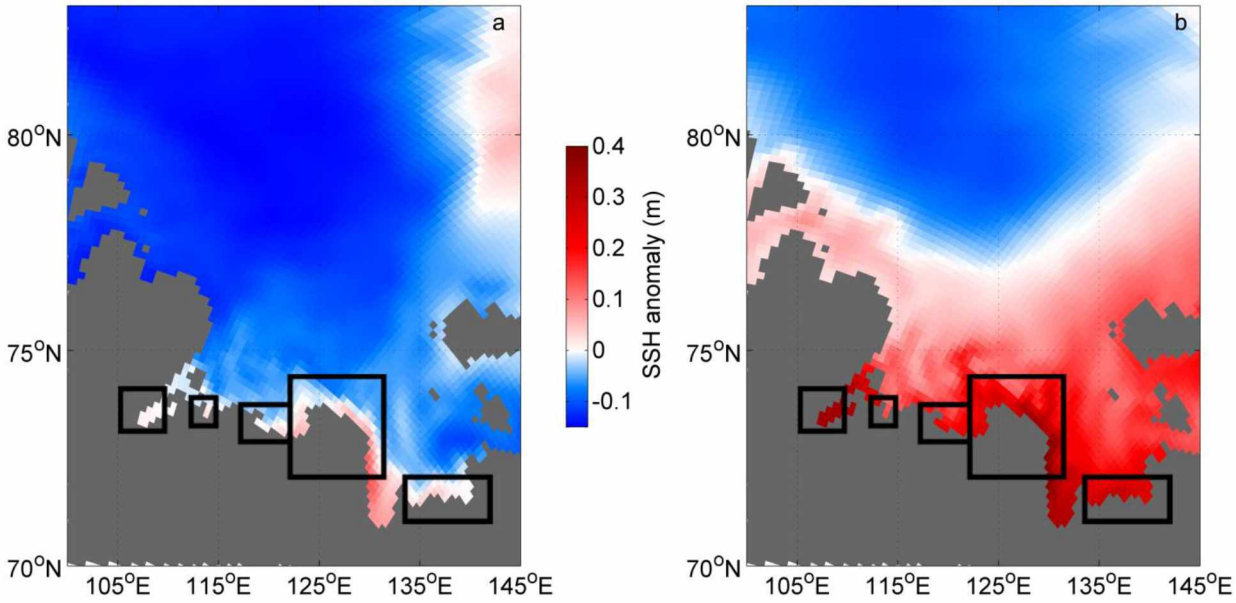


Figure 1.10. Sea surface height anomaly (m) around the Lena delta on 11 August 1996 (a) without and (b) with the "real" freshwater flux and non-linear free surface enabled. Model land mask is in grey. Areas of river discharge are marked with black boxes (W-E: Khatanga, Anabar, Olenek, Lena, Yana).

### *1.8. Tables*

Table 1.1. Summary of availability of observed river discharge and statistics. Superscript numbers denote data sources: 1 – ArcticRIMS, 2 – RArcticNET, 3 – USGS NWIS. The column marked "basin" shows which major river basin was used to assign temperatures to the smaller rivers.

| River Name | Discharge | | Basin |
|---|---|---|---|
| | Date range | Annual mean (± 1 st. dev., $km^3\ yr^{-1}$) | |
| Tana[1] | July 1911 – Nov 2000 | 5.30 ± 7.78 | Ob' |
| Tuloma[1,2] | July 1934 – Dec 1992 | 6.01 ± 3.88 | |
| Ponoy[1,2] | Jan 1935 – Jan 1977 | 5.13 ± 6.19 | |
| Onega[1,2] | Jan 1943 – Aug 2009 | 16.35 ± 17.02 | |
| Kovda[1] | Jan 1956 – Dec 1988 | 8.71 ± 3.13 | |
| Umba[1,2] | Aug 2000 – Aug 2009 | 2.67 ± 1.46 | |
| Belomorkanal[1,2] | Jan 1956 – Dec 1988 | 8.19 ± 2.64 | |
| Severnaya Dvina[1,2] | Jun 1886 – Sept 2009 | 104.59 ± 122.21 | |
| Mezen[1,2] | Sept 1920 – Aug 2009 | 20.28 ± 25.44 | |
| Pechora[1,2] | Oct 1916 – Dec 1998 | 146.73 ± 162.05 | |
| Ob'[1,2] | Jan 1936 – Aug 2009 | 409.08 ± 339.53 | |
| Nadym[1,2] | Jan 1955 – Aug 2009 | 15.45 ± 16.38 | Yenisey |
| Poluy[1,2] | May 1953 – Dec 1999 | 4.12 ± 4.76 | |
| Pur[1,2] | Sept 1969 – Aug 2009 | 23.86 ± 26.42 | |
| Taz[1,2] | Jan 1962 – Dec 1996 | 34.05 ± 39.78 | |
| Yenisey[1,2] | Jan 1936 – Aug 2009 | 592.06 ± 662.83 | |
| Khatanga[1,2] | July 1961 – Sept 1994 | 163.57 ± 164.29 | |
| Anabar[1,2] | Jan 1954 – Dec 1999 | 14.22 ± 29.77 | Lena |
| Olenek[1,2] | Jan 1964 – Dec 1999 | 36.98 ± 75.13 | |
| Lena[1,2] | Jan 1936 – Aug 2009 | 534.92 ± 682.89 | |
| Yana[1,2] | Jan 1972 – Aug 2009 | 36.11 ± 53.06 | |
| Yndikirka[1,2] | Oct 1936 – Dec 1998 | 50.46 ± 73.62 | |
| Alazeya[1,2] | May 1962 – Dec 1999 | 1.12 ± 1.56 | |
| Kolyma[1,2] | Jan 1978 – Aug 2009 | 101.52 ± 148.20 | Kolyma |
| Amguema[1,2] | Jan 1944 – Dec 1988 | 12.14 ± 16.61 | |
| Anadyr[1,2] | Jan 1958 – Dec 1988 | 31.31 ± 49.98 | |
| Kobuk[3] | Sept 1976 – Oct 2012 | 13.48 ± 15.65 | Yukon |
| Yukon[3] | Oct 1975 – Sept 2012 | 214.12 ± 168.58 | |
| Kuskokwim[3] | Jul 1951 – Sept 2012 | 37.74 ± 30.31 | Kuskokwim |
| Mackenzie[2] | Sept 1972 – Dec 2000 | 283.26 ± 194.43 | Mackenzie |

Table 1.2. Summary of observed river water temperature and computed heat fluxes. Smaller rivers were assigned river water temperatures from these 7 rivers (see Table 1.1). Temperature range (in square brackets) shows the range of annual maximum discharge temperatures.

| Basin | Discharge Temperature | | | |
|---|---|---|---|---|
| | Data source | Date range | Max Temp (°C) [range] | Max heat flux (TW, month) |
| Ob' | ART-Russia | May 1936 – Dec 1998 | 15.8 [14.7 – 22.7] | 1.97 (July) |
| | PARTNERS/ AGRO | Jul 2003 – Dec 2011 | | |
| Yenisey | ART-Russia | Jun 1936 – Oct 2001 | 16.2 [14.7 – 22.0] | 2.10 (June) |
| | PARTNERS/ AGRO | Jul 2003 – Dec 2011 | | |
| Lena | ART-Russia | June 1936 – Dec 1995 | 14.0 [10.6 – 19.9] | 2.32 (July) |
| | PARTNERS/ AGRO | Aug 2003 – Nov 2011 | | |
| Kolyma | ART-Russia | July 1929 – Oct 2001 | 15.5 [13.3 – 20.8] | 0.64 (June) |
| | PARTNERS/ AGRO | Aug 2003 – Nov 2011 | | |
| Yukon | USGS NWIS | Apr 1975 – Sept 2012 | 17.6 [10.8 – 20.6] | 0.92 (June) |
| Kuskokwim | USGS NWIS | Jun 1951 – Sept 2010 | 15.3 [12.0 – 21.0] | 0.12 (July) |
| Mackenzie | PARTNERS/ AGRO | Jun 2003 – Feb 2012 | 16.7 [14.6 – 19.6] | 1.20 (July) |

# Chapter 2. Modeled flow pathways in the Chukchi Sea[1]


***Abstract***

The Chukchi Sea is among the most productive of the Arctic shelf seas, and receives input of water, nutrients and organisms from both the Pacific Ocean (through the Bering Strait) and the East Siberian Sea (through Long Strait). With the entire Pacific-Arctic sector undergoing rapid changes, including transitioning to longer ice-free seasons, understanding the dynamics of this region is increasingly important. However, observations can be restricted due to weather, ice or other logistical difficulties. In order to provide a more complete understanding, regional models are often used, but boundary conditions such as volume transport through the straits are based on observations which contain omissions, incorrect estimates, or errors.

By using a high-resolution (~1/6°) model with a domain encompassing the entire Arctic Ocean and surrounding seas, we are able to improve resolution of current pathways in the Chukchi Sea compared to coarser resolution global models. Our model also resolves surface stratified layers and seasonally present coastal currents. We compared model output to available observations from a mooring array in Bering Strait, and found that the model strongly correlates to observations ($r > 0.6$, $p < 0.05$), and captures most of the variability in the Bering Strait. We then used the model output to augment observations in the Bering Strait. Modelled long-term mean Bering Strait transport is $1.03 \pm 0.29$ Sv (1 Sv = $10^6$ $m^3$ $s^{-1}$), with the Alaskan Coastal Current contributing 24%. Long-term heat and freshwater (including contributions from sea ice) transport estimates are increased by 64% and 32% respectively compared to observations.

We also estimate long-term mean transport in the key outflow pathways from the Chukchi Sea, which do not have regular or repeated observations (i.e. Herald Canyon, Central


[1] Whitefield, J., Winsor, P., Weingartner, T. Modeled flow pathways in the Chukchi Sea, prepared for submission to Continental Shelf Research.

Channel, Barrow Canyon, and Long Strait). Long-term flow magnitude of the Siberian Coastal Current is smaller than previously thought (14.5 mSv), suggesting that the long-term influence of the Siberian Coastal Current is negligible, although it may be important on seasonal time scales, and within the current itself. Mean current vector maps also reveal the existence of a recirculating flow to the south of Hanna Shoal, which in future should be considered as one of the many important input pathways within the Chukchi Sea.

### *2.1. Introduction*

The accelerating loss of sea ice in the Pacific-Arctic (Duarte et al., 2012), combined with a longer ice-free period (Wood et al., 2015), is affecting the Chukchi Sea one of the most productive regions of the Arctic (Grebmeier and Maslowski, 2014), which supports ~15% of total Arctic primary production (Sakshaug, 2004). Water enters the Chukchi through the 85 km wide by ~50 m deep Bering Strait (Figure 2.1), which is the only direct oceanic connection between the Pacific and Arctic Ocean. This water is a combination of nutrient-rich, salty water from the deep Bering Sea and the Gulf of Anadyr (Bering Sea Water, BSW), and water from the Bering Shelf, which is colder and fresher. Also flowing through this narrow channel is a buoyant current that hugs the Alaskan Coast, the Alaskan Coastal Current (ACC; Coachman et al., 1975). The ACC is present seasonally during summer and autumn (Coachman et al., 1975; Woodgate and Aagaard, 2005) and forced by freshwater input from regional rivers (Aagaard et al., 2006). Water (including nutrients and planktonic organisms) also enters the Chukchi Sea through Long Strait from the west through the Siberian Coastal Current (SCC), which is a seasonally present wind- and buoyancy-influenced current. The SCC occasionally reaches as far south as the Bering Strait (Weingartner et al., 1999), but is generally deflected offshore while approaching the strait

where it mixes with BSW in the western Chukchi Sea (Weingartner et al., 1999; Pisareva et al., 2015).

Due to seasonal ice cover and logistical difficulties, there is a dearth of observations from the western Chukchi Sea particularly during the winter months. Long Strait is an important pathway for exchange of nutrients and plankton between the Chukchi Sea and the East Siberian Sea, but has only been studied opportunistically (e.g., Weingartner et al., 1999). In general, the flow pathways of the various water masses (and nutrients/organisms contained therein) from both straits, and their interactions with waters from the East Siberian shelf and the Arctic basin, are not well understood. Ocean circulation models have been increasingly used to explore the circulation over broader space and time scales than are possible from observations, recognizing that models are assumption dependent and require evaluation by comparison to observations.

Not all models have sufficient resolution to distinguish the many flow pathways in the Bering Strait and Chukchi Sea adequately. Some models designed to study Arctic Ocean climate variability have run with a closed Bering Strait (e.g. Maslowski et al., 2000). Others have used a coarse spatial resolution such that a single grid cell represents the Bering Strait with a constant transport value (e.g. Steele et al., 2001; Clement et al., 2005), or lack sufficient resolution to reproduce exchanges through the Bering Strait. Consequently, models can yield estimates of large-scale physical processes that differ substantially from observations. For example, total integrated Arctic freshwater content in the Ocean Circulation and Climate Advanced Model from the National Oceanography Centre was ~58,000 $km^3$ compared to 74,000 $km^3$ from observations (Serreze et al., 2006; Jahn et al., 2012).

Regional models focused on the Pacific-Arctic region (e.g., Winsor and Chapman, 2004; Spall, 2007) have used a higher spatial resolution sufficient to resolve the straits. Regional

models tend to be forced with transports derived from observations, such as a long-term mean (as in Winsor and Chapman, 2004) or a seasonal cycle (Spall, 2007), and can face challenges such as limited data (e.g. Long Strait transport observations are limited to 1990-91; Woodgate et al., 2005a, hereafter referred to as W05a). Bering Strait transport has been observed with a high-resolution mooring array since 1990, yet there are still times and locations where there are no data, which causes uncertainties in estimates of volume, heat and freshwater transport. There is also considerable horizontal velocity shear within the Bering Strait which makes spatial extrapolation of measurements prone to errors in the estimated transport (Clement et al., 2005).

Long-term Bering Strait transport is often reported with the caveat that the ACC is not considered (e.g. Woodgate et al., 2005b, hereafter referred to as W05b), due to the general lack of observations in the coastal domain. To date, only two years (2003 and 2004) of ACC observations have been published (Woodgate et al., 2006), but because their shallowest instruments were located at 18m (as with all other Bering Strait moorings) the shallow, buoyant, relatively warm and fresh water masses most characteristic of the ACC may not be detected. Thus, the effect of stratification, and the ACC specifically, to heat and freshwater fluxes have not yet been resolved by the Bering Strait mooring array.

Here we present results from a high-resolution (~1/6°) model with a domain encompassing the entire Arctic Ocean and surrounding seas, which resolves flow pathways in the Chukchi Sea. The model resolution is roughly twice the baroclinic Rossby radius of deformation (~10 km; W05b), so it only coarsely resolves surface stratified layers and seasonal coastal currents not visible in mooring observations. We use this large-domain, high-resolution regional model to augment observations in the key pathways to the Chukchi Sea allows transport estimates from regions not regularly monitored (i.e. Long Strait), or of specific parameters that

cannot be easily observed (e.g. ice contribution to freshwater transport). By combining simulations and observations, we improve our understanding of the flow pathways and their variability, leading to a better appreciation of the current state and potential future of the productive Chukchi ecosystem as it undergoes climate-mediated transition to a new state. We begin by describing our model and methods used to compare the results to observations in section 2, and then present these results in section 3. We discuss our results in context of the observations in section 4, before summarizing and concluding in section 5.

### *2.2. Methods*

#### *2.2.1. Model Set-up*

We employed a simulation from a regional Arctic configuration of the Massachusetts Institute of Technology general circulation model (MITgcm; Marshall et al., 1997), coupled to the MIT sea ice model (Losch et al., 2010). The model is mapped to a cube-sphere grid projection, which results in an even ~1/6° (~18 km) grid spacing and avoids singularities at the poles. This set-up was developed as part of the Estimating the Circulation and Climate of the Ocean, Phase II (ECCO2) project (Menemenlis et al., 2005; Menemenlis et al., 2008), and is described in detail in Condron et al. (2009), Manizza et al. (2009) and Manizza et al. (2011). The regional configuration used here applies boundary conditions from monthly means output from a previously completed set of ECCO2 integrations from the global set-up.

The 18-km horizontal and 10-m vertical grid spacing allows the model to resolve 6 grid cells and 5-6 depth layers in the Bering Strait. Simulations were output as monthly means over a 35-year period (1979 – 2013), although the first 11 years were not used for long-term mean estimates. Model integrations used to create initial conditions used a coarse (1° × 1°) resolution

forcing, which resulted in riverine freshwater being input on or past the shelf break. Use of the higher resolution ARDAT forcing in this simulation resulted in an equilibration period (cf. Whitefield et al., 2015), with riverine freshwater inputs now reproduced more accurately, and discharge remaining on the shelves. Thus, as the model was adjusting to the new data forcing, this 11-year period was omitted from long-term mean calculations.

#### *2.2.1.1. Atmospheric forcing*

The model was forced every 6 hours using atmospheric data from the Japan Meteorological Agency's Japanese 25 year reanalysis (JRA-25; Onogi et al., 2007). Climatological means of the JRA-25 winds show the strongest winds in the region occur over the Bering Strait in the winter. These northerly winds oppose the direction of the mean Bering Strait throughflow. Easterly winds prevail over the East Siberian Sea and also oppose the mean flow, but maximum wind speeds occur during the summer. Winds over the Lena Delta are transitional; they are southerly during winter months, become easterly by the spring, then weaken and reverse to southerly by the beginning of winter. These winds are indicative of the weakening/strengthening and movement of the Siberian High pressure system.

#### *2.2.1.2. Discharge*

River discharge was implemented using an updated version of the ARDAT data set (Whitefield et al., 2015), a 1/6° resolution monthly-mean set of both river discharge and temperatures. ARDAT v1 contains 30 Arctic rivers, supplying ~3,000 $km^3$ $yr^{-1}$ of freshwater to the Arctic shelves, and 38.4 TW of heat. ARDAT contains monthly climatologies of discharge and water temperatures from observational data sets from the mid-1900s until the present. Here,

the new ARDAT data set contains additional water temperature observations from the Lammers et al. (2007) ART-Russia data set. The monthly mean ARDAT discharge forcing is applied to the model as a volume flux measured as yearly runoff (m $y^{-1}$), as opposed to discharge ($m^3$ $s^{-1}$) values. Thus, the ARDAT discharge values are divided by the area of the corresponding model grid cell, and multiplied by a scale factor to convert to yearly values (but remain as a monthly seasonal cycle); effects of water temperature are applied to the model as a positive heat flux (i.e. warming the ocean).

The largest rivers that supply freshwater to coastal currents that flow into the Chukchi are the Yndigirka, Kolyma and Amguema on the western side, and the Yukon and Kuskokwim from the southeast (Table 2.1). The Anadyr River is also to the south of the Bering Strait, and its waters pass through the strait's western channel. We also include values from the Lena, as its discharge is thought to dilute the SCC before flowing across the East Siberian Sea and through Long Strait (Weingartner et al., 1999), and so may have influence over the Chukchi Sea. In addition to freshwater, these rivers also supply considerable heat seasonally (Table 2.1).

### *2.2.2. Model validation*

To assess the performance of the model, we performed point-to-point comparisons between observations from a sub-surface mooring array and the nearest model grid point. The observational array consists of seven moorings distributed across Bering Strait, equipped with near-bottom Seabird SBE16 CTDs, and either upward-looking Acoustic Doppler Current Profilers (ADCPs) or Aanderaa RCM9 single-point current meters at a depth similar to the CTDs. Three moorings were located in the Russian exclusive economic zone (EEZ; western side) and four in the US EEZ (eastern side). Comparisons were only performed when there were

simultaneous model outputs and observations (Table 2.2). For consistency of comparisons, we only use single-point current meters for the velocity comparisons; mooring A4 was only equipped with an upward-looking ADCP, thus no velocity comparisons were made at this location (Table 2.2).

We performed quantitative comparisons between the observations and the model output following Taylor (2001) and Danielson et al. (2011). The first of our comparative metrics was a least-squares correlation. All r-values presented here have a corresponding p-value of $< 0.05$, which denotes a significant result for this study. However, it is not possible to comment on the variation of the signal with just a correlation value (Taylor, 2001). Therefore, our second comparative metric is the root mean square difference (RMSD), defined as

$$RMSD = \sqrt{\frac{\sum_{k=1}^{n}(O_k - M_k)^2}{n}}$$

where n = total number of records, $O_k$ = observed value, and $M_k$ = modeled value. As two signals become more similar, the RMSD tends to zero, thus a small RMSD value is desirable.

We use the standard deviation of each observational and modeled time series ($\sigma$) as our third metric to assess the contribution of differences in the amplitude of the time series to the RMSD (Taylor, 2001). In order to directly compare different moorings as well as different variables, we normalized both $\sigma$ and the RMSD; we denote $\sigma$' as the normalized standard deviations, with $\sigma_{obs}' = 1$, and $\sigma_{model}' = \sigma_{model}/\sigma_{obs}$, and the normalized RMSD (NRMSD) = $RMSD/\sigma_{obs}$.

### *2.2.3. Chukchi Sea sub-domain*

The water flowing into the Chukchi Sea through the Bering Strait exits through four main routes. One route hugs the Alaskan Coast and passes through Barrow Canyon, one passes through Herald Canyon east of Wrangel Island, and one route is between Herald and Hanna Shoals, known as the Central Channel (cf. Weingartner et al., 2005). The fourth, between Wrangel Island and the Siberian mainland, is Long Strait. By defining a box to enclose these four pathways, we are next able to provide estimates of the proportions of Bering Strait throughflow that is transported through each channel.

Our "box" comprises four sections (Figure 2.1b), corresponding to each of the four outflow pathways. The Long Strait section runs from Cape Blossom on the southwest tip of Wrangel Island to Cape Billings, Siberia. The next section is along a model grid line from the east side of Wrangel Island to Herald Shoal, and the third section runs from Herald Shoal to Hanna Shoal. The final section again follows model grid lines from Hanna Shoal to Point Barrow, Alaska.

### *2.2.4. Calculation of fluxes*

Volume transport for each model cell ($Q$, with units of $m^3\ s^{-1}$) was calculated by first multiplying velocity perpendicular to the section ($v$) by the cross-sectional area of the cell ($dA$). The transports in each cell were then summed over all cells comprising the section to obtain the total volume transport estimate. Cell volume transport was also multiplied by heat and freshwater content to obtain corresponding fluxes, before being summed across each section. Heat fluxes were calculated using $H = \rho\, C_p\, (T_{water} - T_{ref})\, Q$, where $H$ is heat flux (with units of terawatts, TW, where 1 TW $\equiv 10^{12}$ W), $\rho$ is water density (kg $m^{-3}$), $C_p$ is specific heat capacity of water (J

$kg^{-1}$ $°C^{-1}$), $T_{water}$ is the temperature of the seawater, $T_{ref}$ is the reference temperature (in this case -1.9 °C, the freezing point of seawater). Freshwater fluxes were calculated using $F = Q(1 - S/S_{ref})$ $dx$ $dz$, where $F$ is the freshwater flux (with units of either $km^3$ $month^{-1}$ or $km^3$ $yr^{-1}$, depending on the period over which output was averaged), $S$ is the salinity of the seawater, $S_{ref}$ is a reference salinity (in this case 34.8, the mean salinity of the Arctic Ocean, and consistent with Woodgate et al., 2006), $dx$ is the width of the model grid cell, and $dz$ is the cell thickness.

### *2.3. Results*

#### *2.3.1. Model-observation comparison*

Simulated velocities are well-correlated to the observations (Figure 2.2). At the moorings where velocity observations were concurrent with model output (A1, A2 and A3), the model NRMSD is 0.71 – 0.96, and the model only reproduces 34-56% of the observed standard deviation (Figure 2.2). There is a weak correlation (r = 0.28) at A1, but the model correlates strongly (r = 0.63 – 0.77) at A2 and A3. Modeled temperatures at all moorings are well-correlated to the observations (r > 0.9), and NRMSD are between 0.42 – 0.48. Standard deviations at A1 and A2 are ~25% greater than the observations suggest, ~25% smaller at A4 and within 7% at the A3 mooring (Figure 2.2). The model correlates strongly to the observed salinity record at the A1 and A2 moorings, but only weakly to A3 and A4 (Figure 2.2). Standard deviations at A3 and A4 are much smaller than observed (only 13 – 28%), which could contribute to the weak correlations.

### *2.3.2. Chukchi Sea water masses*

An additional check on the model performance was to create a T/S diagram (Figure 2.3) illustrating the various water masses over the top 100 m of the Chukchi Sea, using 280,440 individual climatological monthly mean values. This plot was then visually compared with observational data from Gong and Pickart (2015). The water masses used here are consistent with previous studies. However, as noted in Gong and Pickart (2015), water mass properties have interannual and interseasonal variability, and each definition should not be considered static. Detailed definitions of the water masses can be found in Gong and Pickart (2015), but in brief, we define the warmest waters as Alaskan Coastal Water (ACW; $T \geq 3$ °C, $S \geq 30$), and the coldest waters as Pacific Winter Water (PWW; $T < 1$ °C, $S > 31.5$). These winter waters are further split in to two sub-classes, based on age since formation – Newly Ventilated PWW (with temperatures near to the freezing line), and Remnant PWW (with -1.6 °C $< T <$ -1 °C). Atlantic Water (AW) makes up the most dense waters, and seasonal melt waters (MW) create the least dense waters (Early Season Melt Water – ESMW – and Late Season Melt Water – LSMW). All intermediate waters fall within the category of Chukchi Shelf Water (CSW; -1 °C $< T < 3$ °C, $30 < S < 33.6$).

Modeled temperatures and salinities show that both classes of PWW are created across the Chukchi Sea shelf, and a small intrusion of AW is seen at the far north of Herald Canyon, suggesting that the model is reproducing upwelling of AW here, but not in Barrow Canyon as suggested by Gong and Pickart (2015), although this is likely due to our sub-domain not reaching far enough north to see upwelling in this region. Atmospheric cooling in the fall is also visible, with the warm ACW reducing in temperature without an associated change in salinity. The

model also creates MW during the summer progressing from ESMW in May, June and July, to LSMW in August, September and October.

### *2.3.3. Chukchi Sea inflow – the Bering Strait*

Based on the results from the Taylor analysis (see Section 2.2.2), the model is a reasonable approximation of the observations in the Bering Strait. The model thus enables a first estimate of heat, freshwater and volume contained in the ACC and stratified surface layers, and the first to include estimates of freshwater in solid form (i.e. ice and snow). Simultaneously, the model removed an estimated 25% error associated with horizontal interpolation, velocity variability, and under-estimation of the Strait-wide mean velocity by the mooring (W05b).

#### *2.3.3.1. Velocity and volume transport*

To determine the velocity and volume transport values while accounting for the ACC, we used a long-term mean velocity from the entire Bering Strait section, rather than from a single point. Minimum velocities, <21 cm $s^{-1}$, occur in the Bering Strait during November and December, and velocities remain within 25% of the winter values until May (Figure 2.4a). In the ice-free summer months, velocities are between 28 – 33 cm $s^{-1}$. Transport also follows this seasonal cycle, ranging between 0.84 Sv and 1.35 Sv (Figure 2.4a). Long-term mean transport through the Bering Strait is 1.05 ± 0.61 Sv (all values herein are shown as mean ± standard deviation), based on a long-term mean velocity of 26.4 ± 18.1 cm $s^{-1}$ and a cross sectional area (CSA) of 3.99 $\times 10^6$ $m^2$. The large standard deviation is due to the high variability between months; transport values can reach less than 0.1 Sv (December 1991), or as high as 1.67 Sv (59% above the long-term mean) in May 1997. To estimate the Bering Strait volume transport without

contributions from the ACC, and hence the total contribution from the ACC itself, we used the same approach as W05b (i.e. using a single point to the north of the Bering Strait multiplied by the Bering Strait CSA). We calculate transport using this method as 0.83 Sv, suggesting that the ACC contributes 27% (0.22 Sv) of the Bering Strait throughflow.

#### *2.3.3.2. Temperature and heat transport*

Temperatures in the Bering Strait range from -1.8 ºC (from January until May in most years, but occasionally beginning to warm as early as March) to a maximum of 5 °C in September (Figure 2.4b). Heat transports (using a reference temperature of -1.9 °C; see section 2.4) range from <0.5 TW in the winter months to a peak of 35 TW in August (Figure 2.4c). There is some interannual variability in the timing of the heat flux maximum, which occurs as late as October (e.g., 35.5 TW in October 1991). Long-term mean heat transport is 12.0 ± 13.2 TW, with the large standard deviation a result of the high interannual variability in both temperature and volume transports. Long-term mean heat fluxes in the summer months (between May and October) is 21.3 ± 12.1 TW, with values ranging from ~16.2 TW in 2002 and 2009 to 31.7 TW in 2007. The largest monthly-mean heat flux occurred during September 2007 (49.3 TW, an increase of 70.1% on the climatological September heat flux) coincident with a year of minimal Arctic sea ice cover, and coupled with a 7-month period of warmer than normal temperatures (i.e. falling outside a 95% confidence interval).

#### *2.3.3.3. Salinity and freshwater transport*

There is large interannual variability in the seasonal salinity cycle, with typical maximum salinities of 33 occurring during March and April (Figure 2.4d). Yearly maximum salinity can be

up to 0.34 above the long-term mean value (e.g., 1990, 2013). Minimum salinities of 32.1 occur during the September – January cooling period, with the subsequent increase related to a reduction in freshwater runoff and to the onset of ice formation in winter. Anomalously fresh months (all falling outside the 95% confidence interval) occurred in December 2004 (0.9 below the mean), and March/April 1996, September 1998 and March 2001 (all ~0.5 below the mean).

The Bering Strait is seasonally ice free between July and October, although it can be ice free as early as June or as late as November (Figure 2.4e), with maximum sea ice (SI) volume typically attained during May. Long-term mean SI transport, calculated over only the months with ice, is 91.3 ± 222.4 $km^3$ $yr^{-1}$; equivalent freshwater transport contained in the sea ice is 83.5 ± 197.2 $km^3$ $yr^{-1}$. By converting SI and snow volume to freshwater equivalent, we are able to include a sea ice component to estimates of freshwater transport, which has a minimum during March and a maximum during the summer months (Figure 2.4f). The magnitude of the total monthly mean freshwater transport in the Bering Strait section is 122 – 257 $km^3$ $month^{-1}$, and long-term mean freshwater transport is 2251 ± 776 $km^3$ $yr^{-1}$, of which only 3.7% is transported in the form of sea ice.

### *2.3.4. Chukchi Sea outflow – the northern channels*

The model estimates long-term mean transport in Barrow Canyon of 0.48 ± 0.48 Sv. This high standard deviation is a consequence of the wind-forced nature of the flow in this region; depending on wind direction, flow through Barrow Canyon can be completely reversed, and of a similar magnitude. Long-term mean transport through Herald Canyon is of a similar magnitude to Barrow Canyon (0.41 ± 0.30 Sv), with similarly high standard deviation for the same reasons. The long-term mean flow through the Central Channel is 0.06 ± 0.29 Sv, surprisingly small

compared to the other northern channels. The high standard deviation suggests that, like the other two northern channels, flow direction here is highly variable. Subsequently, Central Channel often becomes a net inflow to the Chukchi Sea. One factor that is likely to be contributing to the relatively small magnitude of transport is that, compared to the other sections, a large portion of the transect does not cover the channel. Thus, we further divided the Central Channel transect into two portions – the southern sub-section covers the Central Channel itself, while the northern sub-section, ~1/3 the length of the southern sub-section, covers the shallower region to the southwest of Hanna Shoal. The long-term mean flow through the southern sub-section (Central Channel) is 0.16 ± 0.16 Sv out of our Chukchi Sea domain, while there is a predominantly southward inflow through the northern sub-section of 0.10 ± 0.18 Sv; a south-easterly flow brings water back into the region through the northern sub-section.

Volume transport in Long Strait is less than in the other channels, and is always negative (i.e. mean monthly flow is always out of the Chukchi Sea). Magnitudes range from 0.12 Sv in May to 0.02-0.03 Sv in September and October, with a long-term mean value of 0.07 ± 0.13 Sv westward. As with the other channels, the relatively high standard deviation indicates flow through Long Strait is variable, and occasionally even a source of waters to the Chukchi Sea. Long Strait throughflow is more variable in the summer than in the winter, unlike the Bering Strait. Anomalously large events occurred in 1994, where 0.30 Sv was imported to the Chukchi Sea through Long Strait during August, and in August/September 2013, where >0.35 Sv was exported.

A simple summation of the long-term mean volume transport values for each of the four pathways results in a volume of 1.03 ± 0.68 Sv leaving the Chukchi Sea (Figure 2.5). The remaining 2.3% (0.02 Sv) needed to balance Bering Strait inflow is lost through conversion of

liquid water to solid form (i.e. ice formation in the Chukchi Sea), and an imbalance of evaporation and precipitation.

### *2.3.5. Stratification and velocity shear*

As seasonal sea-ice recedes, solar heating and ice melt leads to stratification of the surface waters in the Chukchi Sea. Additionally, buoyant surface currents create stratified regions close to the coast. In the model, there is a long-term mean difference of 0.5 °C between surface waters and those at 50m, and a salinity difference of 1-2. In order to analyze transport in the surface and bottom layers, the depth of the maximum Brunt-Väisälä frequency was calculated for all model points in the Chukchi Sea. The Brunt-Väisälä frequency ($N^2$) is given by

$$N^2 = -\frac{g}{\rho}\frac{\partial \rho}{\partial z}$$

where $g$ is the gravitational acceleration (m $s^{-2}$ and defined to be positive), $\rho$ is potential density (kg $m^{-3}$), and $z$ is depth (m). Long-term monthly mean values of $N^2$ are always positive, showing that the modeled water column is always stable ($N^2 < 0$ implies unstable stratification, resulting in convection or overturning). The model recreates a surface stratified layer which persists at 20-30 m, as well as reproducing seasonal strengthening and weakening of the pycnocline at this depth. During the summer, strong stratification exists in the region to the west of Wrangel Island, which then bifurcates around both sides of Wrangel Island. This is indicative of Lena discharge being advected into the western Chukchi Sea. To the east of the Chukchi Sea, values indicate weak stratification, suggesting that the model is reproducing the ACC as a barotropic current.

By using the depth of maximum $N^2$ as an interface, we split the barotropic transport estimates above in to estimates for the surface and lower layers (Figure 2.5b and 2.5c). Flow through the Bering Strait is equally split between surface and lower layers, as with Central

Channel. In Herald Canyon and Barrow Canyon, there is some current shear, with only 1/3 of total transport in the surface layer. Shear is the most pronounced in Long Strait, with 14% of the total flow in the surface layer. This reduction is caused by the buoyant SCC flowing in to the Chukchi Sea, and the deep flow being solely an export route.

While flows are barotropically balanced (i.e. sum of upper and lower layer transport through Bering Strait equals the sum of transports through the outflow channels), the flow in through each layer in the Bering Strait does not equal the flow out in each respective layer. This is indicative of mixing occurring in the central/southern Chukchi Sea shelf, with surface Bering Strait waters being mixed downwards and exiting the shelf in the bottom layer, and also due to the surface layers being more susceptible to wind stresses.

### *2.3.6. Long-term mean flow pathways*

A vector map of the depth integrated volume transport across the Chukchi Sea shelf region produces a simplified flow diagram of the different pathways (Figure 2.6a). Flow out of the Bering Strait divides into two routes – the western branch, which typically contains water from the Bering Sea shelf and Gulf of Anadyr, primarily passes through Herald Canyon with some water flowing out through Long Strait (with an inflowing Siberian Coastal Current). The eastern branch, containing the Alaskan Coastal Current and other nearshore waters, flows through the Central Channel and Barrow Canyon. There is a second split in the western branch, north of Herald Canyon, while some of the western branch re-joins the eastern branch. The eastern branch splits in to the two well-documented pathways through Barrow Canyon and the Central Channel, but the model also shows a recently described pathway that recirculates water from the Central Channel to Barrow Canyon to the south of Hanna Shoal (see Pickart et al., in

review). However, these pathways change seasonally. During autumn and winter (Figure 2.6b), flow in the western branch is almost completely through Herald Canyon, and flow in Long Strait is almost zero. By spring, the Long Strait outflow has re-established (Figure 2.6c), but breaks down again in the summer (Figure 2.6d) to be replaced by a model-recreated Siberian Coastal Current. In the summer, magnitudes of transport are at their greatest in all the northern channels.

The high standard deviations of the long-term mean throughflow in each channel are indicative of considerable variability. The Central Channel section is a net inflow to the Chukchi shelf during the summer, although the weak northward flow through the Central Channel itself is counteracted by a southward flow in the northern portion. All other channels are exit pathways, with flow predominantly through Barrow Canyon (57.5% in August). Conversely, outflow is split relatively equally in late summer – early fall (35.2% through Barrow Canyon, 24.6% through Central Channel, and 34.9% through Herald Canyon; Figure 2.7). The fall outflow differs from the late winter and spring outflow in that only 6-10% of the Chukchi outflow passes through the Central Channel at that time (Figure 2.7). As implied by the flow diagrams, this variability suggests that as the southward flow through the northern portion of the Central Channel increases, a greater proportion of water from Herald Canyon and the western Chukchi Sea flows eastwards across the middle shelf, and can enter the Barrow Canyon outflow through the pathways to either the north or south of Hanna Shoal.

### *2.4. Discussion*

The results from the model presented here, although still relatively coarse, still resolve the surface layers and seasonal coastal currents not observed by the Bering Strait mooring array. In addition, our results show long-term mean transports (and their relative contributions) through

the main Chukchi Sea outflow pathways, and allows us to suggest seasonal variations in currents throughout the Chukchi Sea shelf region. Due to the comparative coarseness of the model (~16 km compared to the typical Rossby radius of ~5 km in this region), we next discuss our model results in context with published observations from differing sources.

### *2.4.1. Bering Strait inflow*

The conclusion of W05b was that the mooring at A3 is a good approximation of water flowing through both the east and west channels of the Bering Strait. As such, the velocity at A3 (20.9 cm $s^{-1}$) was combined with a representative cross sectional area of the Bering Strait to obtain a long-term mean transport value of 0.89 Sv. Data from the CTD on the A3 mooring were then used to derive long-term mean heat and freshwater transport values. The CSA used for the previously published estimates is larger than the one used here ($4.25 \times 10^6$ $m^2$ compared to $3.99 \times 10^6$ $m^2$) due to differences between the model and actual bathymetry.

Model estimates of long-term mean transport without contributions from the ACC are similar to observations, but our finding that the ACC contributes an additional 0.22 Sv is greater than the increase suggested by W05b. This difference may result from partial resolution of errors associated with horizontal interpolation of observations, as the model resolution is still coarse compared to the width of Bering Strait and to the baroclinic radius of deformation. Although model estimates of long-term mean transport (not including the ACC contributions) and monthly mean summer transport are similar to the observational estimates of W05b, our winter transport estimates are twice as large as those derived from observations.

The seasonal range of the modeled temperature cycle is comparable to the 1950 – 1988 NODC data average (-1.8 °C – 4.9 °C; Björk, 1989), but is warmer than observations presented

in W05b. For example, the warmest temperatures in the model are as much as 2.5 °C warmer than observations in August/September/October. Ship-borne CTD transects (not shown here) in summer and autumn months show the surface waters are 1-2 °C warmer than near bottom measurements, with this layer not being observed by the >40 m-deep moored CTDs. With the combined increase in both volume transport and mean temperatures compared to observations, published values using A3 data (7.3 TW, Woodgate et al., 2006) underestimate heat transport by 64%. Although large, this increase results in heat fluxes within the 12.1 – 13.6 TW range of total annual mean heat transport suggested by Woodgate et al. (2006).

The modeled monthly mean salinities are fresher than the NODC average, but similar to W05b (model values are 32.1 – 33.0 compared to 31.5 – 32.4 in Björk, 1989). The model does not capture all of the observed interannual variability; observed maximum salinities (1991, 1999 and 2000; W05b) are ~ 1 above the mean value, but maximum salinity in the model only reaches 0.34 above the mean. However, the model does capture some of the anomalous events, with fresher than normal months in March 2001 and December 2004 being seen by both the model and the mooring array.

Given that observational estimates of freshwater transport through Bering Strait are from near-bottom CTDs, freshwater transport in stratified layers, the ACC and sea ice are not accounted for (cf. Woodgate et al., 2012). Observational estimates of sea ice transport through Bering Strait have been attempted, using data from an upward looking ADCP in bottom tracking mode (Travers, 2012). Modeled estimates of sea ice transport are 60% of the observational estimates (91.3 $km^3\ yr^{-1}$ vs. 140 $km^3\ yr^{-1}$), although it is difficult to determine whether the model underestimates ice volume due to averaging the ice thickness over the grid cell, or whether the

ADCP-based calculations overestimate due to measuring keels and ridges that are not representative of the entire Bering Strait.

By converting sea ice volume to a liquid equivalent, our modeled long-term freshwater transport estimate is 2251 $km^3$ $yr^{-1}$, which is only 9.5% less than the 2465 $km^3$ $yr^{-1}$ calculated by Condron et al. (2009), but 32% more than the estimates of Woodgate et al. (2006) who reported an annual mean freshwater transport of 1700 $km^3$ $yr^{-1}$. However, the contribution of the ACC and stratification to freshwater transport in our model is at the low end of the approximately 800 – 1000 $km^3$ $yr^{-1}$ extra suggested by Woodgate et al. (2006). The long-term mean salinity in the model Bering Strait section is the same as the A3 observations (32.5; W05b), which suggests stratification contributes surprisingly little to this increase in freshwater transport. Inclusion of the ACC accounts for 88% of the discrepancy with the observations, and the sea ice component of the FW transport accounts for the remaining 12%.

### *2.4.2. Outflow pathways*

Although it is suggested by W05a that the outflows through the four northern channels are of comparable size (~ 0.1 – 0.3 Sv), this conclusion was based on a single year of moored observations. While relatively long-term observations of fluxes through Barrow Canyon are available (Itoh et al., 2013), as are some quasi-synoptic estimates of flow in Herald Canyon (Pickart et al., 2010; Pisareva et al., 2015), W05a is the only mooring record available from Herald Canyon and Long Strait.

Our estimates of the Chukchi Sea outflows show that flow magnitudes are similar through Herald and Barrow Canyons, and greater than the range suggested by W05a. However, our long-term mean volume transport through Barrow Canyon is similar to estimates from an 8-

year mooring array at the mouth of the Canyon (0.45 Sv; Itoh et al., 2013). Estimates of flow through Herald Canyon are also higher than the estimates of 0.36 Sv from Pickart et al. (2010), although this is due to the observational value being from synoptic data. A model section located at approximately the same location as Transect 2 in Pickart et al. (2010) and using velocities from a single model time step yields a transport value of 0.33 Sv.

Observations of transport in Long Strait have only been conducted from September 1990 to October 1991 (W05a). During this time, the mooring did not observe waters from the Siberian Coastal Current, and transport through Long Strait was inferred from near-bottom velocity from the northern part of Long Strait. W05a used a CSA of $5.9 \times 10^6$ $m^2$ for Long Strait, whereas the CSA of our section in the model is larger at $7.48 \times 10^6$ $m^2$. This difference is due to W05a using only a portion of the CSA in order to omit transport within the unobserved Siberian Coastal Current, whereas we include the coastally-trapped Siberian Coastal Current in our Long Strait transport estimates. This current flows southeastward along the coast in the opposite direction to the flow in the rest of the strait, and thus our estimated long-term mean transport is only 41% of the estimates from W05a, despite our use of a larger CSA. In short, the model suggests that the transport through Long Strait is not as large as has been estimated, although the observational estimates are crude.

The westward outflow from the Chukchi Sea is supposedly balanced by input from the Siberian Coastal Current (W05a), so as with the ACC, we attempted to remove the influence of the SCC from the Long Strait section by removing the two southernmost columns from the model section along with the top grid cell of the third column, which appear to account for the bulk of the SCC in the model. Flow in the SCC section is always eastwards, with a long-term mean volume transport in the SCC of 14.5 mSv, maximum transport of 24.3 mSv in October, and

minimum transport in the winter of <11 mSv. The mean eastward flow in the SCC is only 10-50% of the westward flow in the northern section, suggesting that the long-term influence of the SCC and associated salt, heat and nutrient inputs is also negligible, although it may be important on seasonal time scales and certainly within the region influenced by the SCC.

The recirculating flow around the south of Hanna Shoal has only recently been suggested. Ship-borne ADCP transects undertaken during June-July 2011 as part of the Impacts of Climate on Ecosystem and Chemistry of the Arctic Pacific Environment (ICESCAPE) program found volume transport of between 0.06-0.2 Sv (Pickart et al., in review) in a current to the south of Hanna Shoal. Coupled with our long-term mean estimates, we are confident that this is a persistent feature, and should be considered as part of the overall flow pathways in the Chukchi Sea.

### *2.5. Summary and conclusions*

We used results from 24 years of a 35-year long integration of a large-domain, high-resolution regional model to augment observations through the key flow pathways within the Chukchi Sea, from both the Pacific Ocean (through the Bering Strait) and the East Siberian Sea (through Long Strait) and into the Arctic Ocean basin. Understanding and documenting changes in the Arctic shelf seas (such as those caused by a transition to longer ice-free periods; Wood et al., 2015) and the broader impacts on the productive Chukchi Sea are important, and can only be achieved by combining observations and model output. Using this approach, we modeled regions that do not have regular or repeated observations (i.e. Long Strait), and estimated specific parameters that cannot be easily observed (e.g. ice contribution to freshwater transport).

By comparing estimates of transport through the model sections to observations, we found that the model reproduces transport values over quasi-synoptic, short- and long-term time scales. We were also able to quantify the contributions from stratification, seasonally-present coastal currents such as the ACC and SCC, and freshwater in the form of sea ice, as well as reduce potential errors due to horizontal interpolation, velocity variability, and under-estimation by the observational mooring array. Although observational estimates of the long-term mean Bering Strait volume transport are often reported as 0.8 Sv, W05b state that interpolation errors and variability can add up to an additional 15% to this value. Underestimation of Bering Strait velocity through use of the A3 mooring ~60 km north of Bering Strait, rather than data from within the Bering Strait proper, can further increase this error to up to 25%. Our model estimates the underestimation to be closer to 30% (based on a calculated long-term mean volume transport of 1.05 Sv), due almost entirely to the ACC.

Using physical models to help interpret biological observations is a first step in multi-disciplinary approaches to understanding how the Chukchi Sea ecosystem currently responds to variable climate forcing, and how it may respond in the future. While our results are a step forward to understanding the Chukchi Sea dynamics, it is critical that observational data and models work in tandem to describe the current state and predict the future of the productive Chukchi ecosystem and its inputs.

### *2.6. References*

Aagaard, K., Weingartner, T.J., Danielson, S.L., Woodgate, R.A., Johnson, G.C., Whitledge, T.E., 2006. Some Controls on Flow and Salinity in Bering Strait. Geophysical Research Letters 33, L19602.

Björk, G., 1989. A One-Dimensional Time-Dependent Model for the Vertical Stratification of the Upper Arctic Ocean. Journal of Physical Oceanography 19, 52-67.

Clement, J.L., Maslowski, W., Cooper, L.W., Grebmeier, J.M., Walczowski, W., 2005. Ocean Circulation and Exchanges through the Northern Bering Sea – 1979-2001 Model Results. Deep Sea Research II 52, 3509-3540.

Coachman, L.K., K. Aagaard, Tripp, R.B., 1975. Bering Strait: The Regional Physical Oceanography. University of Washington Press, Seattle.

Condron, A., Winsor, P., Hill, C., Menemenlis, D., 2009. Simulated Response Of The Arctic Freshwater Budget To Extreme NAO Wind Forcing. Journal of Climate 22, 2422-2437.

Danielson, S., Curchitser, E., Hedstrom, K., Weingartner, T., Stabeno, P., 2011. On Ocean and Sea Ice Modes of Variability in the Bering Sea. Journal of Geophysical Research 116 (C12), C12034.

Duarte, C.M., Lenton, T.M., Wadhams, P., Wassmann, P., 2012. Abrupt Climate Change in the Arctic. Nature Climate Change 2, 60-62.

Gong, D., Pickart, R.S., 2015. Summertime Circulation in the Eastern Chukchi Sea. Deep Sea Research Part II: Topical Studies in Oceanography 118, 18-31.

Grebmeier, J.M., Maslowski, W., 2014. The Pacific Arctic Region: Ecosystem Status and Trends in a Rapidly Changing Environment. Springer, New York.

Itoh, M., Nishino, S., Kawaguchi, Y., Kikuchi, T., 2013. Barrow Canyon Volume, Heat, and Freshwater Fluxes Revealed By Long-Term Mooring Observations between 2000 and 2008. Journal of Geophysical Research: Oceans 118, 4363-4379.

Jahn, A., Aksenov, Y., Cuevas, B., Steur, L., Häkkinen, S., Hansen, E., Herbaut, C., Houssais, M.N., Karcher, M., Kauker, F., 2012. Arctic Ocean Freshwater: How Robust Are Model Simulations? Journal of Geophysical Research 117, C00D16.

Lammers, R.B., Pundsack, J.W., Shiklomanov, A.I., 2007. Variability in River Temperature, Discharge, And Energy Flux from the Russian Pan-Arctic landmass. Journal of Geophysical Research 112, G04S59.

Losch, M., Menemenlis, D., Campin, J.-M., Heimbach, P., Hill, C., 2010. On The Formulation of Sea-Ice Models. Part 1: Effects of Different Solver Implementations and Parameterizations. Ocean Modelling 33, 129-144.

Manizza, M., Follows, M.J., Dutkiewicz, S., McClelland, J.W., Menemenlis, D., Hill, C., Townsend-Small, A., Peterson, B.J., 2009. Modeling Transport And Fate Of Riverine Dissolved Organic Carbon In The Arctic Ocean. Global Biogeochemical Cycles 23, GB4006.

Manizza, M., Follows, M.J., Dutkiewicz, S., Menemenlis, D., McClelland, J.W., Hill, C., Peterson, B.J., Key, R.M., 2011. A Model of the Arctic Ocean Carbon Cycle. Journal of Geophysical Research 116, C12020.

Marshall, J., Adcroft, A., Hill, C., Perelman, L., Heisey, C., 1997. A Finite-Volume, Incompressible Navier Stokes Model For Studies of the Ocean on Parallel Computers. Journal of Geophysical Research 102, 5753-5766.

Maslowski, W., Newton, B., Schlosser, P., Semtner, A., Martinson, D., 2000. Modeling Recent Climate Variability in the Arctic Ocean. Geophysical Research Letters 27, 3743-3746.

Menemenlis, D., Campin, J.-M., Heimbach, P., Hill, C., Lee, T., Nguyen, A., Schodlok, M., Zhang, H., 2008. ECCO2: High Resolution Global Ocean and Sea Ice Data Synthesis. Mercator Ocean Quarterly Newsletter 31, 13-21.

Menemenlis, D., Hill, C., Adcroft, A., Campin, J.M., Cheng, B., Ciotti, B., Fukumori, I., Koehl, A., Heimbach, P., Henze, C., Lee, T., Stammer, D., Taft, J., Zhang, J., 2005. NASA Supercomputer Improves Prospects for Ocean Climate Research. EOS Transactions AGU 86, 89.

Onogi, K., Tsutsui, J., Koide, H., Sakamoto, M., Kobayashi, S., Hatsushika, H., Matsumoto, T., Yamazaki, N., Kamahori, H., Takahashi, K., 2007. The JRA-25 Reanalysis. Journal of the Meteorological Society of Japan 85, 369-432.

Pickart, R.S., Pratt, L.J., Torres, D.J., Whitledge, T.E., Proshutinsky, A.Y., Aagaard, K., Agnew, T.A., Moore, G., Dail, H.J., 2010. Evolution and Dynamics of the Flow through Herald Canyon in the Western Chukchi Sea. Deep Sea Research Part II: Topical Studies in Oceanography 57, 5-26.

Pisareva, M.N., Pickart, R.S., Spall, M., Nobre, C., Torres, D., Moore, G., Whitledge, T.E., 2015. Flow of Pacific Water in the Western Chukchi Sea: Results from the 2009 RUSALCA Expedition. Deep Sea Research Part I: Oceanographic Research Papers, 105, 53-73.

Sakshaug, E., 2004. Primary and Secondary Production in the Arctic Seas, in: The Organic Carbon Cycle in the Arctic Ocean, R. Stein and R. MacDonald (eds), Springer, New York, pp. 57-81.

Serreze, M.C., Barrett, A.P., Slater, A.G., Woodgate, R.A., Aagaard, K., Lammers, R.B., Steele, M., Moritz, R., Meredith, M., Lee, C.M., 2006. The Large-Scale Freshwater Cycle of the Arctic. Journal of Geophysical Research 111, C11010.

Spall, M.A., 2007. Circulation and Water Mass Transformation in a Model of the Chukchi Sea. Journal of Geophysical Research: Oceans (1978–2012) 112 (C5), C05025.

Steele, M., Ermold, W., Hakkinen, S., Holland, D., Holloway, G., Karcher, M., Kauker, F., Maslowski, W., Steiner, N., 2001. Adrift in the Beaufort Gyre: A Model Intercomparison. Geophysical Research Letters 28, 2935-2938.

Taylor, K.E., 2001. Summarizing Multiple Aspects of Model Performance in a Single Diagram. Journal of Geophysical Research 106, 7183-7192.

Travers, C.S., 2012. Quantifying Sea-Ice Volume Flux Using Moored Instrumentation In The Bering Strait. University of Washington, Seattle, p. 85.

Weingartner, T., Aagaard, K., Woodgate, R., Danielson, S., Sasaki, Y., Cavalieri, D., 2005. Circulation on the North Central Chukchi Sea Shelf. Deep Sea Research Part II: Topical Studies in Oceanography 52, 3150-3174.

Weingartner, T., Danielson, S., Sasaki, Y., Pavlov, V., Kulakov, M., 1999. The Siberian Coastal Current: A Wind- And Buoyancy-Forced Arctic Coastal Current. Journal of Geophysical Research 104, 29697-29713.

Whitefield, J., Winsor, P., McClelland, J., Menemenlis, D., 2015. A New River Discharge And River Temperature Climatology Data Set For The Pan-Arctic Region. Ocean Modelling 88, 1-15.

Winsor, P., Chapman, D.C., 2004. Pathways of Pacific Water across the Chukchi Sea: A Numerical Model Study. Journal of Geophysical Research 109 (C3), C03002

Wood, K.R., Bond, N.A., Danielson, S.L., Overland, J.E., Salo, S.A., Stabeno, P., Whitefield, J., 2015. A Decade of Environmental Change in the Pacific Arctic Region. Progress in Oceanography 136, 12-31.

Woodgate, R.A., Aagaard, K., 2005. Revising the Bering Strait Freshwater Flux into the Arctic Ocean. Geophysical Research Letters 32, L02602.

Woodgate, R.A., Aagaard, K., Weingartner, T.J., 2005a. A Year in the Physical Oceanography of the Chukchi Sea: Moored Measurements from Autumn 1990-1991. Deep Sea Research II 52, 3116-3149.

Woodgate, R.A., Aagaard, K., Weingartner, T.J., 2005b. Monthly Temperature, Salinity, and Transport Variability of the Bering Strait Through Flow. Geophysical Research Letters 32, L04601.

Woodgate, R.A., Aagaard, K., Weingartner, T.J., 2006. Interannual Changes in the Bering Strait Fluxes of Volume, Heat and Freshwater Between 1991 and 2004. Geophysical Research Letters 33, L15609.

Woodgate, R.A., Weingartner, T., Lindsay, R., 2012. Observed Increases In Bering Strait Oceanic Fluxes From The Pacific To The Arctic From 2001 To 2011 And Their Impacts On The Arctic Ocean Water Column. Geophysical Research Letters 39, L24603.

*2.7. Figures*

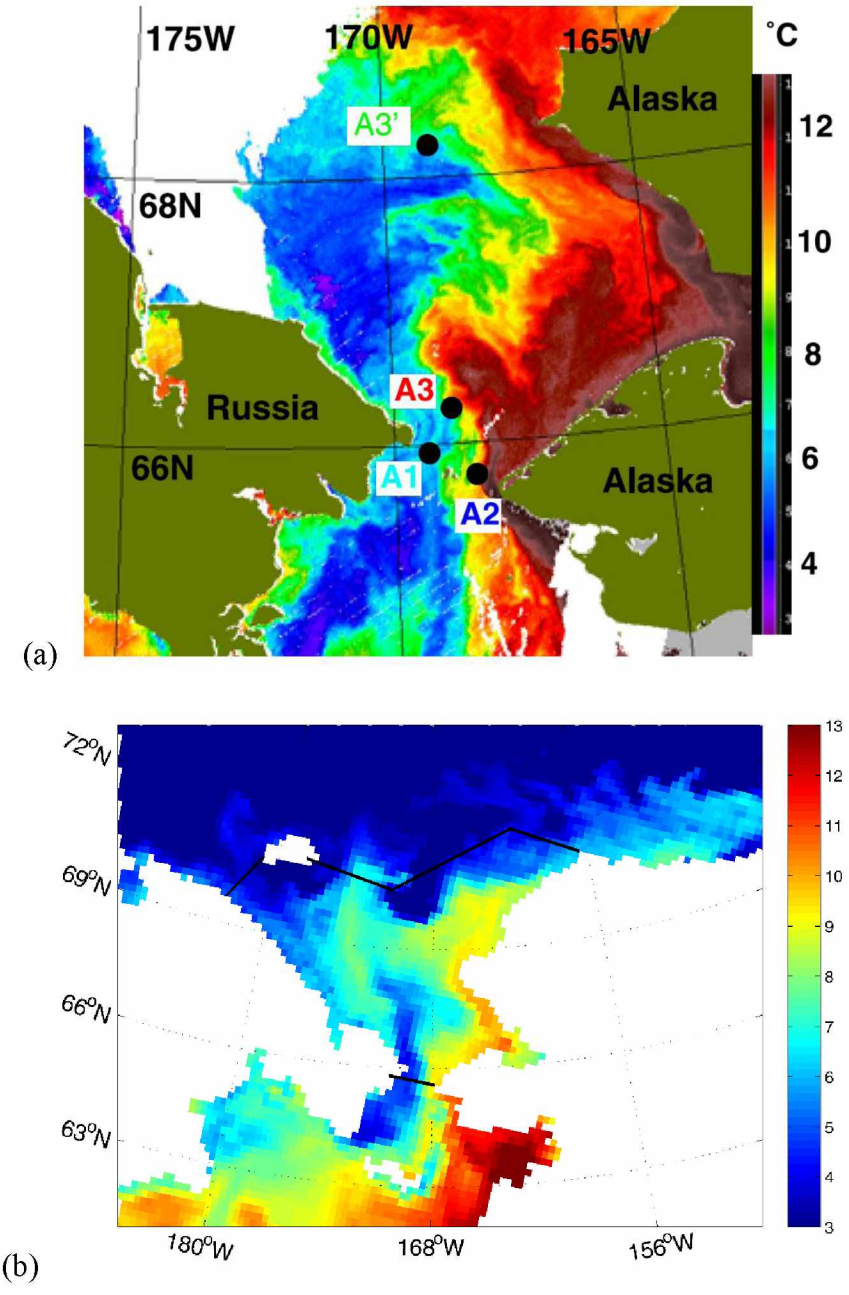


Figure 2.1. (a) Summer (August 2004) sea surface temperature (SST) in the Bering Strait region, showing mooring locations (dots) and NCEP wind points (x), taken from Woodgate et al. (2005b); (b) equivalent summer SST from the model, with solid lines showing locations of the sub-domain used in section 3.3; (c) schematic flow diagram of the Chukchi Sea, adapted from Danielson et al. (2014).

(c)

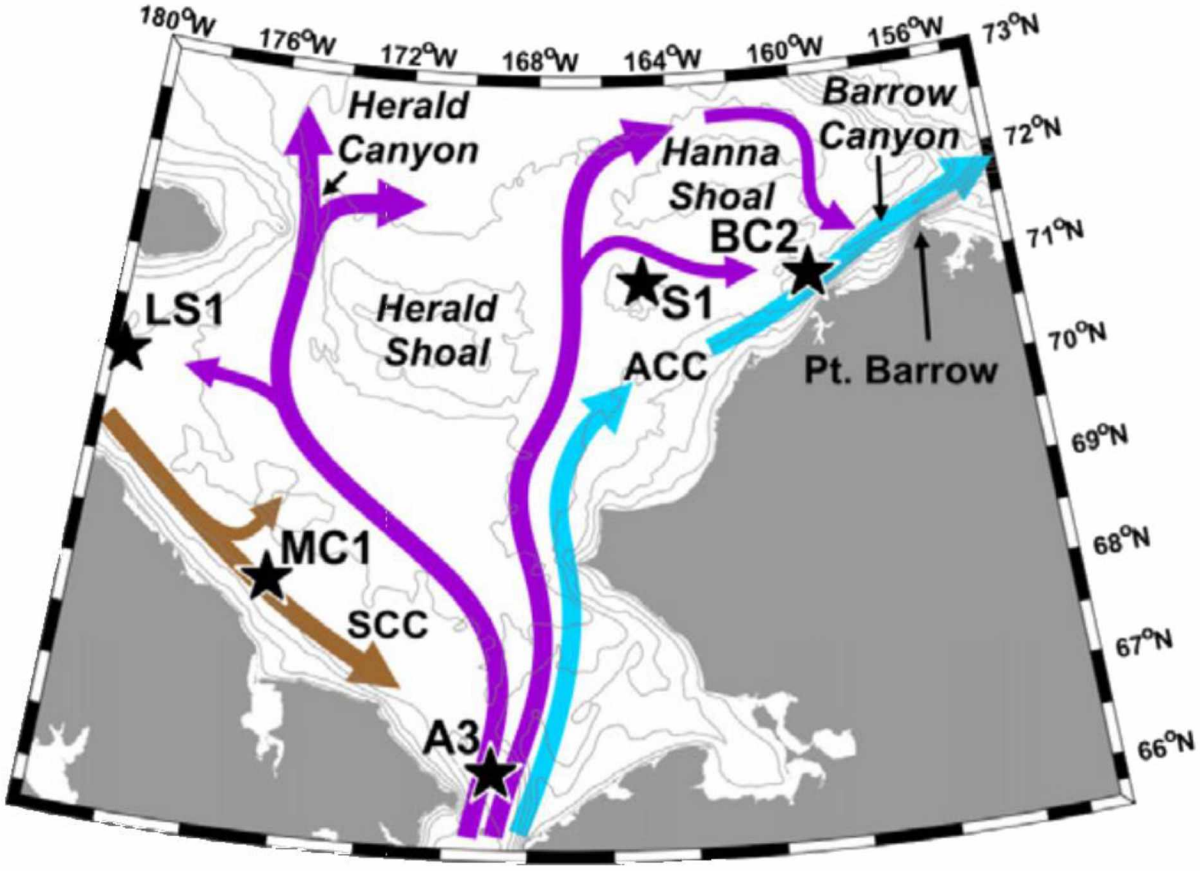


Figure 2.1. cont.

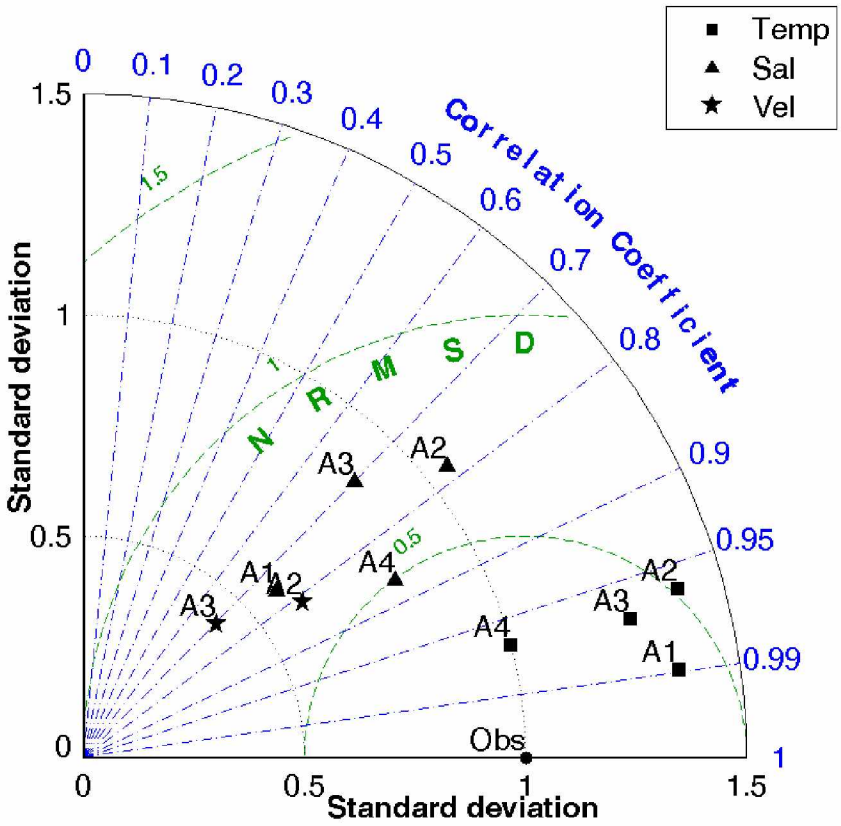


Figure 2.2. Taylor diagrams resulting from comparison of model output to mooring data for (■) temperature, (▲) salinity, and (★) velocity. Normalized root mean square deviation (NRMSD) is normalized so that NRMSD = 0 is identical to the observations, and standard deviation (σ) is normalized so $\sigma_{norm} = 1$ is identical to the observations.

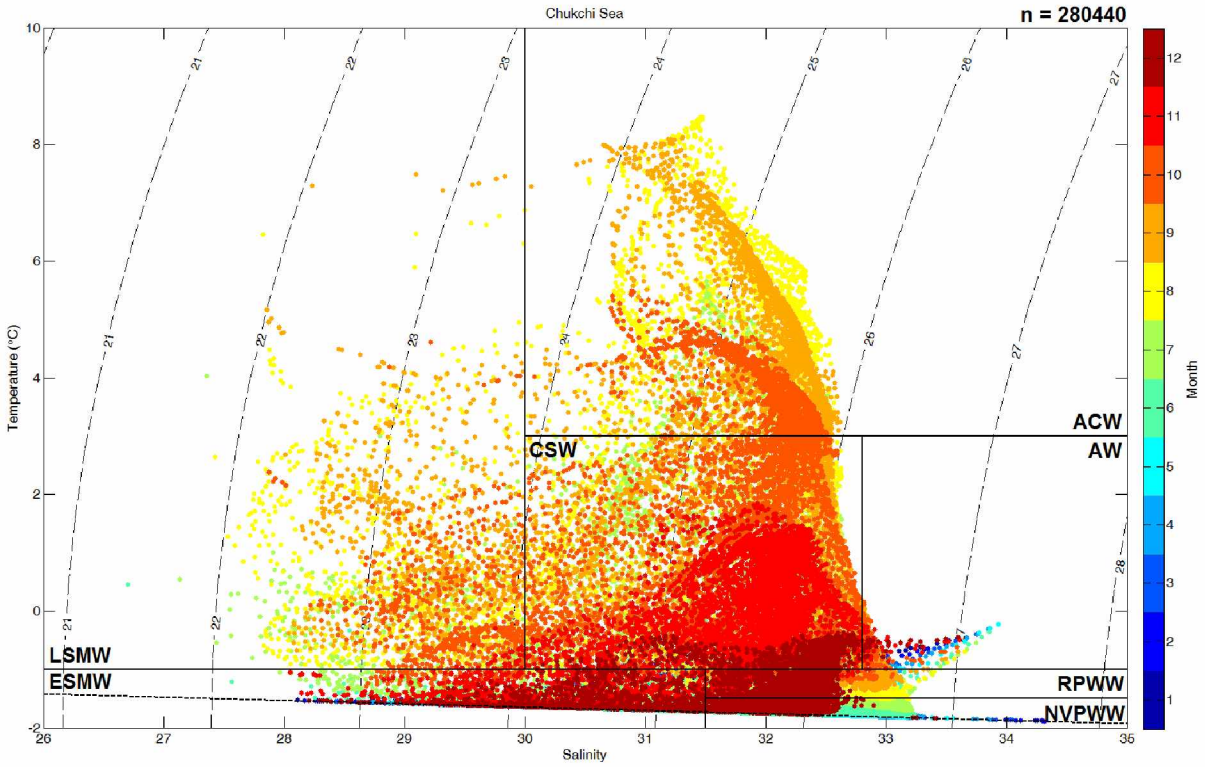


Figure 2.3. Temperature-salinity plot of the modeled water masses in the Chukchi Sea shelf (depth < 100 m), with color of dots indicating month. Curved dashed lines indicate potential density contours, and the freezing line is denoted by the thick black line. Thick solid lines delineate water mass types, with water mass classes labelled (see text for abbreviations).

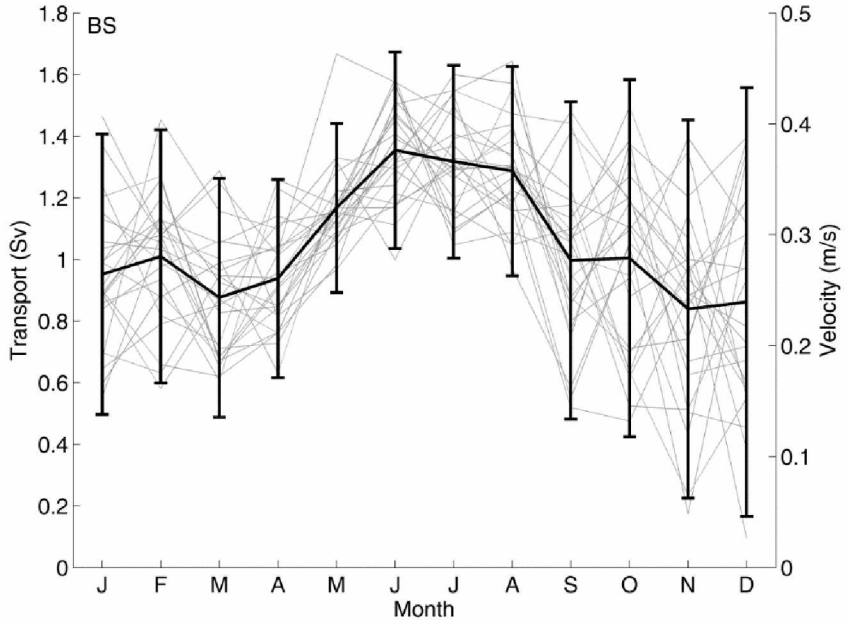


(a)

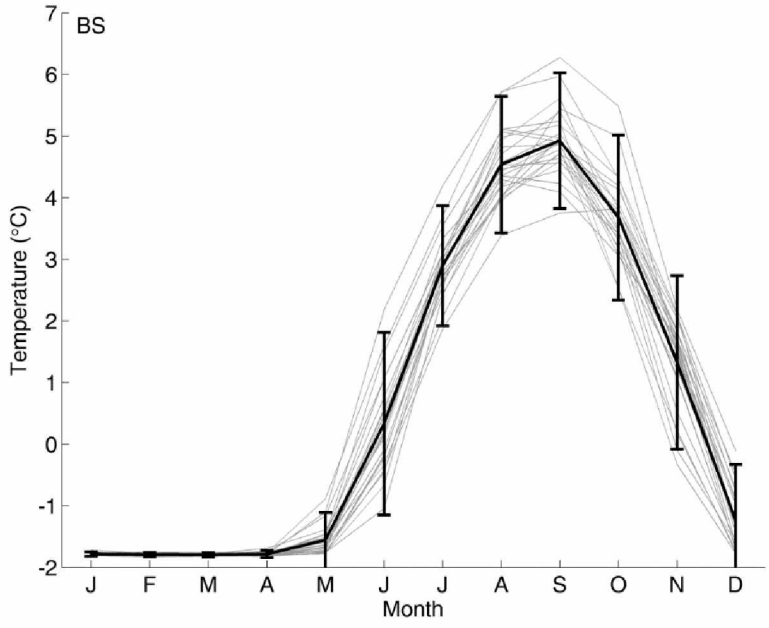


(b)

Figure 2.4. Long-term mean climatology for (a) volume transport and water velocity; (b) water temperature; (c) heat flux; (d) salinity; (e) ice volume transport (the Strait is ice-free between July and October); (f) total freshwater transport in Bering Strait, with error bars showing the 95% confidence limit (~1.96 σ). Grey lines show monthly mean values for each year of the model run.

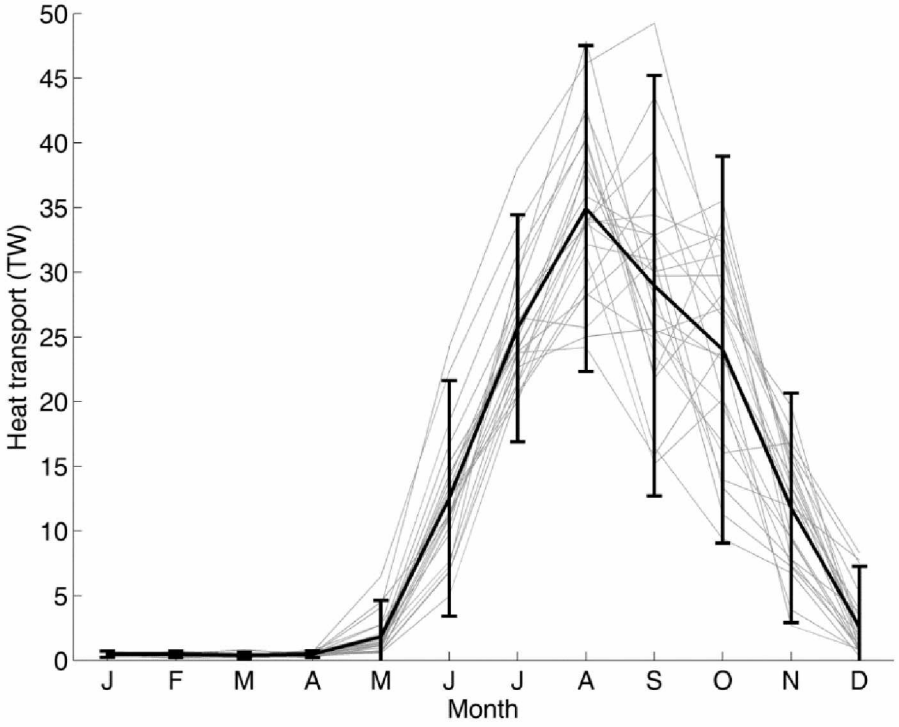


(c)

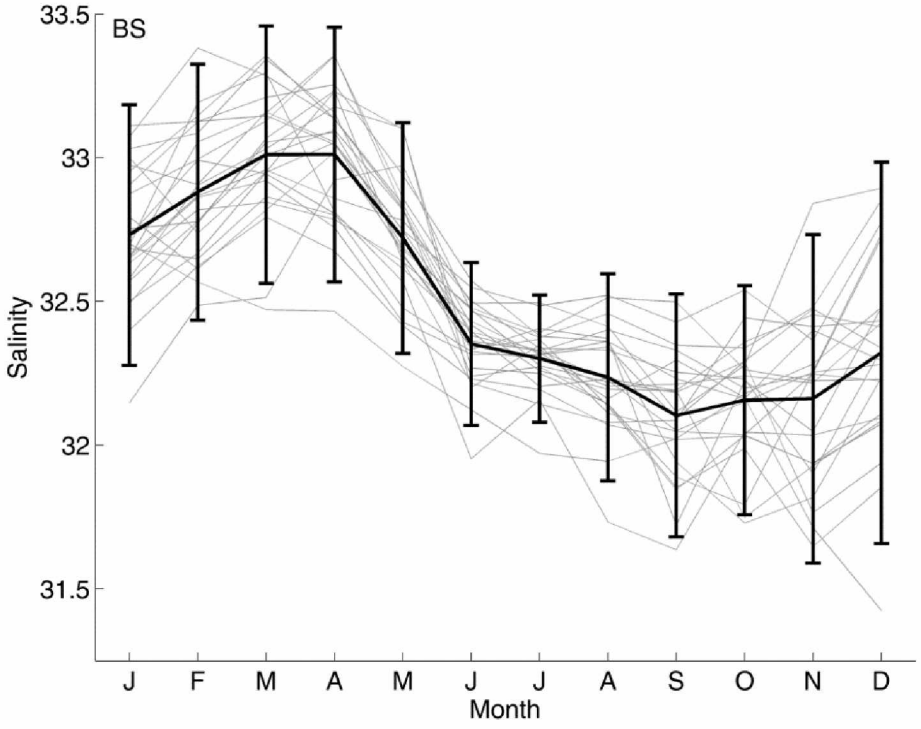


(d)

Figure 2.4. cont.

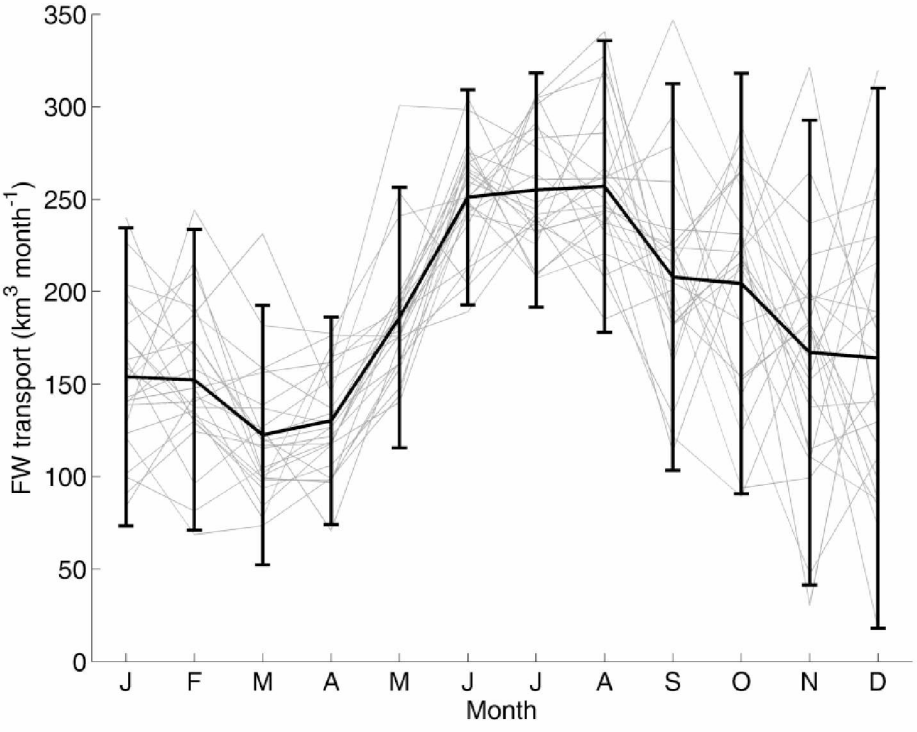


(f)

Figure 2.4. cont.

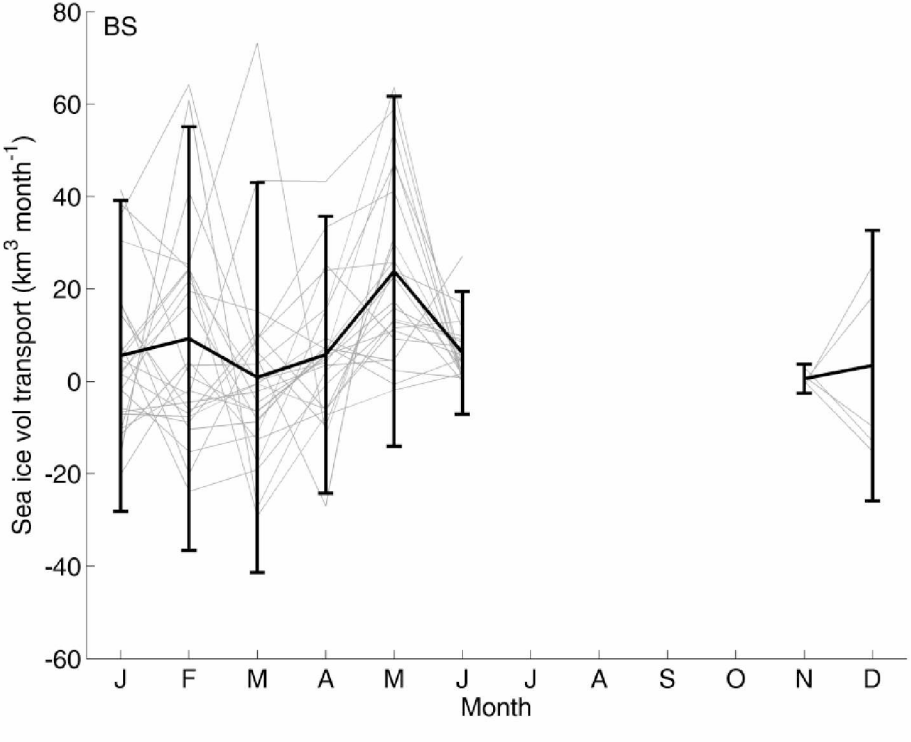
BS
Sea ice vol transport (km3 month-1)
80
60
40
20
0
-20
-40
-60
J
F
M
A
M
J
J
A
S
O
N
D
Month

(e)

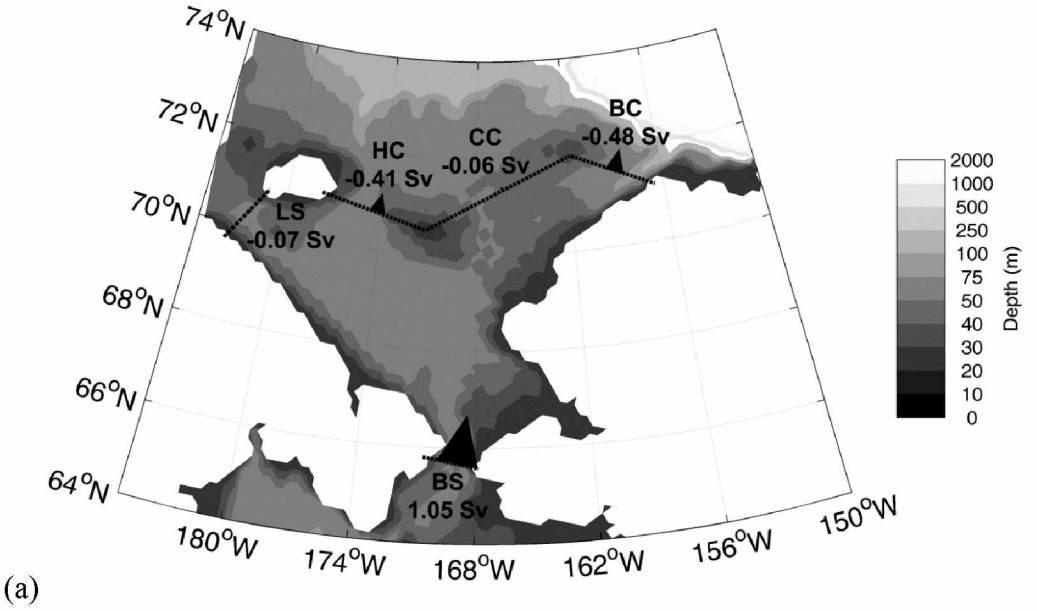


(a)

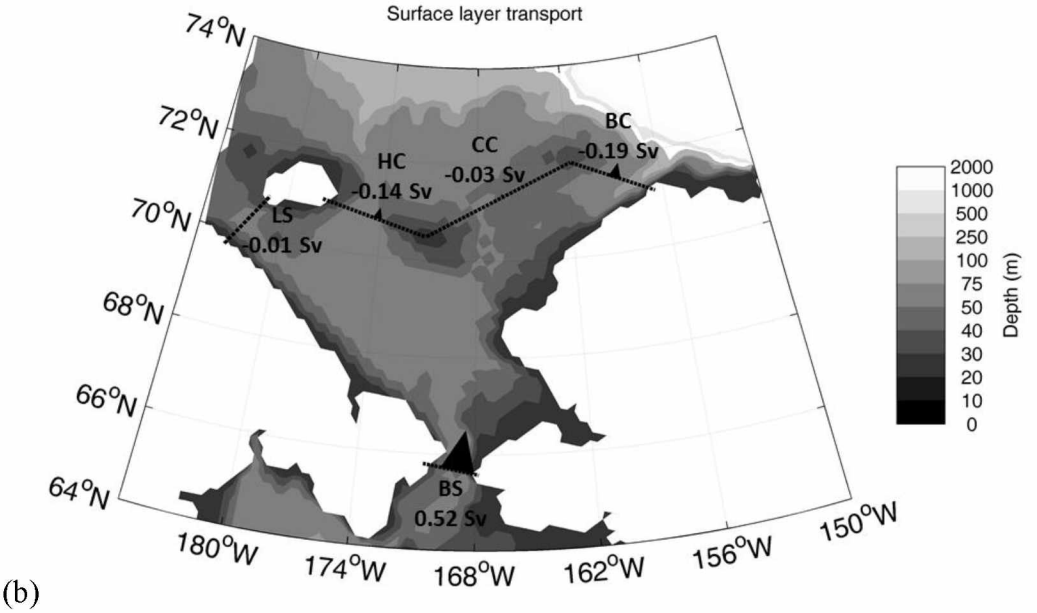


(b)

Figure 2.5. Long-term mean (a) depth integrated, (b) surface layer, and (c) deep layer transport values (see section 3.5. for layer definitions) across Long Strait (LS), Herald Canyon (HC), Central Channel (CC), and Barrow Canyon (BC) (1 Sv ≡ $10^6$ $m^3$ $s^{-1}$). Negative values denote flow out of the Chukchi Sea shelf region.

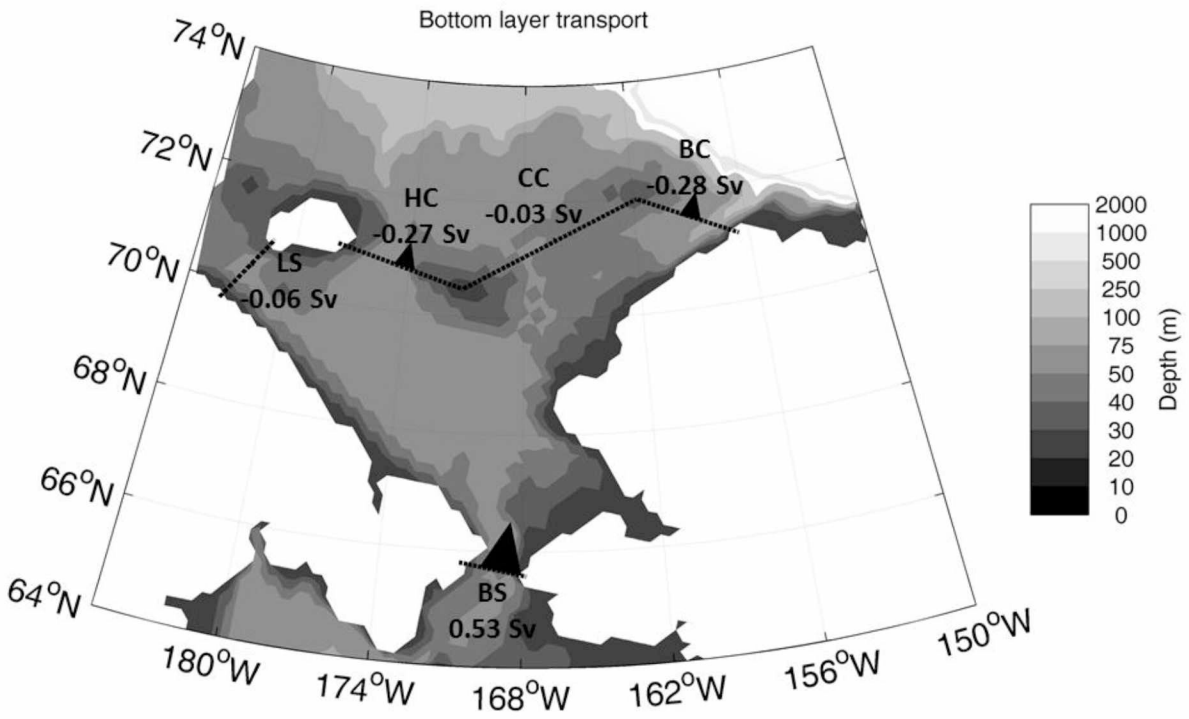


(c)

Figure 2.5. cont.

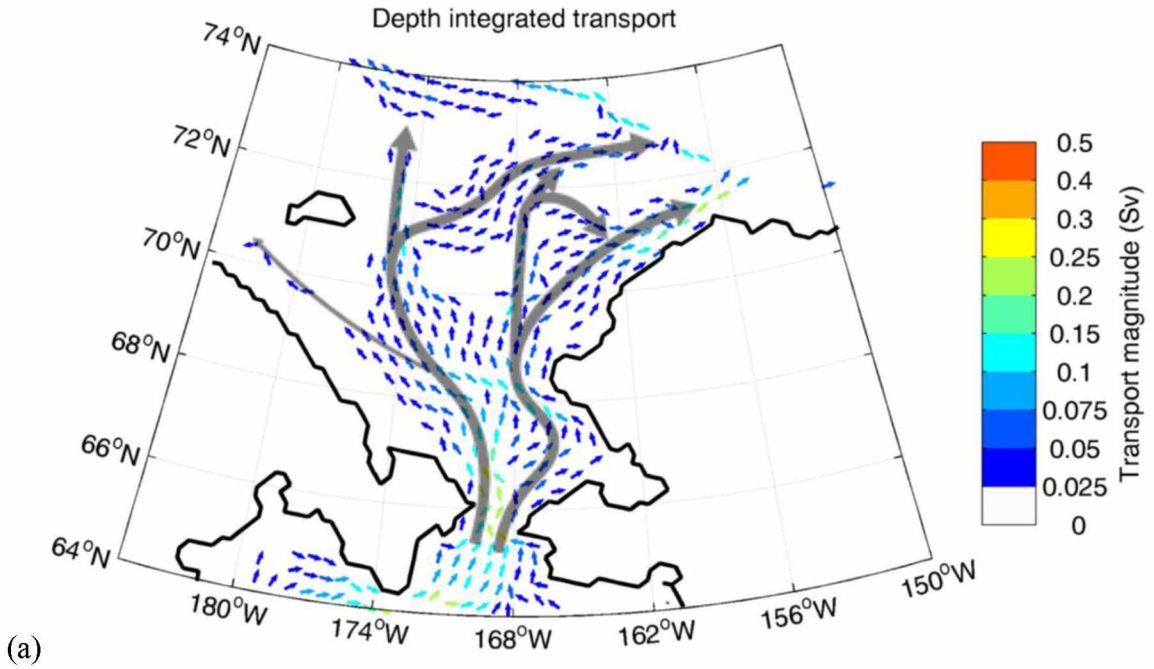


(a)

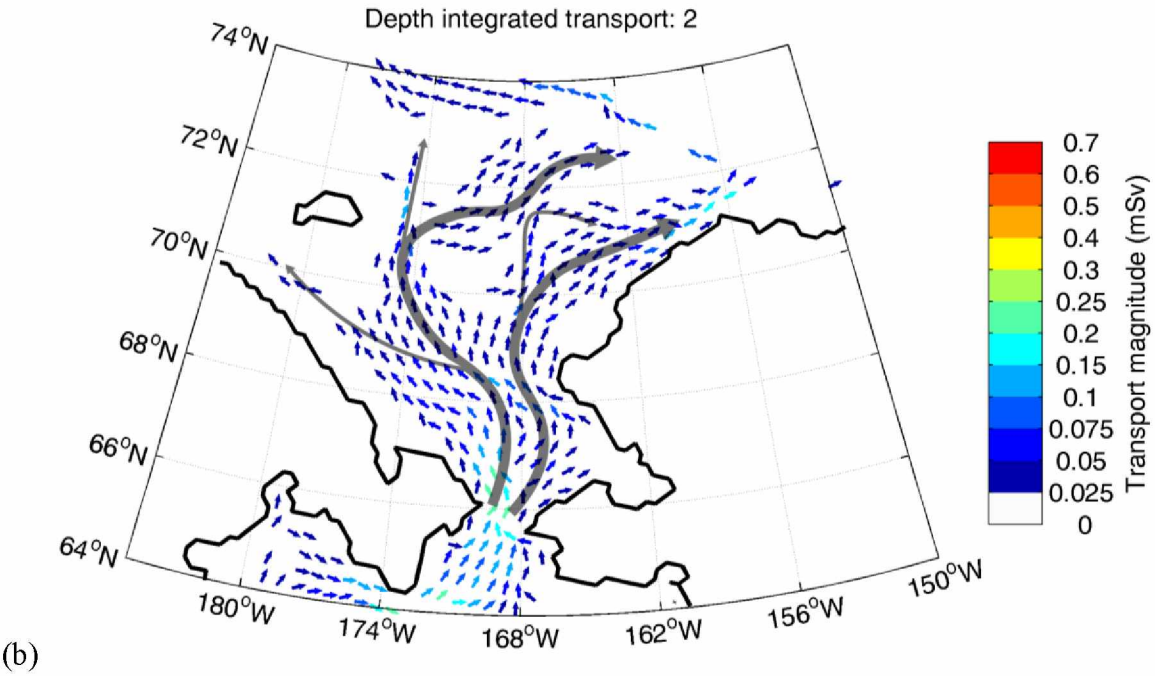


(b)

Figure 2.6. Mean depth integrated volume transport vectors for (a) entire model run, (b) winter months, (c) spring months, and (d) summer months. Schematic arrows showing flow pathways are overlaid for clarity. Areas with no small arrows have transport < 0.025 mSv.

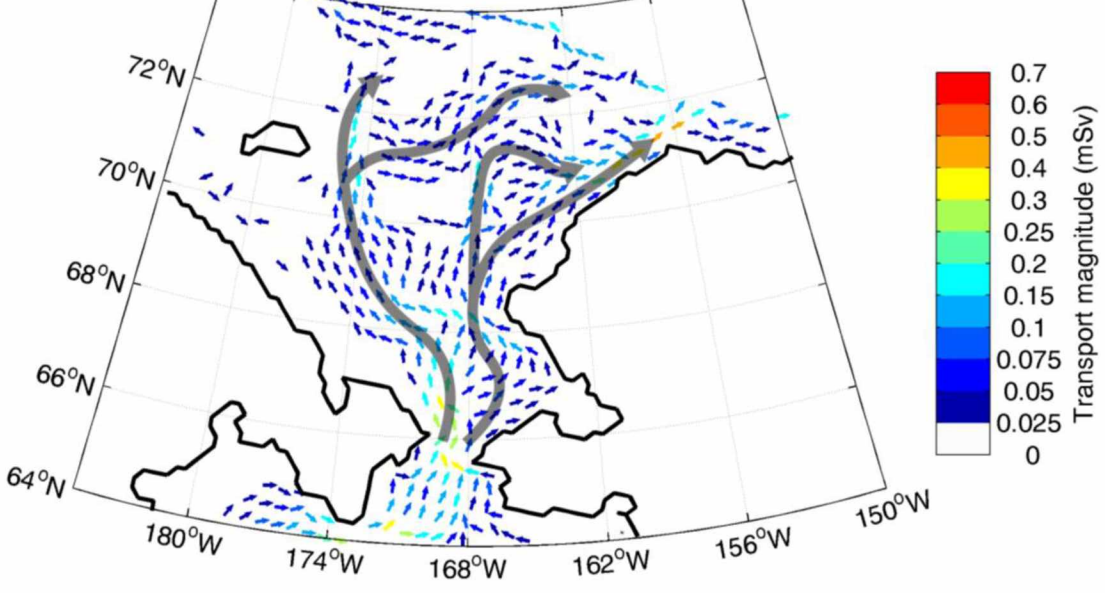


(d)

Figure 2.6. cont.

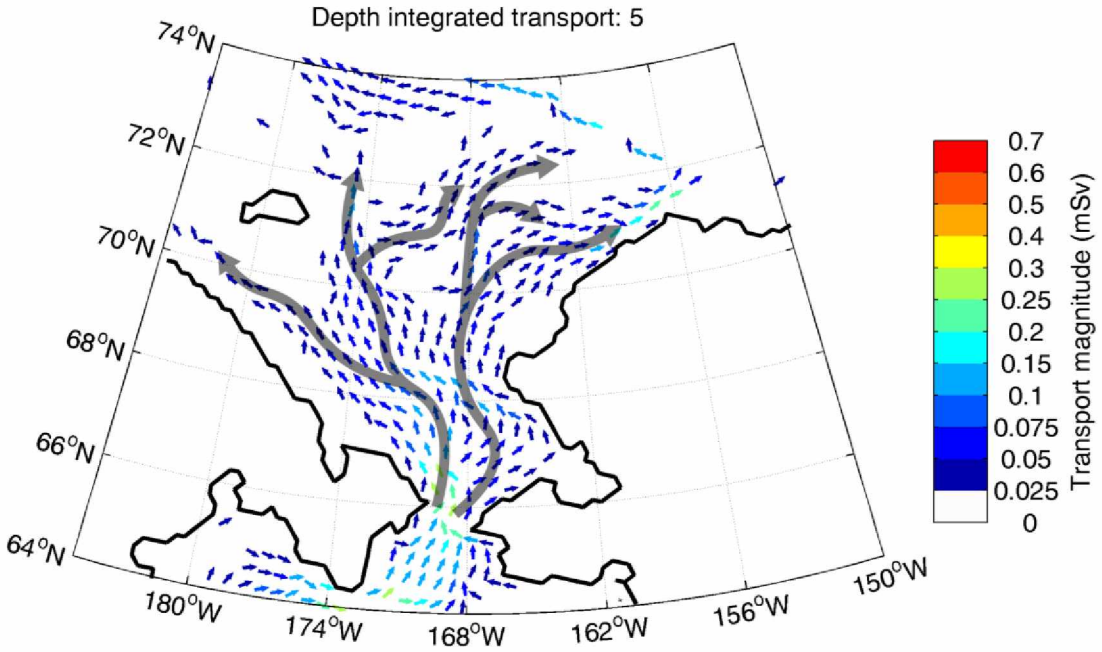
Depth integrated transport: 5
74°N
72°N
70°N
68°N
66°N
64°N
180°W
174°W
168°W
162°W
156°W
150°W
0.7
0.6
0.5
0.4
0.3
0.25
0.2
0.15
0.1
0.075
0.05
0.025
0
Transport magnitude (mSv)

(c)

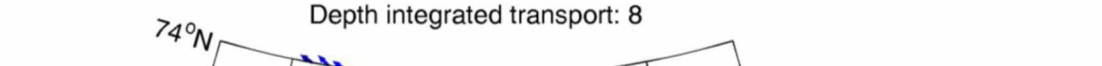
Depth integrated transport: 8
74°N

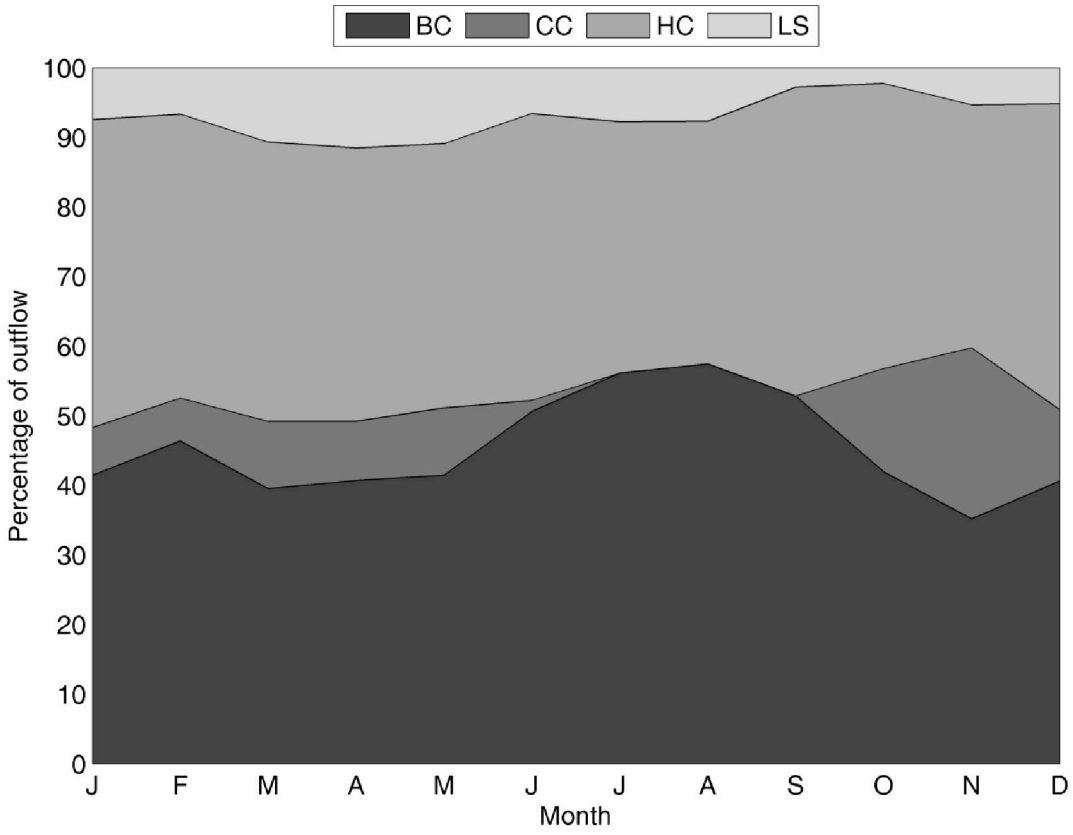


Figure 2.7. Area plot showing climatology of relative outflow division in the four northern channels – Long Strait (LS), Herald Canyon (HC), Central Channel (CC), and Barrow Canyon (BC). Note that a zero contribution for a channel means that it is an inflowing period.

### *2.8. Tables*

Table 2.1. Values from the ARDAT data set for selected rivers which supply freshwater to the Chukchi Sea.

| River | Annual mean discharge ($km^3\ yr^{-1}$) | Peak discharge temperature (°C) |
|---|---|---|
| Lena | 535 | 14.0 |
| Yndigirka | 50 | 14.2 |
| Kolyma | 101 | 15.5 |
| Amguema | 12 | 15.4 |
| Yukon | 214 | 17.6 |
| Kuskokwim | 38 | 15.3 |

Table 2.2. Availability of data from Bering Strait observations at four locations, with N showing how many months were used in Figure 2. No single point current meter was deployed at A4, therefore no velocity comparisons were performed at this grid point.

| Mooring | Variable | Date range | N |
|---|---|---|---|
| A1 | T | Sept 1992 – Sept 1994, Aug 2006 – Aug 2010 | 74 |
| | S | | |
| | V | Sept 1990 – Sept 1991, Sept 1992 – Sept 1994 | 38 |
| A2 | T | Jan 1995 – Sept 1996, July 1997 – Nov 2003, Aug 2004 – July 2011 | 180 |
| | S | | |
| | V | Sept 1990 – Sept 1996, July 1997 – July 1998, July 1999 – Sept 2001, Jun 2002 – Aug 2007 | 176 |
| A3 | T | July 1997 – July 2011 | 169 |
| | S | | |
| | V | Sept 1990 – Dec 1991, July 1997 – Aug 2008 | 137 |
| A4 | T | Sept 2001 – July 2006, Aug 2007 – July 2011 | 107 |
| | S | | |
| | V | --- | 0 |

## Summary and Conclusions

A new climatological data set of river discharge and river water temperature was created and incorporated into a pan-Arctic model with 1/6° horizontal resolution to improve the model's recreation of near-shore buoyant currents. Model integrations were first compared to output from a simulation using a 1° resolution discharge data set (which did not include river water temperature), and then used to estimate contributions of coastal currents to the heat, freshwater and volume fluxes through the Bering Strait, the only pathway for Pacific water to enter the Arctic Ocean.

Both basin-wide and local responses to the higher resolution data set were investigated. After compiling monthly mean observations for 30 Arctic rivers in a climatological data set, we applied the data set to a 35-year long integration of a regional sub-domain of a global model. Previously, this model used a 1° resolution forcing which resulted in discharge being input on or past the shelf break, meaning discharge was rapidly advected to the interior of the Arctic basin. In addition to the higher resolution data set, a non-linear free surface was enabled in the model.

We initially analyzed differences of both freshwater content and heat fluxes on the Arctic shelves, a region that was defined as having depth <200 m. While the seasonal cycle of freshwater content was unchanged with the inclusion of the new river data set, magnitude was increased by 3,700 $km^3$, reflecting both the direct input of river water to the shelf region (total river discharge in the data set is ~2,800 $km^3$ $yr^{-1}$), but also the indirect effect of river water on the sea-ice balance. For heat fluxes to the shelf region, both the seasonal cycle and magnitude were changed. Winter heat fluxes were reduced to <0.01 TW, and mean summer heat fluxes from riverine sources increased by 8 TW, equivalent to ~50% of the heat flux needed to explain the decreasing sea-ice trend over the last few decades. By using the new data set, heat flux maxima

now coincides with times of peak river discharge and warmest river temperatures, as opposed to being driven only by solar radiation. The additional summer heat fluxes reduced basin-wide sea-ice extent by ~10% when compared to the results from the model using the coarser forcing, which suggests that inclusion of riverine heat could lead to more conservative sea-ice extent estimates. Regional effects were even greater, with a ~36% decrease in sea-ice around the Mackenzie delta. However, it is likely that the current model configuration still underestimates the effects of river discharge and heat locally.

Comparison of model output to satellite derived sea surface temperatures showed that the model was considerably cooler than observations, with differences resulting from two main factors. Firstly, the model's surface grid layer is 10 m thick, and river discharge is input to this layer. Observations show that the depth of the Mackenzie River plume is only ~5 m (Wood et al., 2013), and so the volume of seawater heated by the model was much larger than in observations, resulting in lower simulated temperatures. The second factor is that the model (in its current configuration) does not recreate plume turbidity. Arctic rivers are typically heavily sediment laden, with the sediment transported far offshore. The sediment plume has a much lower albedo, and absorbs more solar radiation than the surrounding water, making the plume able to regain heat lost by advection and mixing.

Regardless of these underestimates, enabling a non-linear free surface in the model meant that where there was heat and freshening from the Arctic rivers, sea surface height was also raised. This positive anomaly, coupled with a greater area of open water exposed to winds, consequently increased along-shore geostrophic velocities, leading to a quasi-continuous, fast-moving nearshore boundary current akin to the riverine coastal domain (RCD; Carmack et al., 2015). However, the Rossby radius of deformation in this region is typically 5-15 km, meaning

that the RCD is not well resolved in the current model configuration. Higher resolution model runs (with similarly high resolution river discharge and river temperatures) would be needed to more accurately investigate the existence of the RCD, and its effects of larval and/or zooplankton transport in this region.

With improved reproduction of near-shore buoyant currents in the model, the second part of this thesis was to look at contributions of these currents in the Bering Strait, a key gateway for waters from the Pacific Ocean to enter the Arctic Ocean, and a region where longer ice-free seasons could potentially cause ecosystem shifts. Due to logistical difficulties, only opportunistic observations are available for most of the Chukchi Sea. A high-resolution mooring array has been deployed in the Bering Strait since 1990, but data is still published with uncertainties in volume, heat and freshwater transport due to data gaps (cf. Woodgate et al., 2012). Thus, we used the pan-Arctic model to resolve flow pathways through the Bering Strait and over the Chukchi Sea shelf in order to improve understanding of both the current and future states of one of the most productive Arctic seas.

Preliminary point-to-point comparisons between the model and observations from the long-term mooring array showed strong correlations, and that the model reasonably approximates the Bering Strait throughflow. This allowed us to then estimate heat, freshwater and volume transports in both the Alaskan Coastal Current and stratified surface layers (including freshwater transported as ice or snow) not captured by the mooring array. We suggested a volume transport contribution of 27% from the Alaskan Coastal Current, which subsequently led to increases in heat and freshwater fluxes of 64% and 32% respectively. In the case of freshwater transport, 88% of the increase came from inclusion of the coastal current, and the remaining 12% from the sea-ice component. However, modeled estimates of sea-ice transport

were 60% of observational estimates, although it is difficult to determine whether the model underestimates ice volume due to averaging over a ~16 km-wide grid cell, or whether acoustically derived observations overestimate due to measuring ice keels that are not representative of the whole Bering Strait.

With a revised estimate of inflow to the Chukchi Sea through the Bering Strait, we finally used model output to determine seasonal variations of the current pathways across the Chukchi Sea, as well as volume transport through the four major outflow pathways (Long Strait, Herald Canyon, Central Channel and Barrow Canyon) which have relatively few observations. We found that the majority of the water exiting the Chukchi Sea leaves through either Barrow Canyon or Herald Canyon, and modeled volume transport through Long Strait was only 41% of observed estimates, suggesting that the influence of Long Strait to the western Chukchi Sea may be negligible over longer time periods. However, high variability showed that it may be important on seasonal time scales. The model also resolved an eastward flow to the south of Hanna Shoal, in agreement with earlier circulation models (e.g. Winsor and Chapman, 2004) and observations (e.g. Weingartner et al., 2005). Flow pathways exhibited interannual variability in the eastern Chukchi Sea, and we suggested that variability in the southern Hanna Shoal recirculation explain changes in species abundance on the eastern Chukchi Sea shelf – years with a strong eastward flow led to the presence of more oceanic copepod species advected with the more nutrient-rich Bering Sea water, and years with reduced or reversed (i.e. westward) flow resulted in Arctic copepod species being present.

While the model crudely recreates buoyant coastal currents and newly observed flow pathways, further improvements to simulations can still be made. In the present configuration, the model resolution is roughly twice the baroclinic Rossby radius of deformation, and as stated

previously, vertical resolution is also still coarse, with riverine inputs added to the model over greater depths than observations. The first potential improvement to this, and other models, is to give greater focus to riverine influence in the Arctic Ocean by increasing resolution in both horizontal and vertical directions. Similarly, once the model resolution is increased, so should that of the forcing fields, otherwise a problem comparable to the original one presented here will occur; riverine inputs to the model will not be accurately represented. A second improvement to the simulations would be to use a time-varying river discharge and river temperature forcing. Although time-varying river forcing files were not used here, preliminary work has been undertaken at NASA's Jet Propulsion Laboratory and the University of Bonn with aims to incorporate discharge data derived from the Gravity Recovery and Climate Experiment (GRACE) into the data set created in Chapter 1 of this thesis. A more complex hydrological model could be used to determine a continuous coastal runoff, instead of just point sources at rivers, and could also derive discharge temperature data to complete the data omissions from the presently available discharge and river temperature time-series.

Thus, in order to resolve fine-scale oceanic features in the changing Arctic, and to reduce uncertainties in both observational estimates and model constraints, both higher model resolution and increased observations are needed. The results from this thesis in increasing the skill at which the riverine coastal domain, and other buoyant coastal currents, are reproduced in models leads to incrementally greater understanding of the nearshore region and its influences – knowledge vital to being able to analyze larger scale connections, not only between the terrestrial and marine ecosystems, but also on the Arctic-wide and global scales as regions undergo predicted changes to altered states as a result of the changing climate.

***References***

Carmack, E., Winsor, P., Williams, W., 2015. The Contiguous Panarctic Riverine Coastal Domain: A Unifying Concept. Progress in Oceanography 139, 13-23.

Weingartner, T., Aagaard, K., Woodgate, R., Danielson, S., Sasaki, Y., Cavalieri, D., 2005. Circulation on the North Central Chukchi Sea Shelf. Deep Sea Research Part II: Topical Studies in Oceanography 52, 3150-3174.

Winsor, P., Chapman, D.C., 2004. Pathways of Pacific Water across the Chukchi Sea: A Numerical Model Study. Journal of Geophysical Research 109 (C3), C03002.

Wood, K.R., Overland, J.E., Salo, S.A., Bond, N.A., Williams, W.J., Dong, X., 2013. Is There A "New Normal" Climate in the Beaufort Sea? Polar Research 32, 19552-19560.

Woodgate, R.A., Weingartner, T., Lindsay, R., 2012. Observed Increases In Bering Strait Oceanic Fluxes From The Pacific To The Arctic From 2001 To 2011 And Their Impacts On The Arctic Ocean Water Column. Geophysical Research Letters 39, L24603.

# Appendix. Approval of non-committee co-authors for use of material

**Menemenlis, Dimitris (329C)** <Dimitris.Menemenlis@jpl.nasa.gov> 3 March 2016 at 20:58
To: Jonathan Whitefield <jonathan.whitefield@gmail.com>

Dear Jonathan, this letter is to grant you permission to use the ARDAT Ocean Modelling paper in your thesis. My contribution to this paper was modest and mostly limited to a technical advisory role.

Congratulations and best regards,

Dimitris Menemenlis

Jet Propulsion Laboratory, California Institute of Technology
MS 300-323, 4800 Oak Grove Dr, Pasadena CA 91109-8099, USA
tel: 818-354-1656; cell: 818-625-6498; fax: 818-393-6720

---

**McClelland, James W** <jimm@utexas.edu> 4 March 2016 at 07:39
To: "Jonathan Whitefield (jonathan.whitefield@gmail.com)" <jonathan.whitefield@gmail.com>

Dear Jonathan,

I'm glad to hear that your thesis is nearly complete. You have my permission to include our paper titled "A new river discharge and river temperature climatology data set for the pan-Arctic region" (Ocean Modelling 88:1-15) as a chapter in your thesis.

Best Regards,

Jim McClelland

---
James McClelland
University of Texas at Austin
Marine Science Institute
750 Channel View Drive
Port Aransas, Texas 78373

Phone: 361-749-6756
Fax: 361-749-6777
---